A Measurement of the Difference Between the Phases of the CP-Violation Parameters η^{+-} and η^{00}

Robert K. Black

Submitted for the degree of
Doctor of Philosophy

Department of Physics
University of Edinburgh
September 1988

To my Mother and Father,

and to Tina Szucs.

Acknowledgements

My work at Edinburgh was supported by the Science and Engineering Research Council.

I would like to thank all members of the NA31 collaboration. In particular Don Cundy, for his advice and support, Heinz-Georg Sander, who communicated easily his knowledge of the experiment, and Ken Peach, my supervisor.

For reasons which have nothing to do with this work I thank Tina, Dave and Leslie, Rod, big Davie Walker, Bill, Maria, Cecilia, and Tony.

Abstract

The CERN-Edinburgh-Mainz-Orsay-Pisa-Siegen Neutral Kaon Spectrometer at the CERN SPS has been used to measure the difference between the phases ϕ^{+-} and ϕ^{00} of the CP-violation parameters η^{+-} and η^{00}. We determine $\Delta\phi$ to be 2.4 ± 3.6^0. This is in agreement with the requirements of the CPT-Theorem, and is more accurate than the previous result, $\Delta\phi = 9.8 \pm 5.4^0$.

Contents

List of Figures

List of Tables

Chapter 1

Introduction

Symmetries and conservation laws have long been the foundations upon which an understanding of the physical world is based. The macroscopic symmetries of space and time, which imply conservation of energy and momentum, have guided physics for centuries. In more recent times the discovery of quantum phenomena have led to new conservation laws corresponding to discrete transformations. Charge conjugation (C), changes particle into antiparticle, and C-invariance implies that the results of an experiment will not change when all particles are replaced by their corresponding antiparticles. Invariance under reflection in space (parity operator, P) implies that the mirror image of an experiment should give the same results as the original. Time reversal, T, interchanges initial and final states of an interaction, reversing momenta and angular momenta, and corresponds formally to a reversal of the direction of time.

The CPT-Theorem of Luders and Pauli [1] states that, under weak assumptions in a local field theory, all interactions are invariant under the successive application of C, P and T. Originally it was believed that C, P and T were conserved independently. The discovery of P-violation [2] and C-violation [3] in the weak interaction refuted this belief, and the combined product CP was taken to replace the separate conservation of C and P.

In 1964 CP-violation was discovered [4] by the observation that the long-lived neutral kaon (CP = -1) decays into two pions (CP = +1), albeit with a small branching ratio. This unexpected observation has become one of the great dis-

coveries of particle physics, and the subject of CP-violation in the kaon system is still one of great interest in the late nineteen-eighties.

Despite these symmetries which have fallen by the wayside, the CPT-symmetry is still regarded as a "good" symmetry, although it is not on such strong ground experimentally as, for example, the conservation of energy [5]. Some consequences of the CPT-theorem which can be verified experimentally relate to the properties of particles and antiparticles, which should have the same mass and lifetime, and magnetic moments equal in magnitude but opposite in sign.

In the kaon system one consequence of the CPT-theorem is that the phases ϕ^{+-} and ϕ^{00} of the CP-violation parameters η^{+-} and η^{00} (see Chapter 2) should differ by no more than a fraction of one degree. Experimentally the phase ϕ^{+-} is $44.6^o \pm 1.2^o$ [6], and the most accurate measurement of ϕ^{00} is $55.7^o \pm 5.8^o$ [7]. The best direct measurement of the difference of these phases [7] gives ϕ^{00}-ϕ^{+-} as $12.6^o \pm 6.2^o$, and a fit to results in the Particle Data Booklet gives a phase difference of $9.8^o \pm 5.4^o$.

Given this indication of a phase difference of more than one degree, and given the fundamental role of the CPT-theorem in modern physics (it is very difficult to formulate field theories which are not automatically CPT-invariant), it is desirable to make a more accurate measurement of ϕ^{00}-ϕ^{+-}. The work described here is such a measurement, an analysis of data taken in 1987 with the NA31 Neutral Kaon Spectrometer at the CERN-SPS.

In the following chapters we will discuss theory, experimental set-up, principles of the measurement, cuts and background removal, and results.

Chapter 2

Theory

In this chapter we introduce the phenomenology of CP-violation in the kaon system, and briefly discuss models for CP-violation and the current experimental status. We then introduce possible CPT-violating amplitudes, and show that the current experimental data are not in perfect agreement with theory if CPT-invariance is assumed.

2.1 Introduction to the Kaon System

The strong eigenstates of the neutral kaon system are the $| K^0 >$ and the $| \bar{K}^0 >$, which have strangeness +1 and -1 respectively. The K^0 and $\bar{K}^0$ are strongly produced, but being the lightest strange particles can decay only weakly. The weak interaction does not conserve strangeness, so the $| K^0 >$ and $| \bar{K}^0 >$ states can mix through second-order weak interactions ($\Delta S = 2$), via intermediate states such as $\pi\pi$ or $\pi\pi\pi$.

If CP were conserved (CPT is assumed until we explicitly introduce CPT-violating amplitudes) the eigenstates would be :

$$\begin{aligned} | K_1 > &= \frac{1}{\sqrt{2}}(| K^0 > + | \bar{K}^0 >) \qquad (CP = +1) \\ | K_2 > &= \frac{1}{\sqrt{2}}(| K^0 > - | \bar{K}^0 >) \qquad (CP = -1) \end{aligned} \tag{2.1}$$

Since $< \pi\pi \mid CP \mid \pi\pi >= 1$ for pions in a state of angular momentum zero, the K_1 can decay into two pions but the K_2 cannot. The two-body decay is preferred over a three-body decay because of phase space, so the K_2 is longer lived than the K_1. The discovery of CP-violation was the observation that this long-lived component, the supposedly CP-odd state, decays into the CP-even two pion state.

The observed CP-violation requires, alongside the $\Delta S = 2$ transitions which allow for mixing between $\mid K^0 >$ and $\mid \bar{K^0} >$, $\Delta S = 2$ CP-violating transitions which give the mass eigenstates a CP-impurity. The physical states are now regarded as :

$$\begin{aligned} \mid K_L > &= \frac{1}{\sqrt{2}(1+\mid \epsilon \mid^2)}(\mid K_2 > + \epsilon \mid K_1 >) \\ \mid K_S > &= \frac{1}{\sqrt{2}(1+\mid \epsilon \mid^2)}(\mid K_1 > + \epsilon \mid K_2 >) \end{aligned} \tag{2.2}$$

where ϵ characterises the CP-impurity in these mass eigenstates.

The interesting question which has instigated a massive experimental effort is whether all CP-violation is present in the mass eigenstate, or if "direct" CP-violation ($K_2 \rightarrow \pi\pi$) can occur in addition. We will review the parameters associated with CP-violation, and show how experiments may be sensitive to the presence of direct CP-violation.

2.2 Phenomenology of CP-violation in the Kaon System

CP-violation has only been observed in the decay of the long-lived neutral kaon. We have already introduced the CP-violating decays of K_L into two pions, but CP-violation has also been observed as a charge asymmetry in semi-leptonic decays ($\pi e \nu$, $\pi \mu \nu$) of K_L. We will discuss further only the CP-violating decay into two pions.

By Bose statistics the allowed states for two pions with angular momentum zero

are I=0 and I=2. There are, therefore, four possible amplitudes:

$$\begin{aligned} &A(K_S \to \pi\pi, I=0) && A(K_L \to \pi\pi, I=0) \\ &A(K_S \to \pi\pi, I=2) && A(K_L \to \pi\pi, I=2) \end{aligned} \tag{2.3}$$

In the usual notation of CP-violation these are reduced to three complex numbers by normalisation to $A(K_S \to \pi\pi, I=0)$. We define:

$$\begin{aligned} \epsilon_0 &= A(K_L \to \pi\pi, I=0)/A(K_S \to \pi\pi, I=0) \\ \epsilon_2 &= \frac{1}{\sqrt{2}} A(K_L \to \pi\pi, I=2)/A(K_S \to \pi\pi, I=0) \\ \omega &= \frac{1}{\sqrt{2}} A(K_S \to \pi\pi, I=2)/A(K_S \to \pi\pi, I=0) \end{aligned} \tag{2.4}$$

We define the direct CP-violation term ϵ' as follows:

$$\epsilon' = \frac{1}{\sqrt{2}} A(K_2 \to \pi\pi, I=2)/A(K_1 \to \pi\pi, I=0) \tag{2.5}$$

The parameters of experimental interest, which will allow us to make an experimental measurement sensitive to direct CP-violation are defined as:

$$\begin{aligned} \eta^{+-} &= \mid \eta^{+-} \mid e^{i\phi^{+-}} = A(K_L \to \pi^+\pi^-)/A(K_S \to \pi^+\pi^-) \\ \eta^{00} &= \mid \eta^{00} \mid e^{i\phi^{00}} = A(K_L \to \pi^0\pi^0)/A(K_S \to \pi^0\pi^0) \end{aligned} \tag{2.6}$$

Decomposing the $\pi^+\pi^-$ and $\pi^0\pi^0$ states into their I=0 and I=2 components

$$\begin{aligned} \mid \pi^+\pi^- > &= \frac{\sqrt{2}}{\sqrt{3}} \mid \pi^+\pi^-, I=0 > + \frac{1}{\sqrt{3}} \mid \pi^+\pi^-, I=2 > \\ \mid \pi^0\pi^0 > &= \frac{1}{\sqrt{3}} \mid \pi^0\pi^0, I=0 > - \frac{\sqrt{2}}{\sqrt{3}} \mid \pi^0\pi^0, I=2 > \end{aligned} \tag{2.7}$$

it can be seen, from 2.6 and 2.7, that

$$\begin{aligned} \eta^{+-} &= (\epsilon_0 + \epsilon_2)/(1+\omega) \\ \eta^{00} &= (\epsilon_0 - 2\epsilon_2)/(1-2\omega) \end{aligned} \tag{2.8}$$

By convention the $K^0 \to \pi\pi$ (I=0) amplitude is chosen to be real, except for a final-state interaction leading to a phase shift δ_0 . The $K^0 \to \pi\pi$ (I=2) amplitude has, in general, a non-zero phase relative to the I=0 transition, and similarly has a phase-shift, δ_2, due to final-state interaction.

$$\begin{aligned} < \pi\pi, I=0 \mid K^0 > &= A_0 e^{i\delta_0} \\ < \pi\pi, I=2 \mid K^0 > &= A_2 e^{i\delta_2} \end{aligned} \tag{2.9}$$

The $\bar{K}^0$ amplitudes may be obtained by CPT.

$$\begin{aligned} < \pi\pi, I = 0 \mid \bar{K}^0 > &= A_0^* e^{i\delta_0} = A_0 e^{i\delta_0} \\ < \pi\pi, I = 2 \mid \bar{K}^0 > &= A_2^* e^{i\delta_2} \end{aligned} \tag{2.10}$$

It is easy to show, using 2.1, 2.2, 2.4, 2.9 and 2.10, that :

$$\begin{aligned} \epsilon_0 &= \epsilon \\ \epsilon' &= \frac{i}{\sqrt{2}}(ImA_2/A_0)e^{i(\delta_2-\delta_0)} \end{aligned} \tag{2.11}$$

From the definition of ϵ' (eqn 2.5) it can be seen that non-zero ϵ' explicitly signals the presence of direct CP-violation. The above expression shows that non-zero ϵ' requires a difference between the phase of A_0 and A_2, a difference between the I=0 and I=2 decay channels. Such a difference in these decay channels can only occur if direct CP-violation is present. If all CP-violation were present in the mass eigenstates then ϵ' would be zero.

Let us recall:

$$\begin{aligned} \eta^{+-} &= (\epsilon_0 + \epsilon_2)/(1+\omega) \\ \eta^{00} &= (\epsilon_0 - 2\epsilon_2)/(1-2\omega) \end{aligned} \tag{2.12}$$

From the definitions of ϵ_2, ϵ' and ω (eqns 2.4 and 2.5) it can be seen that :

$$\epsilon_2 = \epsilon' + \epsilon\omega \tag{2.13}$$

Therefore :

$$\begin{aligned} \eta^{+-} &= \epsilon + \epsilon'/(1+\omega) \\ \eta^{00} &= \epsilon - 2\epsilon'/(1-2\omega) \end{aligned} \tag{2.14}$$

The transition $\mid K_S \rightarrow \pi\pi, I = 2 >$ (ΔI=3/2) is strongly suppressed relative to the transition $\mid K_S \rightarrow \pi\pi, I = 0 >$ (ΔI=1/2), so the factor ω is small and may be neglected in the above expressions.Therefore, to a very good approximation :

$$\begin{aligned} \eta^{+-} &= \epsilon + \epsilon' \\ \eta^{00} &= \epsilon - 2\epsilon' \end{aligned} \tag{2.15}$$

These relationships may be demonstrated graphically, following the style of Wu and Yang [8], in the so-called Wu-Yang diagram (see fig 2.1).

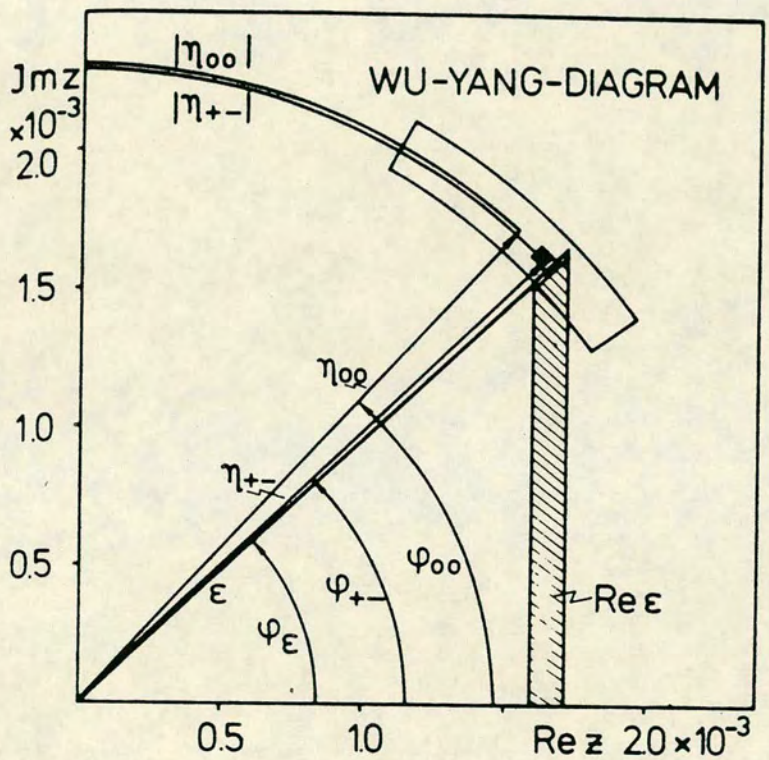

Figure 2.1: The Wu-Yang Diagram

It can be seen that:

$$| \eta^{00}/\eta^{+-} |^2 \;=\; (\epsilon - 2\epsilon')^2/(\epsilon + \epsilon')^2 \tag{2.16}$$

The experimentally measured values of η^{+-} and η^{00} are close, so ϵ' is small relative to ϵ . Using this fact, and the fact that the phases of ϵ and ϵ' are close, we may expand the above expression to arrive at the famous relationship:

$$| \eta^{00}/\eta^{+-} |^2 \;=\; 1 - 6 \, | \, \epsilon'/\epsilon \, | \tag{2.17}$$

The ratio $| \eta^{00}/\eta^{+-} |^2$ is an experimentally measurable quantity, which is simply a double ratio constructed from the rates of K_L^0 and K_S^0 into two neutral pions, and two charged pions, respectively. By measuring these rates and constructing the $| \eta^{00}/\eta^{+-} |^2$ ratio we have an experimental quantity which would be sensitive, if precise enough, to a non-zero ϵ'.

The simplest explanation for CP-violation came from Wolfenstein [9] who proposed a new ΔS=2 transition which would allow for CP-violating transitions between K_S and K_L. The strength of this "superweak" interaction would be 10^{-7} that of the weak interaction. Unfortunately this model is purely phenomenological, the only parameter being ϵ which is measured from the data and is unrelated to quantities outside the kaon system. For this model ϵ' would be zero. An explanation for CP-violation from within the framework of the standard model would be more acceptable.

In 1973 Kobayashi and Maskawa [10] showed that, in the presence of three or more flavour generations, CP-violation could occur due to mixing between the light and heavy quark sectors. Both ϵ and ϵ' effects are predicted by this so-called Kobayashi-Maskawa model. The box diagram of figure 2.2 is thought to be responsible for ϵ effects, and ϵ' effects are thought to be due to the "Penguin" diagram, shown in figure 2.3. The calculation of the magnitude of ϵ' within the Kobayashi-Maskawa model is a difficult problem, requiring the translation of weak interactions of quarks to weak interactions of hadrons. Most recent estimates predict $0.001 < \epsilon'/\epsilon < 0.005$ [20].

NA31 have measured ϵ'/ϵ to be $(3.3 \pm 1.1)10^{-3}$ [11], from an analysis of data taken in 1986. This is the first non-zero measurement of ϵ'/ϵ. As such it is in agreement

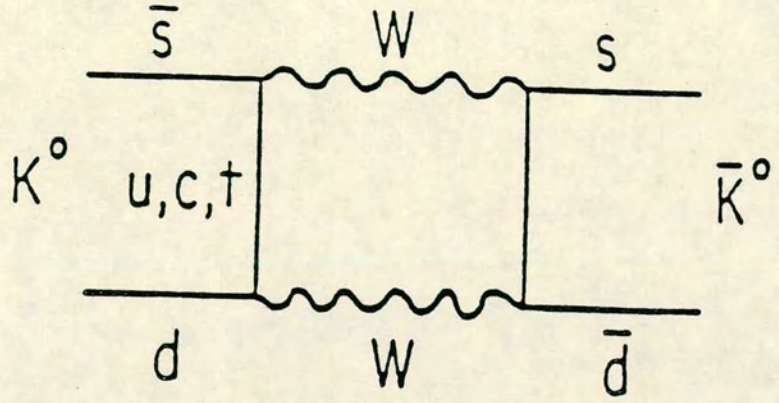

Figure 2.2: The Box Diagram

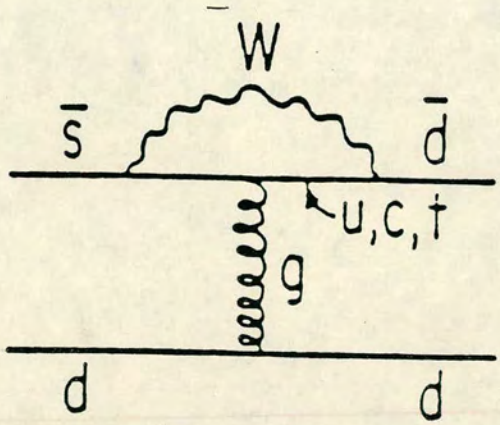

Figure 2.3: The "Penguin" Diagram

with the Kobayashi-Maskawa model but would exclude the Superweak model of Wolfenstein. For such an important result, a three standard deviation effect needs confirmation. NA31, with an upgraded detector, has taken data in 1988 to re-measure ϵ'/ϵ. Physicists in the United States are at present analysing data taken at Fermilab towards the end of 1987.

Having introduced CP-violation we will now introduce possible CPT-violation, and compare theoretical predictions with the current experimental results.

2.3 CPT-Conserving and CPT-violating decay amplitudes

To discuss the accuracy of experimental tests of CPT-violation it is necessary to introduce explicit CPT-violating amplitudes alongside the familiar CPT-conserving amplitudes. We define:

$$\begin{aligned} A(K^0 \to \pi\pi, I=i) &= (A_i + B_i)e^{i\delta_i} \\ A(\bar{K}^0 \to \pi\pi, I=i) &= (A_i^* - B_i^*)e^{i\delta_i} \end{aligned} \tag{2.18}$$

where A_i are CPT-invariant amplitudes, B_i are CPT-violating amplitudes and i, as we have seen, may be 0 or 2. It follows from the definitions of K_1 and K_2 that :

$$\begin{aligned} A(K_1 \to \pi\pi, I=i) &= \sqrt{2}(ReA_i + iImB_i)e^{\delta_i} \\ A(K_2 \to \pi\pi, I=i) &= \sqrt{2}(iImA_i + ReB_i)e^{\delta_i} \end{aligned} \tag{2.19}$$

From these definitions, the amplitudes

$$\begin{aligned} &\text{ReA}_i \text{ are CPT invariant, CP invariant and T invariant} \\ &\text{ImA}_i \text{ are CPT invariant, CP violating and T violating} \\ &\text{ReB}_i \text{ are CPT violating, CP violating and T invariant} \\ &\text{ImB}_i \text{ are CPT violating, CP invariant and T violating} \end{aligned} \tag{2.20}$$

From the definition of ϵ' (see eqn 2.5), we see that:

$$\epsilon' = \frac{1}{\sqrt{2}}(ReB_2 + iImA_2)/(ReA_0 + iImB_0)e^{i(\delta_2 - \delta_0)} \tag{2.21}$$

CPT-invariance requires B_0 and B_2 to be zero, so for CPT to hold :

$$arg\epsilon' = \delta_2 - \delta_0 \pm \pi/2 \tag{2.22}$$

A disagreement of the experimental data with this equality would be a signal of CPT-invariance.

2.4 The Agreement of Data with Theory for ϵ'

According to eqn 2.22, CPT-invariance requires the phase of the CP-violation parameter ϵ' to be $(\delta_2 - \delta_0 \pm \pi/2)$. A summary of data on $(\delta_2 - \delta_0)$ may be found in the Particle Data Booklet. In particular the fitted world average value for $(\delta_2 - \delta_0)$ is $-45.3^o \pm 4.6^o$. Taking the negative sign in equation 2.22 would lead to catastrophic CPT-violation [12], and can be neglected, so agreement with the requirements of CPT-invariance would give the phase of ϵ' to be $44.7^o \pm 4.6^o$.

From equations 2.15 we see that:

$$\epsilon' = \frac{1}{3}(\eta^{+-} - \eta^{00}) \tag{2.23}$$

We now consider the components of ϵ' parallel and orthogonal to η^{+-}. Let these projections be denoted by $\epsilon'_{||}$ and $\epsilon'_{\perp}$. Then

$$\begin{aligned} \epsilon'_{\perp} &= \frac{1}{3} \mid \eta^{+-} \mid (\phi^{+-} - \phi^{00}) \\ \epsilon'_{||} &= \frac{1}{3}(\mid \eta^{+-} \mid - \mid \eta^{00} \mid) \\ &= \frac{1}{3} \mid \eta^{+-} \mid (1 - \mid \eta^{00} \mid / \mid \eta^{+-} \mid) \end{aligned} \tag{2.24}$$

The fitted values for η^{+-}, η^{00}, ϕ^{+-} and ϕ^{00} given in the Particle Data Booklet are

$$\begin{aligned} \eta^{+-} &= (2.275 \pm 0.021)10^{-3} \\ \eta^{00} &= (2.299 \pm 0.036)10^{-3} \\ \phi^{+-} &= 44.6^o \pm 1.2^o \\ \phi^{00} &= 54.5^o \pm 5.3^o \end{aligned} \tag{2.25}$$

and 1986 NA31 results [11] give

$$| \eta^{00} | / | \eta^{+-} | \; = \; 0.991 \pm 0.003$$

This gives

$$\begin{aligned} \epsilon'_{\perp} &= (-0.13 \pm 0.07)10^{-3} \\ \epsilon'_{\parallel} &= (6.825 \pm 2.338)10^{-6} \end{aligned} \tag{2.26}$$

It is evident that the vector ϵ' has a significant component orthogonal to the vector η^{+-} whose phase is approximately $\pi/4$. So experimentally $\epsilon'_{\perp}$ looks to be significantly larger than $\epsilon'_{\parallel}$, and CPT-invariance requires the opposite. We conclude that, for the parameter ϵ', the agreement of the data with the requirements of CPT-invariance is not too good, and the most likely cause of this is the difference between the measured values for ϕ^{+-} and ϕ^{00}.

We see that a difference between ϕ^{+-} and ϕ^{00} signifies a breaking of CPT-symmetry. The logical equivalent of this is, of course, the statement that CPT-invariance requires equality of ϕ^{+-} and ϕ^{00}. It can also be noted, from the definitions of ϕ^{+-} and ϕ^{00} (eqns 2.15) and the measured value of ϵ'/ϵ , that the phases of ϕ^{+-} and ϕ^{00} should be approximately equal to the phase of ϵ (see also fig 2.1). The phase of ϵ is given by:

$$tan^{-1}(2(M_L - M_S)/(\Gamma_S - \Gamma_L)) \; = \; 43.72^{o} \pm 0.14^{o}. \tag{2.27}$$

2.5 Possible CPT-violation in ΔS=0 and ΔS=2 modes

Having discussed the possibility of CPT-violation in $| \Delta S | = 1$ transitions, we now consider ΔS=0 and $| \Delta S |$ =2 modes. We define :

$$\begin{aligned} K_L &= K_2 + \epsilon_L K_1 \\ K_S &= K_1 + \epsilon_S K_2 \\ \epsilon_L &= \epsilon - \Delta \\ \epsilon_S &= \epsilon + \Delta \end{aligned} \tag{2.28}$$

While CPT-violation in $\mid \Delta S \mid = 1$ transitions is parameterised by the amplitudes B_i, CPT-violation in the $\Delta S = 0$ and $\mid \Delta S \mid = 2$ cases is parameterised by ϵ_L and ϵ_S.

Considering mixing between K_1 and K_2 , and using perturbation theory, it can be shown [12] that

$$\begin{aligned}
\epsilon &= \frac{1}{2}(\epsilon_S + \epsilon_L) \\
&= \frac{1}{2}(< \bar{K^0} \mid H \mid K^0 > - < K^0 \mid H \mid \bar{K^0} >)/((M_L - M_S) + \frac{i}{2}(\Gamma_S - \Gamma_L)) \\
\Delta &= \frac{1}{2}(\epsilon_S - \epsilon_L) \\
&= \frac{1}{2}(< \bar{K^0} \mid H \mid \bar{K^0} > - < K^0 \mid H \mid K^0 >)/((M_L - M_S) + \frac{i}{2}(\Gamma_S - \Gamma_L))
\end{aligned} \tag{2.29}$$

From 2.29 we can see that CPT-violation with $\Delta S = 0$ gives a non-zero value of Δ, while CPT-violation with $\mid \Delta S \mid = 2$ will alter the phase of ϵ.

A detailed analysis, comparing experimental results and theoretical predictions in the case of arg ϵ and Δ, has been presented by Barmin et al [12]. They once again reach the conclusion that agreement between experiment and theory could be better, and that the reason for this is again the imprecise measurement of ϕ^{00}.

2.6 How can we measure ϕ^{+-} and ϕ^{00}

From a target where both K_S and K_L are produced, the time dependences of the K_S and K_L amplitudes are as follows :

$$\begin{aligned}
\mid K_S > &\rightarrow \mid K_S > e^{-i(M_S - i\Gamma_S/2)t} \\
\mid K_L > &\rightarrow \mid K_L > e^{-i(M_L - i\Gamma_L/2)t}
\end{aligned} \tag{2.30}$$

where M_L and M_S are the K_L and K_S masses, and Γ_L and Γ_S are the decay widths, the reciprocals of the proper lifetimes τ_L and τ_S.

The parameter η^{+-} or η^{00} measures the ratio of the respective two pion decay amplitudes, so the time dependence of the $K^0 \to \pi\pi$ intensity is given by

$$I_{2\pi}(t) \propto | \, e^{-i(M_S - i\Gamma_S/2)t} + \eta e^{-i(M_L - i\Gamma_L/2)t} \, |^2 \tag{2.31}$$

Therefore:

$$I_{2\pi}(t) \propto e^{-\Gamma_S t} + |\eta|^2 e^{-\Gamma_L t} + 2\,|\eta|\, e^{-\frac{(\Gamma_L+\Gamma_S)t}{2}} cos(\Delta m t - \phi) \tag{2.32}$$

where $\Delta m = M_L - M_S$.

The initial beam is composed of K^0 and $\bar{K}^0$, which are produced incoherently. The interference term will have a different sign for the $\bar{K}^0$ component, so the time dependence is given by :

$$I_{2\pi}(t) \;=\; S(p)[e^{-\Gamma_S t} + |\eta|^2 e^{-\Gamma_L t} + 2\,|\eta|\, D(p) e^{-\frac{(\Gamma_L+\Gamma_S)t}{2}} cos(\Delta m t - \phi)] \tag{2.33}$$

The factor S(p) is a normalisation depending on the production spectrum of the incident beam.

The factor D(p), known as the dilution factor, measures the relative production of K^0 and $\bar{K}^0$ at the target, and is a function of momentum.

$$D(p) = (K^0 - \bar{K}^0)/(K^0 + \bar{K}^0) \tag{2.34}$$

By fitting the observed time distribution of $\pi^+\pi^-$ and $\pi^0\pi^0$ decays to the above formula, it is possible to measure the phases ϕ^{+-} and ϕ^{00}.

Chapter 3

The Experiment

3.1 Introduction

The NA31 experiment, situated in the North Area at the CERN-SPS, was designed, in particular, to measure the parameter ϵ'/ϵ. In a long run during the summer of 1986, approximately one million CP-violating $K_L \to \pi\pi$ decays were recorded. ϵ'/ϵ was measured to be $(3.3 \pm 1.1)10^{-3}$, the first evidence of direct CP-violation [11]. In 1987, during an experimental run of 97 days, the experiment, with modifications to the target stations, took data to measure the difference between the phases ϕ^{+-} and ϕ^{00} of the CP-violation parameters η^{+-} and η^{00}. The experimental configuration during 1986 has been described elsewhere [13]. Here we describe the 1987 experiment, paying particular attention to the points most relevant to this analysis.

In the experiment there are two different target stations, and data taking is alternated between the two targets. This results in two distinct data samples recorded in the same fiducial volume, the events in the two samples being separated in time of flight by typically 3 K_S lifetimes. The $\pi^+\pi^-$ and $\pi^0\pi^0$ decays are recorded simultaneously. Neutral decays are measured with a lead/liquid-argon calorimeter (LAC). Charged decay tracks are observed with wire chambers, and the energy is measured by the combination of the LAC and an iron/scintillator hadron calorimeter. The overall experimental layout is shown in figs 3.1 and 3.2.

K_L	$\pi e \nu$	38.7%
	$\pi \mu \nu$	27.1%
	$\pi^0\pi^0\pi^0$	21.5%
	$\pi^+\pi^-\pi^0$	12.4%
	$\pi^+\pi^-$	0.227%
	$\pi^0\pi^0$	0.094%
K_S	$\pi^+\pi^-$	68.6%
	$\pi^0\pi^0$	31.4%

Table 3.1: The Principal Branching Ratios of K_L and K_S

In the K_L part of the interference beam, the two-pion decays represent only a small fraction of the decays (see table 3.1). In order to maximise the number of two body decays written to tape, it is necessary to have fast data processing and a high level of online rejection of three-body decays. The trigger makes use of scintillation counters, fast information from detector elements, a hard-wired processor, and two IBM 168 emulators (168E's). The data-acquisition system employs FASTBUS, the 168E's, a micro-vax, and a VAX 750 computer. In this chapter we will discuss : 1) the beams 2) the scintillation counters and hodoscopes 3) the wire chambers 4) the calorimeters 5) the trigger system, and 6) the data acquisition system.

3.2 The KN and KF Beams

For a measurement of ϵ'/ϵ, two pion decays must be measured separately in K_L and K_S beams (see eqn 2.17). To investigate interference phenomena, however, it is necessary to detect two pion decays of K_L and K_S simultaneously. Indeed, most information on the interference term is obtained at the point where the decay rates $K_L \rightarrow \pi\pi$ and $K_S \rightarrow \pi\pi$ are approximately the same. This occurs at roughly 10-15 K_S lifetimes from a target where K_L and K_S are produced. In 1986 the distances from the targets to the collimator defining the start of the decay region were 120m (K_L) and 7.1m (K_S). In 1987 these distances were

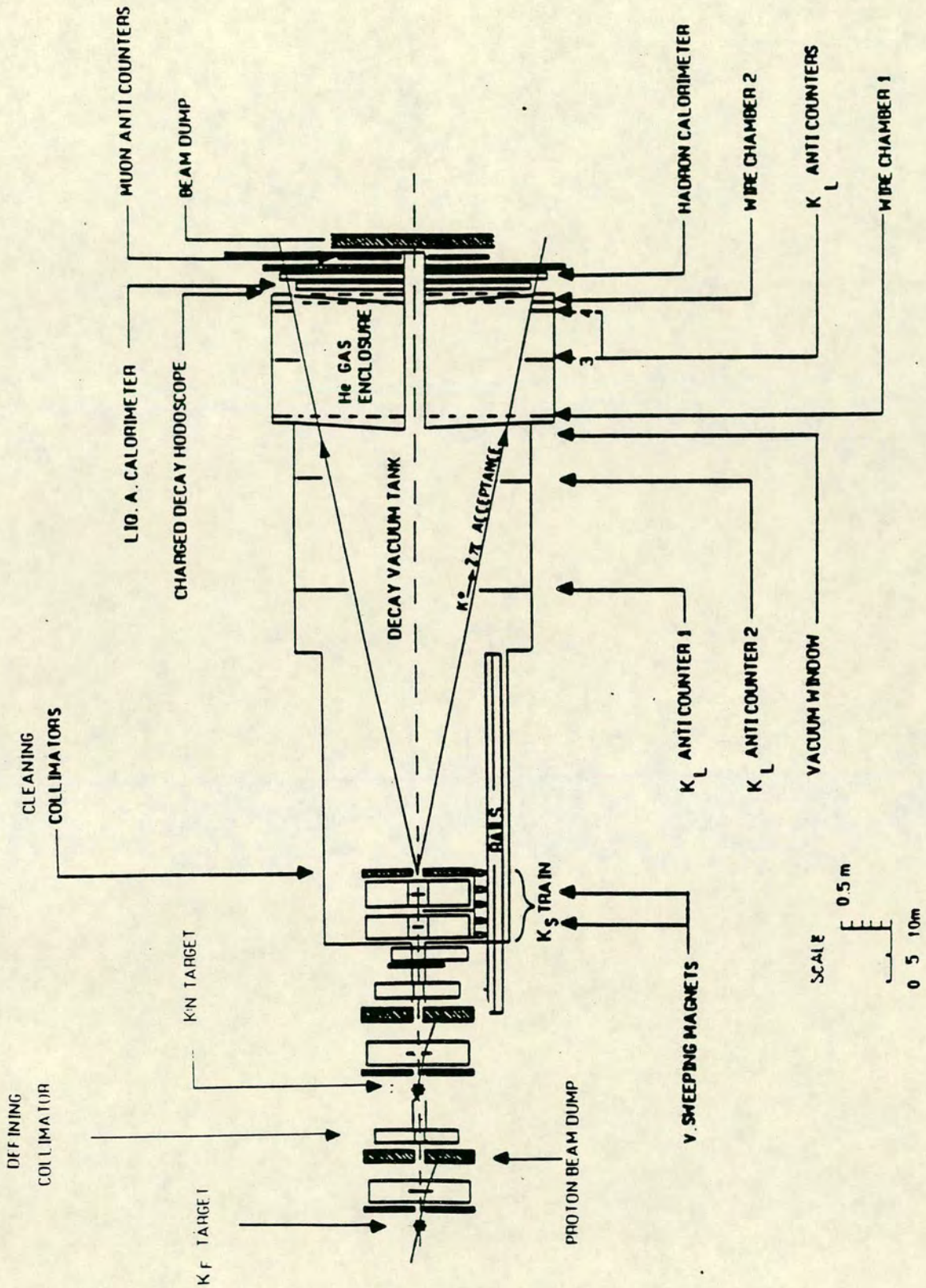

Figure 3.1: Experimental Layout

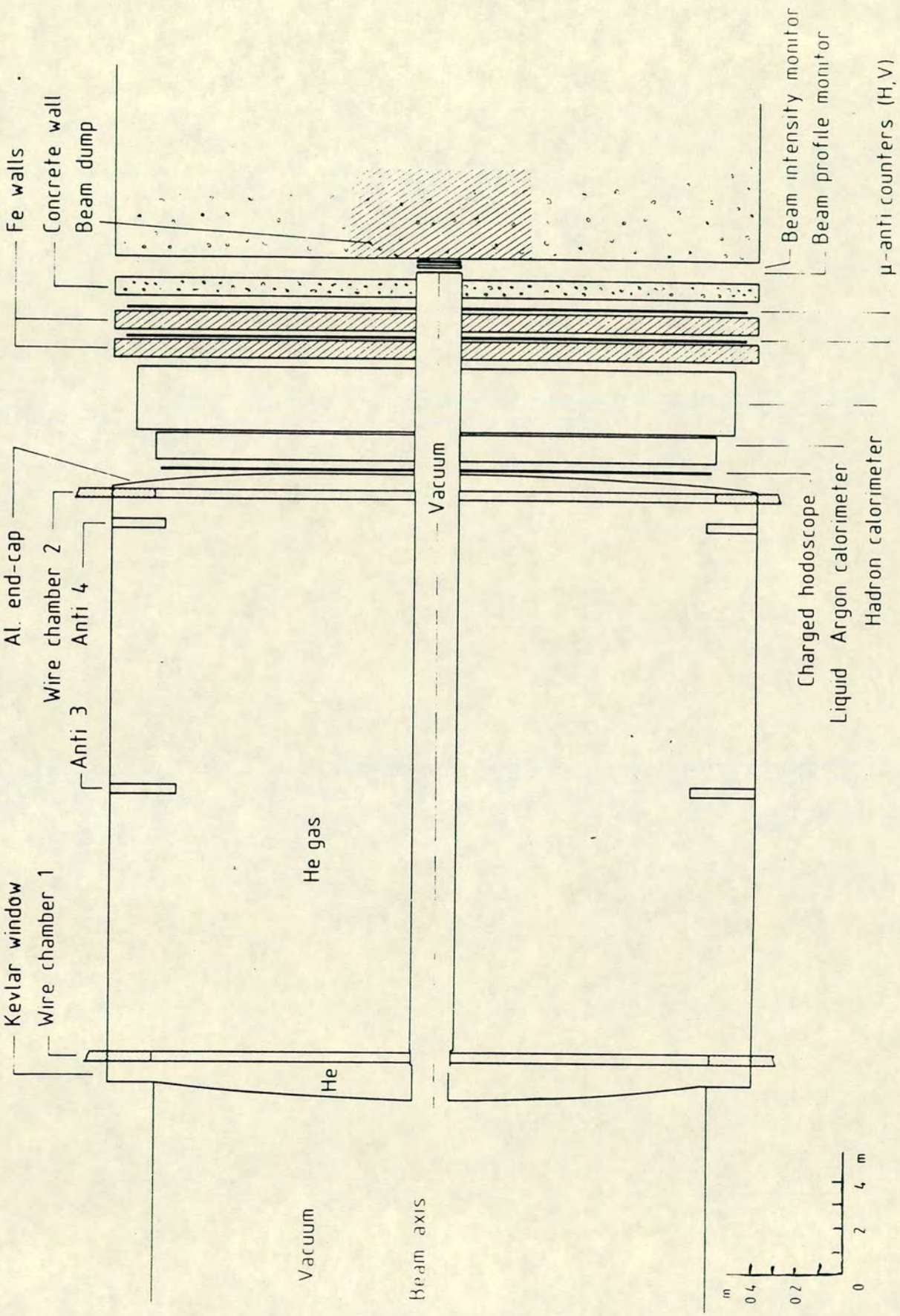

Figure 3.2: Detector Layout

	z	radius
KF Target	-4800cm	-
KF Defining Collimator	-3800cm	2.8mm
KF Cleaning Collimator	00cm	21mm
KN Target	-3360cm	-
KN Defining Collimator	-2360cm	2.8mm
KN Cleaning Collimator	00cm	14mm

Table 3.2: Collimator and Target Geometries

48m (KF - far) and 33.6m (KN - near), where KN and KF refer to the position relative to the NA31 detector.

The two targets are of identical design and construction, differing only in the longitudinal position of the target on the beam line, and the geometry of the collimators. The 450 GeV/c primary protons from the SPS are transported along the H4 beam line at a nominal intensity of 10^{10} protons per pulse. They are steered to intercept one or other target with a downward inclination of 3.6 mrad, resulting in a neutron : kaon flux ratio of 6 : 1.

The target head consists of four beryllium rods, each 10cm long and 2mm in diameter. These are aligned along the axis of the kaon beam and are suspended by aluminium foils. The target is followed downstream by a 160 cm long collimator to reduce the angular acceptance of secondary decays, and a 10.8 Tm bending magnet which deflects the primary proton beam downwards, and deviates charged secondaries away from the neutral beam line. Each target is followed at a distance of 10m by a defining collimator which determines the final angular acceptance of the beam, and by a cleaning collimator at the start of the decay region. The cleaning collimator has an aperture greater than the beam radius, and is designed to get rid of particles produced at the edge of the defining collimator. The collimator and target geometries are given in table 3.2.

It is worth noting here that the radius of the KF beam cone is 4.7 cm at the second wire chamber, whilst the KN beam has a radius of 4.2 cm at the same point.

A schematic layout of the targets for the two interference beams is shown in fig 3.3, and fig 3.4 shows the kaon production spectrum.

3.2.1 The K_S Beam and Calibration Beams

In a measurement of this nature, it is most important that the energy scale of the liquid argon calorimeter be accurately known. All information on neutral decays comes from positions and energies measured in the LAC, so any uncertainty in the neutral energy scale will translate directly into an uncertainty in the measurement of ϕ^{00}. For this reason, we took one tape of K_S data roughly every day of data taking. The K_S target, mounted on a train which is moveable through the vacuum tank, is followed by an anti-counter which defines the start of the K_S decay volume. The neutral energy scale is measured by a fit of observed decay vertices to the position of this anti-counter. This procedure will be discussed in more detail in chapter 7. The lay-out of the K_S target is shown in fig 3.5.

In addition to the K_S beam, provision is also made to supply beams of pions, electrons or muons for calibration purposes. Electrons are produced by converting photons at a target station 400m upstream of the decay volume, and negative pions are selected from the target at which the primary proton beam usually originates. These beams are momentum selected, giving electrons or pions of known energy for calibration of the calorimeters. To obtain muons, the normal beam is stopped just after the target, and sweeping magnets are switched off. This allows muons from pions produced at the target to illuminate the detector uniformly.

3.2.2 The Decay Region

The decay volume is enclosed in a steel vacuum pipe, which is comprised of two sections of internal radii 0.96m and 1.20m. The total length of the vacuum tank is 111m, and the region from which decays are selected lies in the upstream part

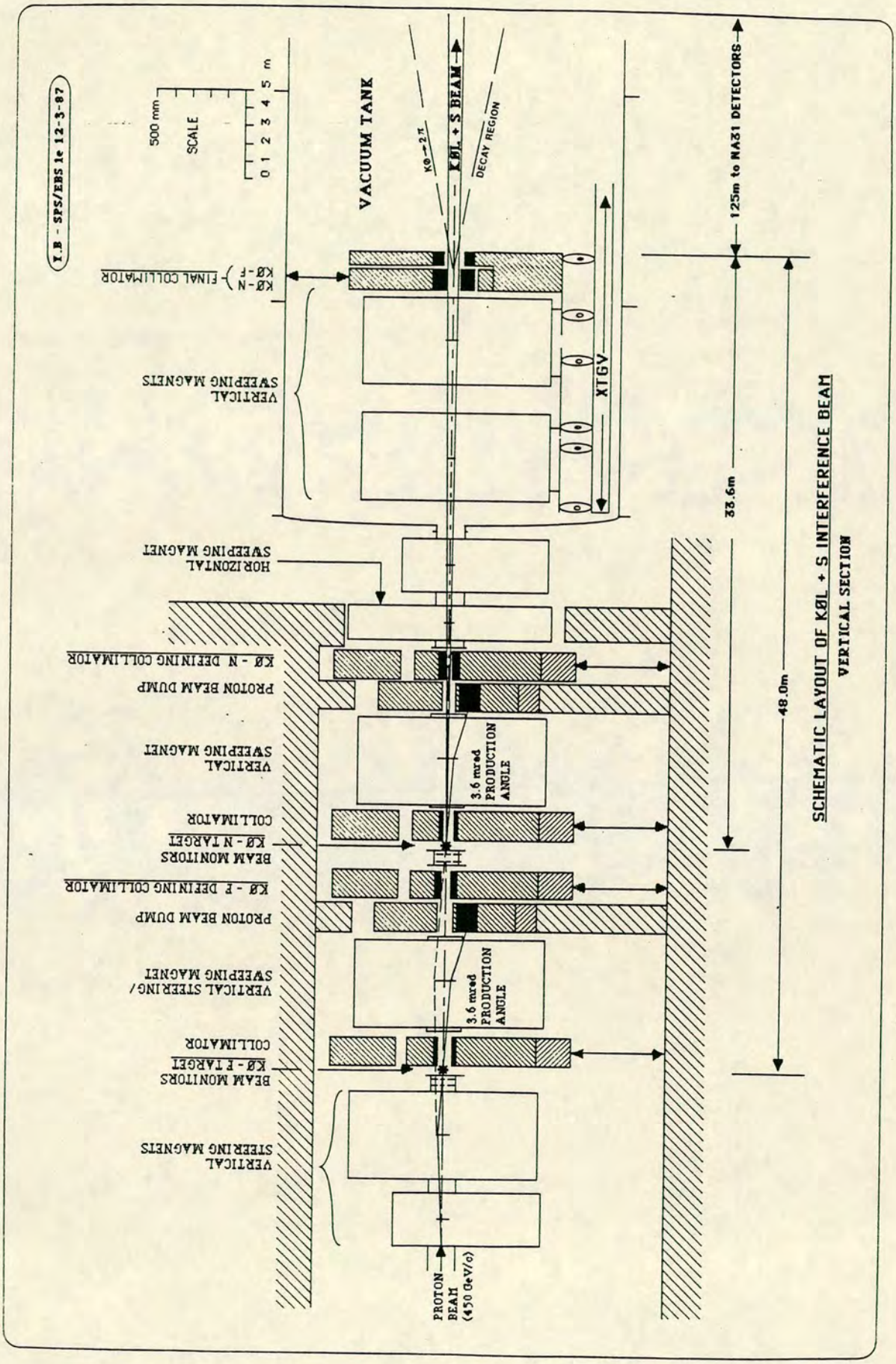

Figure 3.3: Beam Layout

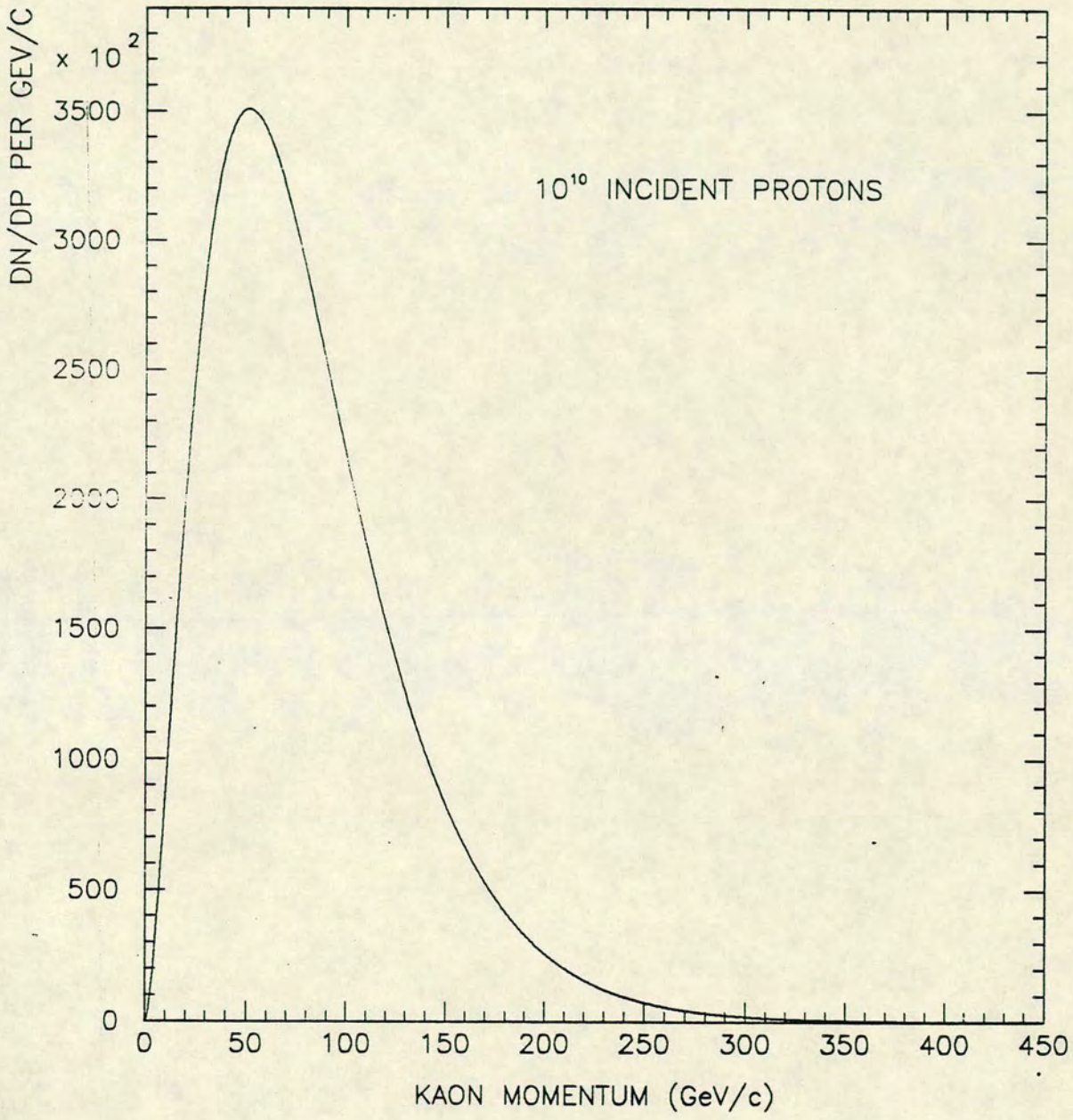

Figure 3.4: Kaon Production Spectrum

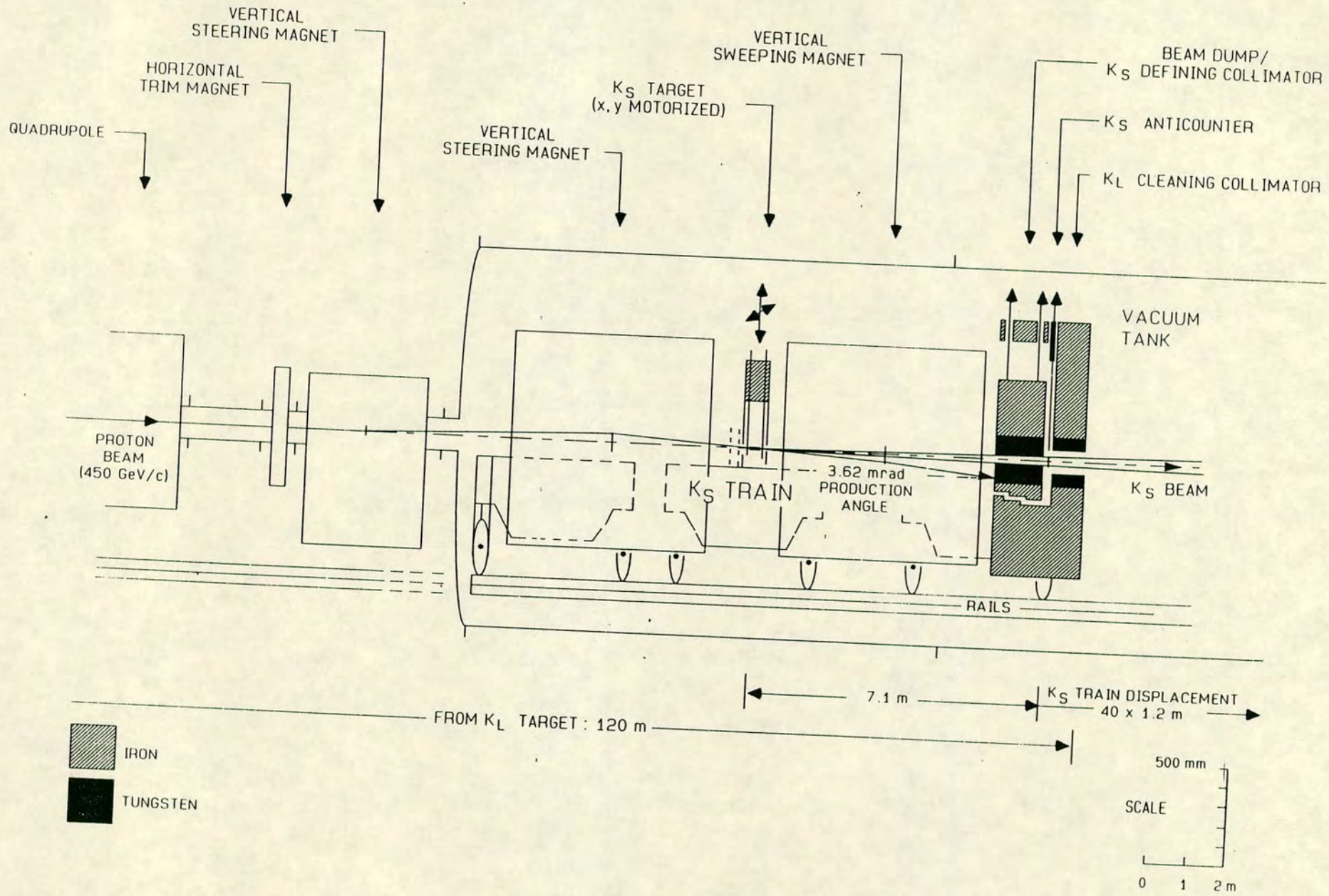

Figure 3.5: Layout of the K_S Target

of the tank. The tube is evacuated to a pressure of 3.10^{-3} Torr. The downstream end of the decay vessel is a thin window of epoxy impregnated kevlar fibre cloth. A beam pipe of 16.4 cm diameter passes through this window, enabling the beam to complete it's path in vacuum. The drift chambers are housed in a cylindrical steel tank, filled with helium to reduce multiple scattering, which lies downstream of the vacuum tank.

3.3 Scintillation Counters and Hodoscopes

Several scintillation counters are used in the experiment. In addition to the K_S anti-counter, which facilitates measurement of the neutral energy scale, scintillation counters are used to define the trigger timing for charged and neutral events, and for online rejection of unwanted three-body decays of K_L.

3.3.1 The K_S Anti-Counter

The beginning of the K_S decay region is defined by a small scintillation counter with 7mm of lead placed directly in front of it. This counter is 20mm downstream of the collimator on the K_S beam train (see fig 3.5). It vetoes upstream decays at the trigger level, and provides a well-defined leading edge to the decay distribution. This is used for measurement of the energy scale of the LAC (see chapter 7).

3.3.2 Charged Trigger Hodoscope

A hodoscope of scintillation counters is placed just in front of the liquid-argon calorimeter to detect charged decay modes and start the trigger for these decays. The hodoscope consists of 18 horizontal strips and 2 vertical strips, each 2cm thick, which cover a circular region of 1.2m radius around the beam pipe (see fig 3.6).

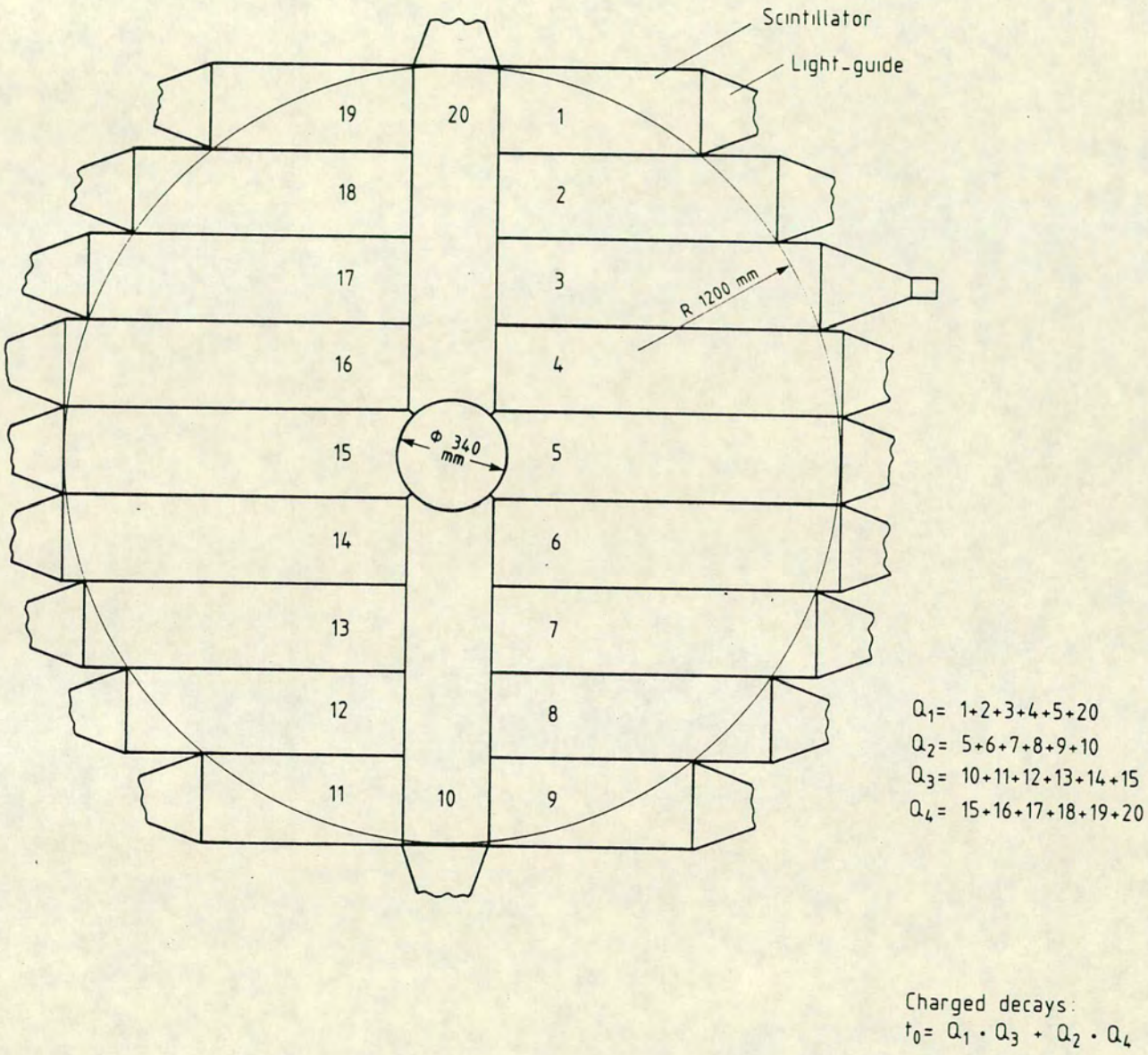

Figure 3.6: Charged Trigger Hodoscope

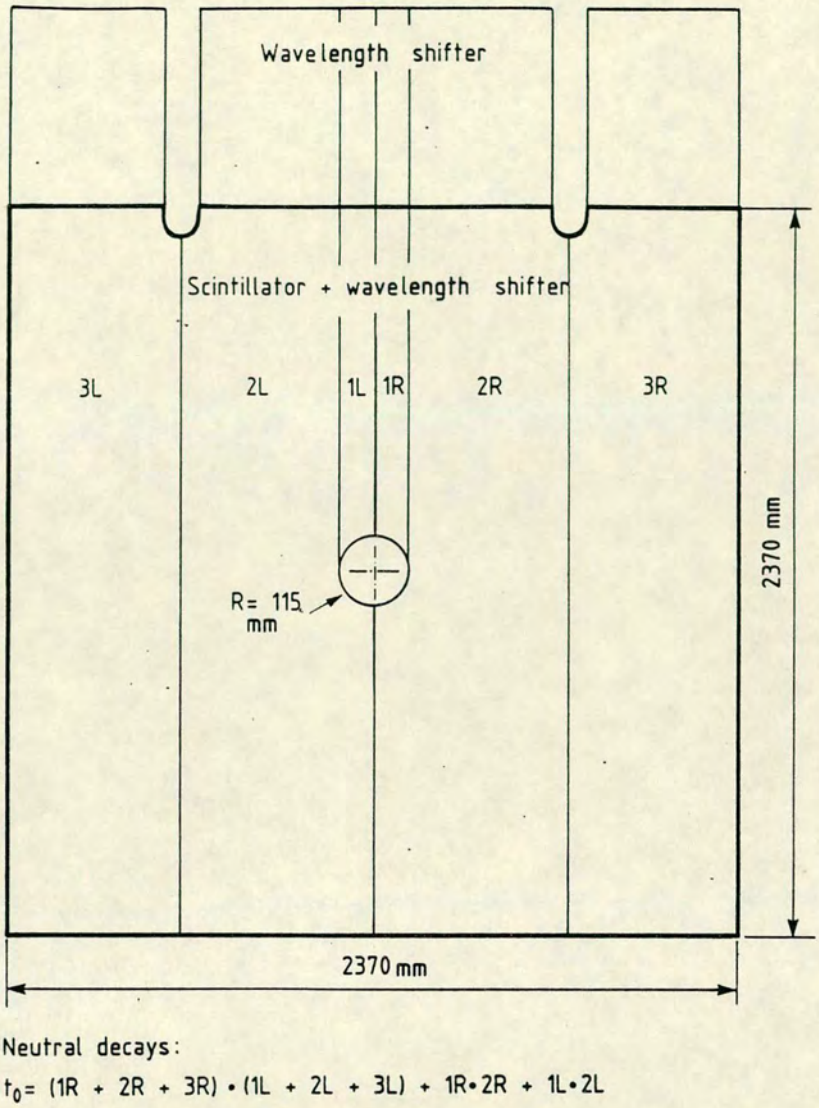

Figure 3.7: Neutral Trigger Hodoscope

3.3.3 Neutral Trigger Hodoscope

In order to start the trigger system for neutral decays, a plane of scintillators (fig 3.7), 12mm thick, is installed inside the liquid-argon calorimeter after 12.5 radiation lengths. The plane is split into six vertical strips. A wavelength-shifter plate, 3mm thick, is placed behind each scintillator and transmits light to a photomultiplier tube. The photomultipliers are located at room temperature on top of the cryostat (see fig 3.13).

3.3.4 Anti-Counter Rings

From table 3.1 it can be seen that $\pi^0\pi^0\pi^0$ decays of K_L are much more abundant than $\pi^0\pi^0$ decays. If two photons from a $\pi^0\pi^0\pi^0$ decay pass outwith the detector, and so go undetected, then the decay may mimic the signature of a $\pi^0\pi^0$ decay. For this reason four large anti-counter rings are placed in the downstream region of the vacuum tank and between the wire chambers in the helium tank (see fig 3.2). These counters detect photons outside the solid angle subtended by the calorimeters, and reduce the amount of $\pi^0\pi^0\pi^0$ background to the $\pi^0\pi^0$ signal by a factor of three. Each counter consists of two planes of scintillator, read out by wavelength-shifter bars which are connected to a single photomultiplier tube. The counters are mounted with 5cm of iron in front of the first scintillator, and 2.5cm of iron between them. There are sixteen counters per ring for the two upstream rings, and eight per ring for the two downstream rings (fig 3.8). These counters are greater than 95% efficient for photons above 1 GeV.

3.3.5 The Muon Anti-Counters

Another unwanted three-body decay of the K_L is $K_L \rightarrow \pi\mu\nu$. To reject these decays online a muon anti-counter is placed downstream of the calorimeters. This detector element was constructed by the Edinburgh group, and during the 1987 run I was responsible for its monitoring and maintenance.

The muon veto consists of two planes of NE110 scintillator, each shielded upstream by an iron screen 80cm thick. These two iron blocks are sufficient to stop nearly all annihilation products from pions in the calorimeters, but will not stop muons. A muon is defined by a coincidence between signals from the first and second planes. A coincidence between two scintillators is chosen in preference to a signal from one scintillator to reduce the number of events vetoed due to random signals or noise in the scintillator elements. When this coincidence is achieved, a signal is sent to the trigger to indicate that the event should not be recorded to tape. Each plane of scintillator is comprised of ten components of 2.7m length, with a lightguide and phototube at each end, and two shorter

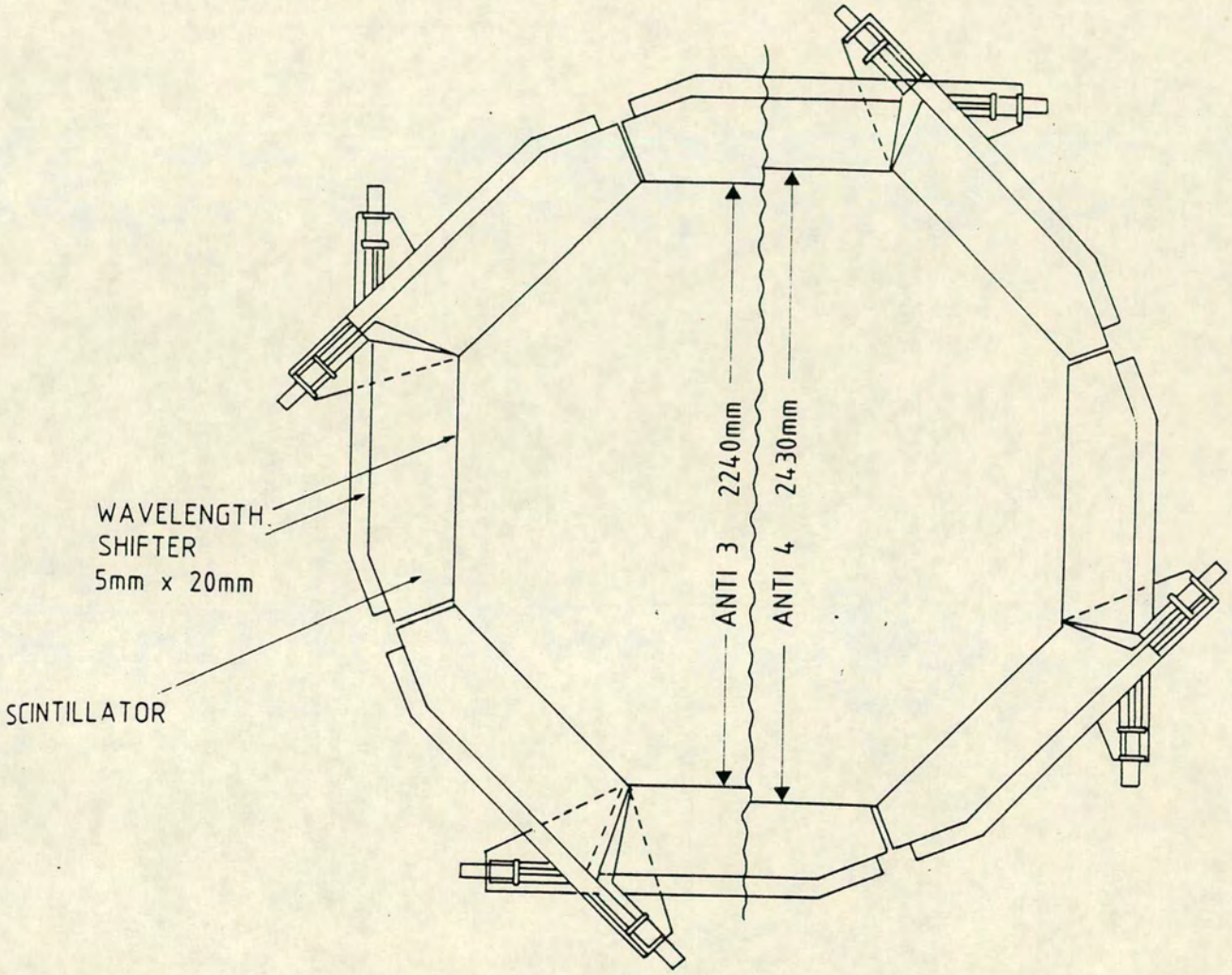

Figure 3.8: Anti-Counter Rings

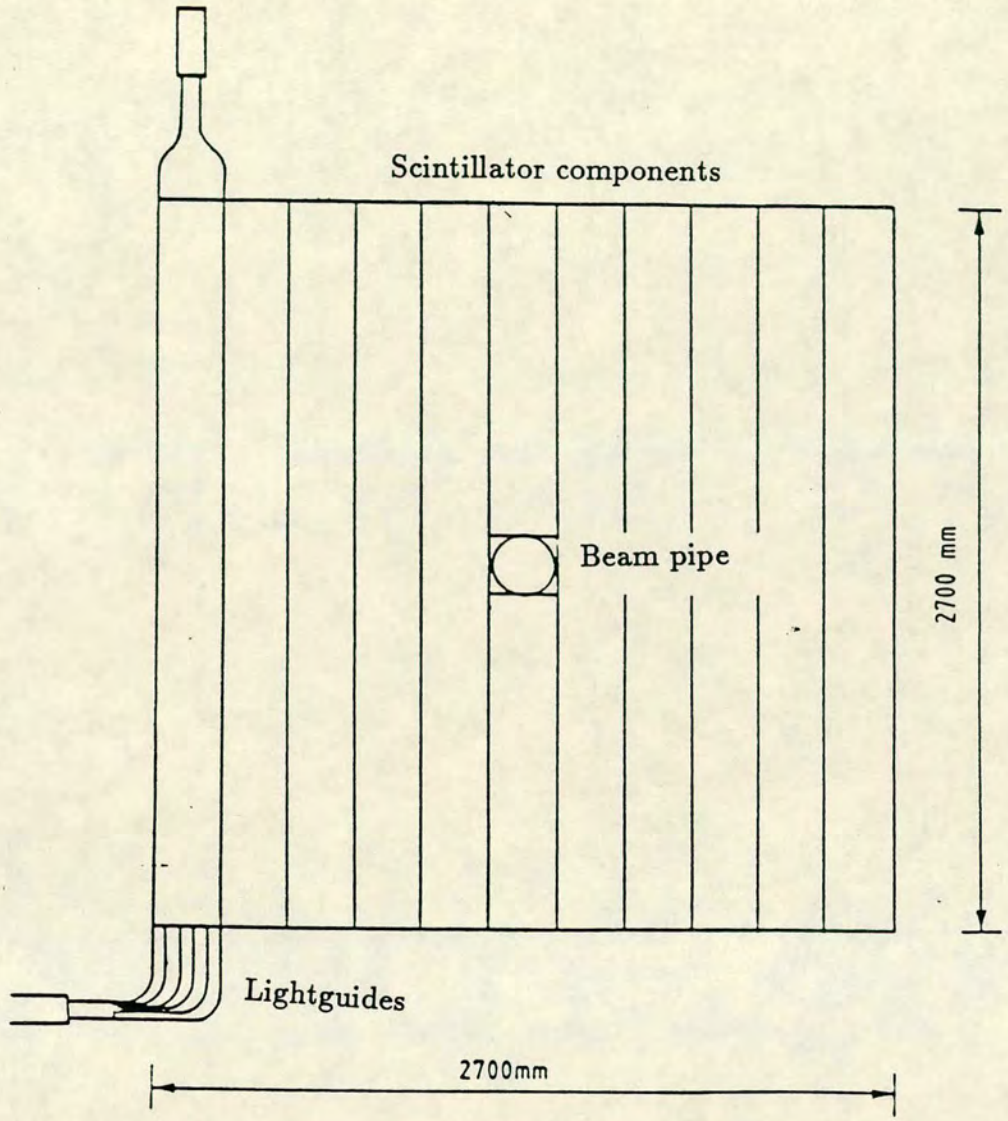

Figure 3.9: Muon Veto PIane

(1.25m), single ended components which sit on either side of the beam pipe (see fig 3.9).

In the upstream plane the components are arranged horizontally, and in the downstream plane vertically. Adiabatic light guides are used for light collection, and EMI9813 fourteen stage phototubes for light detection. To obtain a muon signal we require that both planes of scintillator detect a particle simultaneously. To achieve this signature one cannot compare analog signals from the phototubes - it is necessary to generate a standard logic signal for each component. The signals from the phototubes at each end of the scintillator strip pass through an

analog mixer, which sums the signals. In this way a genuine muon is enhanced relative to random or noise signals which tend to be present at one end only. The mixed signal then enters a discriminator. This device has a set threshold voltage, and only produces a signal if the analog input is greater than the threshold setting. The threshold is set to give maximum discrimination between genuine muons and random or noise signals. Finally, the twenty-two outputs from the discriminators enter a logic unit which provides an AND of the 11-fold OR from each plane. The logic unit provides a signal to the trigger to define whether or not the event should be rejected. All the voltages are set and monitored by a Caviar microcomputer.

3.4 The Multi-Wire Proportional Chambers

3.4.1 Mechanical Construction

The experiment uses two drift chambers of similar construction, separated by 24.5 m and bolted to the helium tank. The first chamber is situated 100m from the start of the decay region. Each chamber consists of four planes (see fig 3.10). The orientation of the wires is vertical in the first plane, horizontal in the second plane, and at 53° and 143° in the third and fourth planes. The wires therefore define two orthogonal coordinate systems offset by 53°. The origins of the two systems are separated so that no more than two wires cross at any point in the projection plane perpendicular to the beam axis (see fig 3.11). This is the optimal choice for resolving any left/right ambiguities.

The NA31 chambers are unusual in that there are no field-shaping wires in the sense-wire plane. The sense wires are $30\mu m$ diameter, of gold-plated tungsten, and are separated by 6mm. The wires are stretched by a force of 1.3 N and soldered to printed boards on the chamber frame. The gap between the anode and cathode planes is 8mm, the cathode planes consisting of $25\mu m$ mylar foils clad with graphite. These planes are glued to vitronite frames, which are sandwiched between aluminium bars for support.

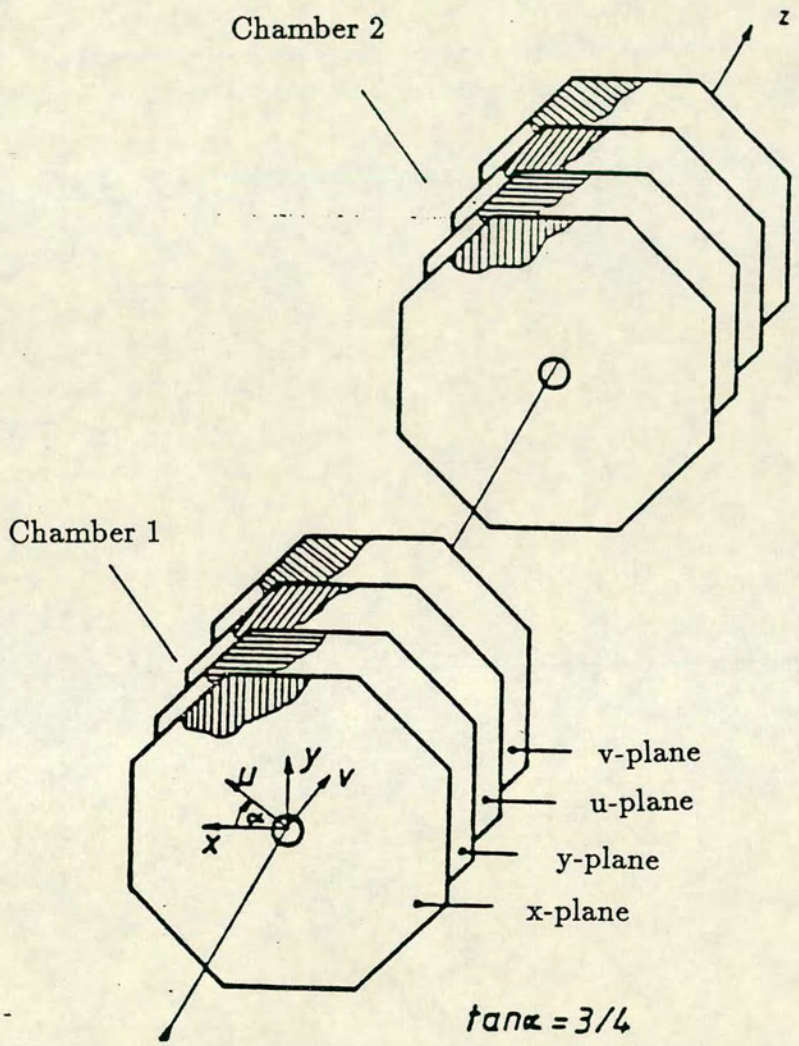

Figure 3.10: Wire Chamber Layout

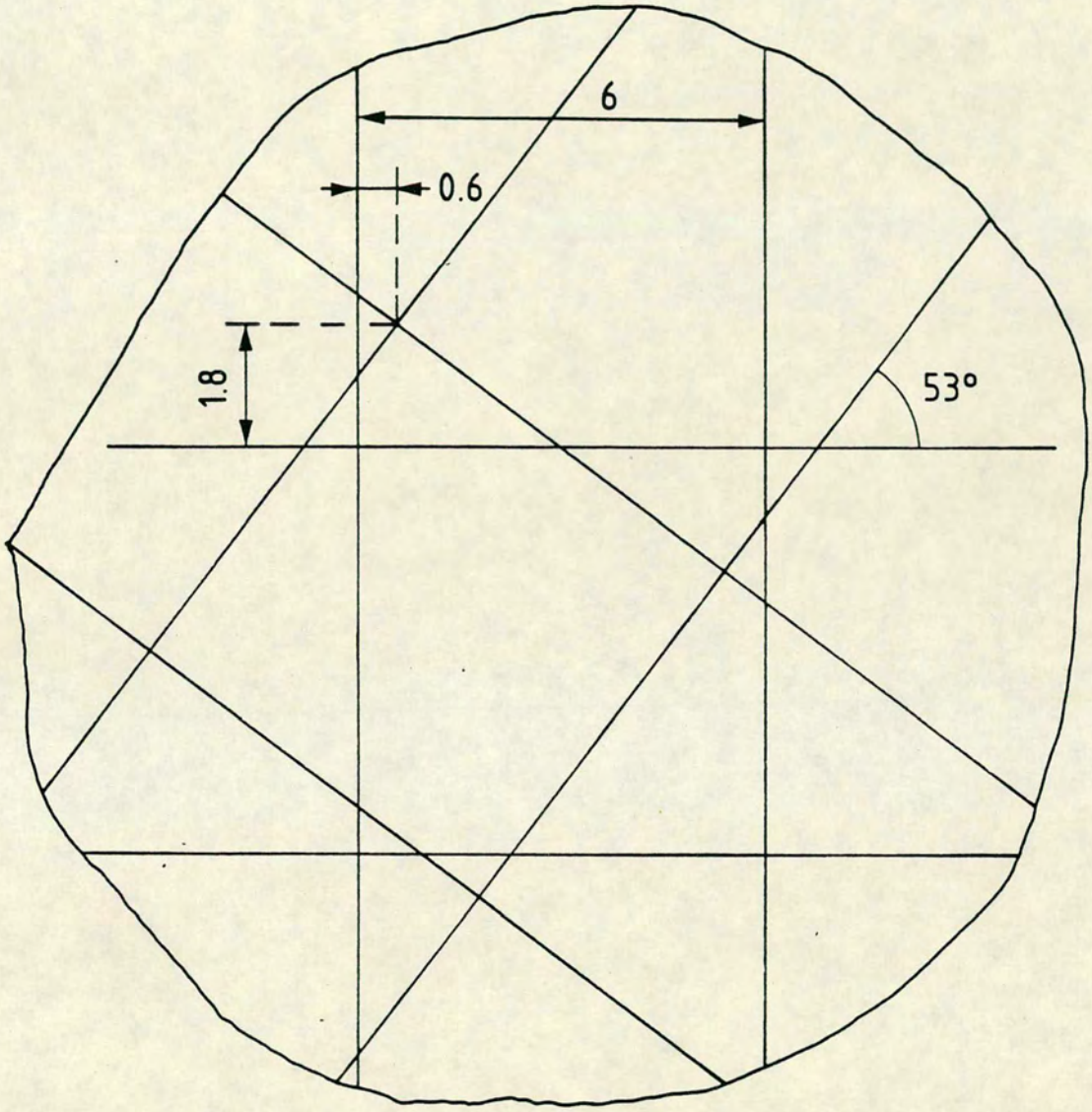

Figure 3.11: Wire Chamber Planes

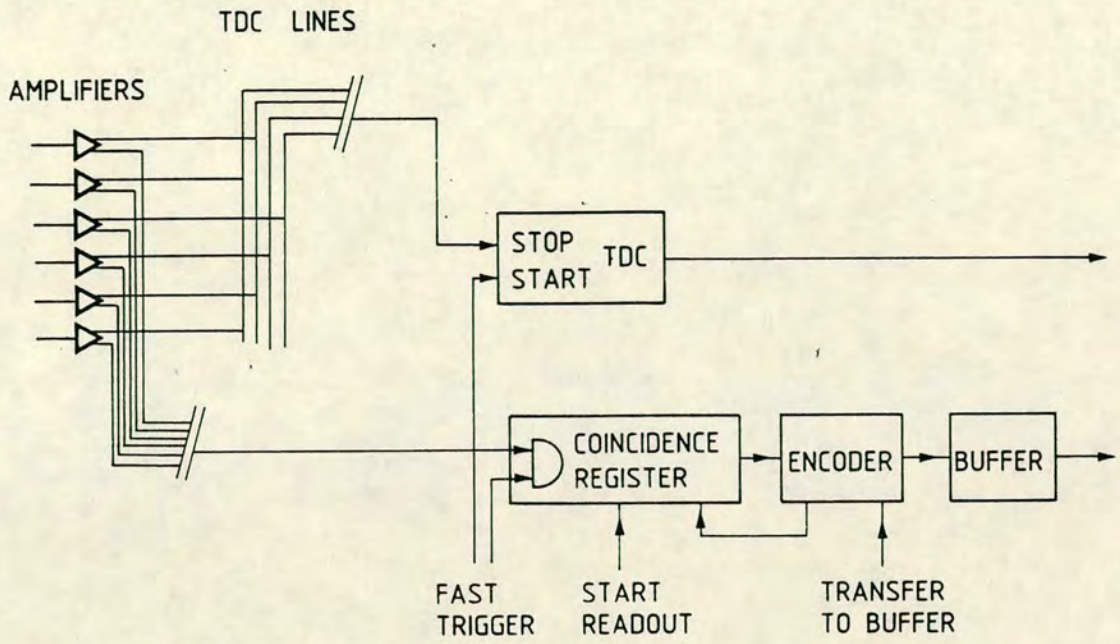

Figure 3.12: Electronics

The chambers contain a gas mixture of argon (70%) and isobutane (30%), bubbling through isopropanol at 3°C. They are operated at 2.85 kV, and the drift velocity is $55\mu m/ns$.

3.4.2 Electronics

Each wire signal is shaped and amplified before being split into two logic pulses, in preamplifier boxes on the chamber frame. One signal is used for the drift-time measurement, the other is sent off to a set of coincidence registers (see fig 3.12).

In the coincidence registers a hit is recorded if it is within 180 ns of the passage of a particle, as defined by the event time t_0 (see section 3.7). The level 1 pre-trigger starts encoding logic to form addresses from the contents of the hit registers. Adjacent wires are grouped into clusters, with at most five wires per cluster. Up to four cluster addresses and widths can be recorded per plane, and the presence of five or more clusters is signalled by an overflow bit. The information on the number of clusters per plane is passed to the trigger logic

for the level 3 decision making. A level 3 trigger initiates the transfer of cluster addresses to a buffer card in the main data-acquisition FASTBUS crate.

For measurement of drift times, the second amplifier outputs are connected in groups. The 432 wires in each plane are divided into six groups, and every fourth wire per group is connected to the same TDC. There are, therefore, 24 TDC's to record the information from each plane. The grouping is made such that two charged tracks from a kaon decay should not fall in the same group. The TDC's are found in the main FASTBUS crate. They employ 100 MHz scalers, which are started by the trigger t_0 and stopped by the wire signal. The time of the start pulse is recorded to an accuracy of 2ns.

3.4.3 Performance

The timing of each wire is determined using muons. The chamber efficiency is determined using charged decays with a reconstructed vertex. To reconstruct a space point, hits in at least three of the four planes are required. The frequency of charged decays where a given plane has no hit defines the efficiency of that plane. The average efficiency per plane is greater than 99.3%, and the estimated loss of good events due to overflow is a few per mille.

The reconstruction accuracy using drift times is estimated by closest approach, of the two tracks in $K^0 \rightarrow \pi^+\pi^-$ decays. The average measurement error in a plane is around $500\mu m$. This is too large to resolve all left/right ambiguities, leading to tails in the distributions and an r.m.s. error of around $750\mu m$ in the measurement of transverse coordinates.

The longitudinal decay vertex resolution is typically 80cm at the centre of the region from which decays are selected, varying by ± 40 cm throughout this region. This is comparable to the vertex resolution in neutral decays.

3.5 The Electromagnetic Calorimeter

3.5.1 Basic Layout

All information on $K_0 \rightarrow \pi^0\pi^0 \rightarrow 4\gamma$ events is provided by the liquid argon calorimeter (LAC), which measures the energies and positions of the photons. The calorimeter is also used to discriminate against unwanted three-body decays of K_L, in both charged and neutral modes. These requirements demand excellent energy and spatial resolution.

The LAC (see fig 3.13) consists of a stack of aluminium coated lead conversion plates, alternated with printed circuit board read-out plates. The calorimeter is physically divided into left and right halves. The plates, weighing approximately 9t, are suspended from the cryostat cover and supported by stainless steel rods. The calorimeter has an active area of 240cm x 240 cm, but the projection of the wire chambers onto the LAC inscribes an octagon of 118cm. This defines the outer radius for photon acceptance in this analysis, the inner radius being defined by a 16cm radius circle centred on the beam pipe.

Fig 3.14 shows the cell structure, consisting of the aluminium clad sandwich-plate, two liquid argon gaps, and a double-sided read-out strip plane. Most of the tie rods traversing the calorimeter, and necessary to maintain spacing, are located outside the region within which photons are accepted. The length of one cell corresponds to 0.31 radiation lengths. The calorimeter is separated into front and back halves by the neutral trigger hodoscope, each half having a total of 80 cells (12.5 X_0). Read-out strips are alternately horizontal (x) and vertical (y). The cells are connected so that, for any particle interacting in the LAC, four energies are recorded; E_x and E_y in the front, and the same for the back. In addition to the physical front/back and left/right divisions, the read-out strips are also discontinuous at the vertical mid-point, so that sets of horizontal and vertical strips form quadrants. There are 96 horizontal and 96 vertical strips per quadrant, each 1.25cm wide. In total there are 1536 read-out channels.

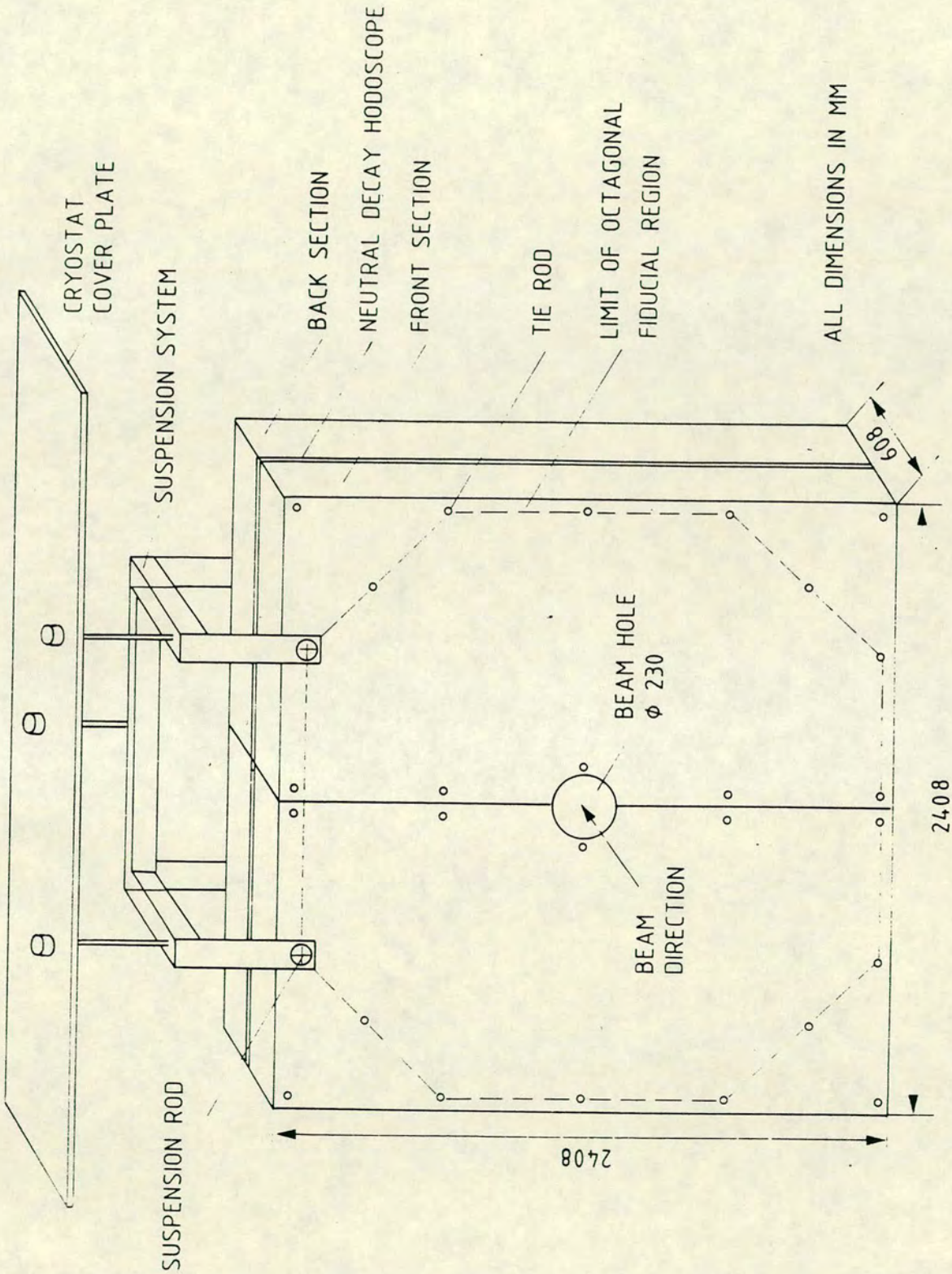

Figure 3.13: The Liquid Argon Calorimeter

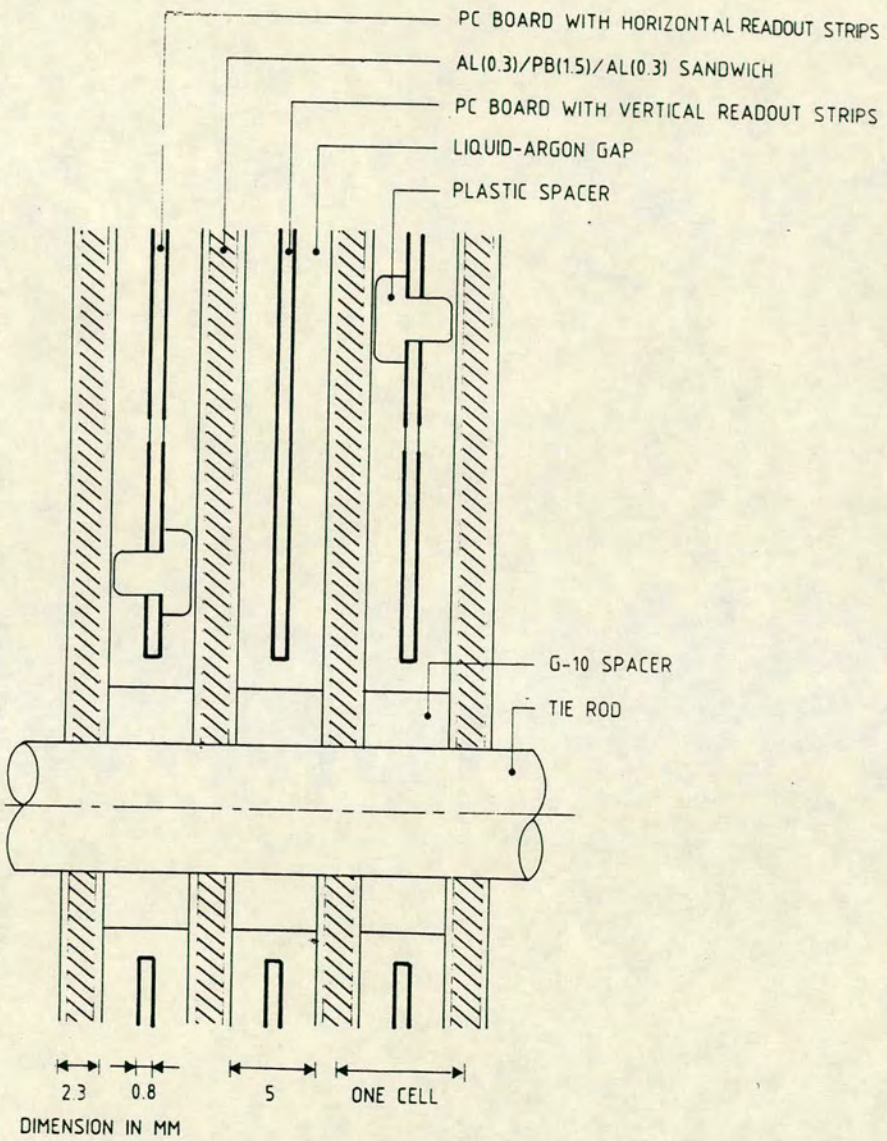

Figure 3.14: The Liquid Argon Cell Structure

3.5.2 LAC Cryogenics

The cryostat is comprised of an inner (liquid-argon) and an outer (vacuum) vessel. The inner vessel is sealed to the outer one by means of an O-ring. The cover plate, which supports the LAC, seals the liquid argon vessel without any vaccum insulation. The assembly is in stainless steel.

Evaporating argon gas is recondensed by a liquid nitrogen heat exchanger. The re-liquified argon flows through an oxygen absorber on its way back to the cryostat. The cryostat is self-regulating, and maintains a constant 1.2 bar pressure.

3.5.3 Read-Out Electronics

The LAC electronics may be considered in three sections; The HV and preamplifier cards, the Sample and Hold Card (SHC), and the FASTBUS ADC system.

The HV card contains a transformer providing power for eight LAC channels, a blocking capacitor, and two calibration capacitors per channel. The preamplifier has two outputs: one goes to the SHC and the other is used for a fast-trigger energy measurement.

With a transformer at the preamplifier input, low frequency noise is dominant. This can be eliminated by double differentiation, so the signal arriving at the SHC is sampled three times.

$$Q_{out} = (Q_B - Q_A) - (Q_C - Q_B) \tag{3.1}$$

where Q_{out} is the total measured charge, and Q_A, Q_B and Q_C are the charge samples. With the time between successive samplings (700ns) being larger than the signal rise-time (400ns), the dependence on exact timing is not critical. There are two SHC outputs: one to the ADC's and the other to the trigger for photon counting.

FASTBUS ADC's, of 96 channels each, are used to digitise the SHC measurements. To minimise queueing time neighbouring channels are fed to different

ADC's. The total conversion and the amount of data are reduced by a zero suppression scheme. Only those channels above a certain threshold (typically 150 MeV), and their three immediate neighbours on either side are converted. Channels in front and back halves of the LAC are correlated so that corresponding channels are always recorded.

3.5.4 Performance of the LAC

Electronic Calibration

To measure pedestals and electronic channel gain, two kinds of events are recorded: 1) using a random clock trigger and 2) with a fixed amount of charge injected into every fourth calorimeter channel. For these events all channels are digitized and recorded. From the random events, the r.m.s. of the pedestals gives 16MeV per channel in electronic noise. Using events where energy is injected to every fourth strip, cross-talk is measured to be less than 1.0%. Electronic channel gains exhibit a small drift correlated to the temperature in the experimental hall, at the level of $0.15\%/^{o}C$. For data analysis channel gains are calculated from long term averages, and corrected for temperature drift.

Energy Resolution

The energy resolution can be regarded in three parts: 1) shower fluctuations, 2) uniformity of response across the calorimeter and 3) electronic noise. To obtain the shower fluctuation component, electron beams of 12, 15, 20, 35, 80, 100 and 120 GeV were used. A Gaussian distribution was fitted, and the energy resolution was calculated to be $7.5\%/\sqrt{E}(\mathrm{GeV})$.

To obtain uniformity of response a scan of all calorimeter strips was performed, with electrons of 80GeV. The response is stable over the calorimeter to within 0.5%. At low energy the electronic noise contributes to the energy resolution. Typical electronic noise for a shower is 100MeV.

The energy resolution is then the sum of the three contributions.

$$\sigma_E = [(0.1/E)^2 + (0.075/\sqrt{E})^2 + (0.005)^2]^{1/2} \tag{3.2}$$

Spatial Resolution

The spatial resolution of the LAC is obtained by comparing reconstructed shower positions with the electron impact point extrapolated from the wire chambers. A Gaussian fit to the difference gives a standard deviation of 0.75mm. This value includes chamber resolution and multiple scattering, and so is an upper limit to the spatial resolution for photons.

The π^0 mass resolution and the energy scale calculations will be discussed in sections 6.2.1 and 7.3.2.

3.6 The Hadron Calorimeter

3.6.1 Detector Description

The hadron calorimeter (fig 3.15) consists of an iron/scintillator sandwich of 1.2m total iron thickness. It is divided longitudinally into two separate modules, each consisting of 24 steel plates, 25mm thick, of dimensions 270cm x 270cm. Each scintillator plane, inserted between steel plates, consists of 44 separate strips of dimension 1.3m x 11.9cm x 4.5mm. There are 24 such scintillator planes in the front module, and 25 in the back. The strips are alternately horizontal and vertical, and since each strip spans only half the calorimeter, the planes have a quadrant structure similar to the LAC. In each module the horizontal or vertical strips are coupled to a 3-inch phototube by a Plexiglas light-guide.

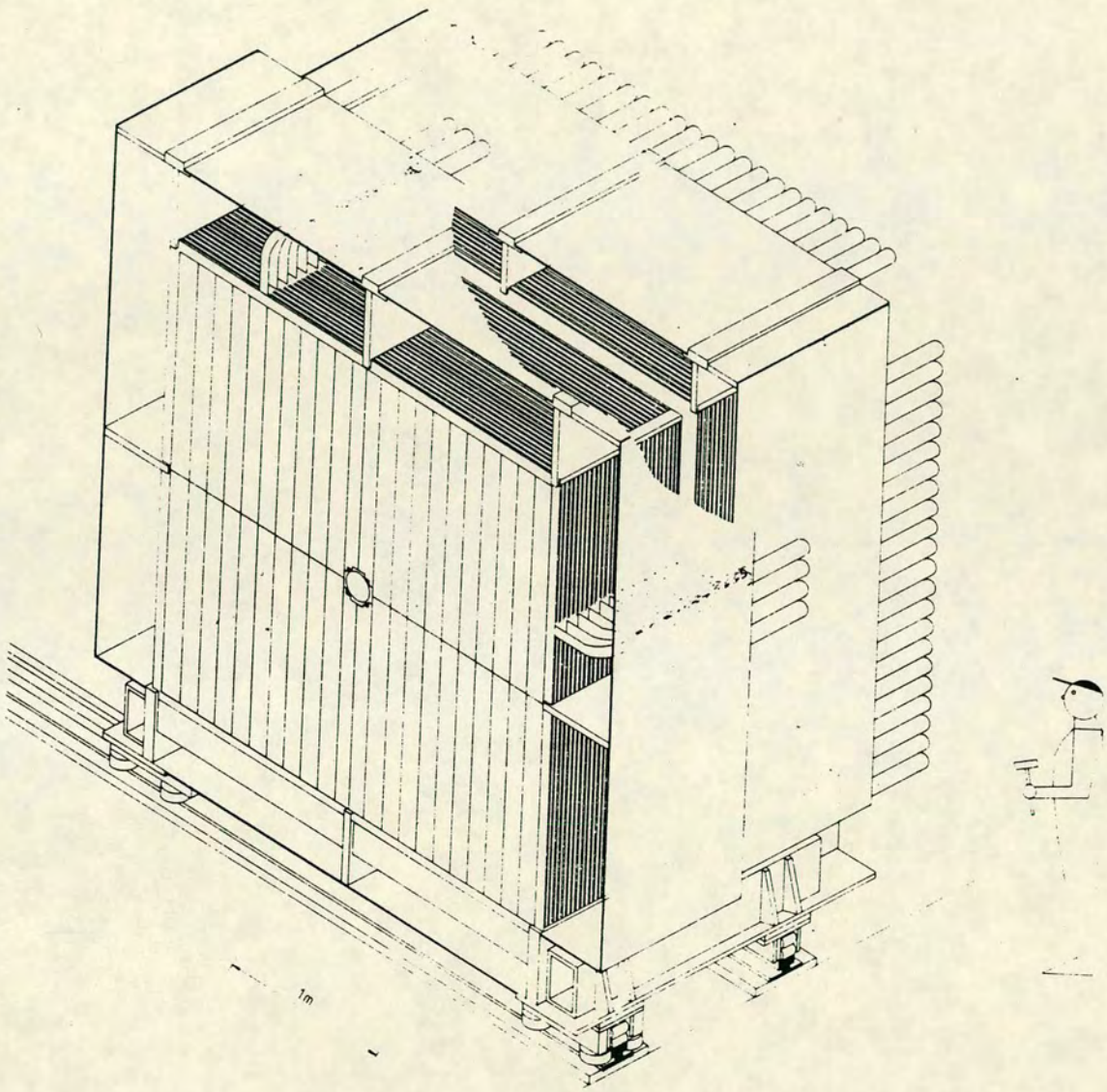

Figure 3.15: The Hadron Calorimeter

3.6.2 Hadron Calorimeter Read-Out

The hadron calorimeter possesses 176 readout channels. The analog signals are fed into linear mixers which match the impedance to twisted-pair output. Subsequent integrators split each signal into two parts. The first part is an integrated phototube signal which simulates the slower signal of the LAC, and is used for energy measurement in the same sample-and-hold/ADC system. The second part forms a fast analog sum which is used as an energy measurement in the trigger. A laser calibration system has been installed to monitor the complete readout chain.

3.6.3 Hadronic Energy Reconstruction

A large fraction of pions deposit a significant amount of energy in the 1.3 nuclear absorption lengths of the LAC. Thus the calorimetric response to hadronic showers is calibrated with the combined system. As described above for the LAC, the relative calibration between individual channels is performed separately for the two calorimeters.

Pedestals are calculated from random triggers recorded during data-taking, and these are subtracted off-line from ADC data. Special muon runs are used to establish relative sensitivities and the light attenuation along scintillator strips. The average energy sharing of hadronic showers is about 35% in the LAC, and 65% in the hadronic calorimeter. The hadronic response of the combined system is obtained using pions of 12-120 GeV. The following algorithm is applied to optimise the total energy resolution:

1. Relative energy units are transformed into GeV. For the hadron calorimeter a scale factor of 0.72 GeV per average muon pulse height has been determined from pions which do not interact in the LAC. For the LAC, an overall factor of 1.3 adjusts the recorded pion energy to the response for electrons of the same energy.
2. Overlapping showers are disentangled assuming an exponential lateral shower profile, and using the energy distribution in the projection

without overlap.

3. To equalize the different responses for hadronic and electromagnetic components, a correction weight is applied to each channel to correct for the shower shape. This is done separately for the two calorimeters.
4. A longitudinal energy correction is applied with an energy-dependent second-order polynomial F(E,R), where R is the ratio of the energy deposited in the LAC to that deposited in the hadron calorimeter. This function corrects for different e/π energy dependence in lead and iron, and corrects for non-linearities in weighting procedures.

The total algorithm results in an energy resolution of

$$\sigma_E = 0.65/\sqrt{E} \qquad (E > 12GeV) \tag{3.3}$$

This compares with an energy resolution of $1.2/\sqrt{E}$ before the algorithm is applied.

3.7 The Trigger System

The trigger system is designed to select $\pi^+\pi^-$ (charged) and $\pi^0\pi^0$ (neutral) decays in a beam containing both K_L and K_S. Since these channels are rare for the K_L, the trigger must be able to discriminate against more common three-body decays, and operate with a high beam intensity to allow collection of high statistics.

Charged and neutral two-pion decays are collected simultaneously. Each event is classified as charged, or neutral, or both, according to trigger conditions. The trigger logic is implemented using programmable units to allow for flexibility of selection criteria; the logic being loaded from the on-line computer. The trigger system consists of a synchronous front end, an asynchronous second part, and a 168E dual processor. Each stage processes and filters events independently, allowing the system to handle several events concurrently. The experiment has a finite memory time, so good $\pi\pi$ decays can be contaminated by overlay with

other events, or with uncorrelated background signals. To monitor this, two 48-channel logical-state analysers are used. These record signals from all scintillation counters, and various trigger elements, at $32\mu s$ intervals.

3.7.1 The Synchronous Part of the Trigger

The synchronous part of the trigger makes decisions in three sequential stages. First, the information from scintillation counters is used for initial timing and fast vetoing. Next, the energy deposition in the calorimeters is used, and finally, use is made of the number of wire chamber hits and energy clusters in the LAC.

Level 1: Scintillation counters and event time

At this level, a pre-trigger is generated by the combination of a cross-coincidence in either of the two scintillation counter hodoscopes, and no signal from any of the scintillator veto counters (see figs 3.8 and 3.9). An event time t_0 is defined by an OR of the coincidence signals from charged and neutral decay hodoscopes. Events with neither a signal in any anti-counter nor a coincidence of the two muon planes generate a pre-trigger. The pre-trigger strobes subsequent electronics, generates a 200ns gate for the wire chambers, starts the TDC's and blocks subsequent events.

Level 2: Fast Energy Measurements and Electron Rejection

At the second level of the synchronous trigger, fast sums of energy deposition in the calorimeters are used. Charged decays have to satisfy a minimum total energy threshold, whilst neutral triggers must pass a minimum energy threshold in the LAC and a maximum total energy threshold in the hadron calorimeter.

The $\pi e\nu$ decays produce an electron and a pion. Electrons can be identified by rapid shower development in the LAC, and an initial rejection of $\pi e\nu$ decays is. made by requiring that no track deposits more than 80% of its energy in the

front half of the LAC. This rejects about 80% of $\pi e\nu$ events, and about 2% of $\pi^+\pi^-$ decays.

If the energy requirements are satisfied, a general trigger is generated. This starts sample-and-hold measurements of calorimetric energy, and encoders of the wire chambers.

Level 3: Wire Chambers and Photon Counting

After passing the level 2 trigger, conditions are imposed on the number of wire chamber peaks and LAC energy clusters. For $\pi^+\pi^-$ events, at least two hits are required in at least two planes of the first wire chamber. For neutral events the energy clusters in the front part of the LAC are counted. If neither the horizontal or vertical projection has more than four clusters, then the event is passed by this stage of the trigger. Cluster positions are later used by the 168E system to reject $\pi^+\pi^-\pi^0$ decays.

If the conditions of these three levels are satisfied, then the asynchronous part of the trigger begins to process the event.

3.7.2 The Asynchronous Part of the Trigger

The Arithmetic Fastbus Interface (AFBI) is used, for neutral events, to reject background three-body events using more accurate digitized energy measurements. While the calorimeter channel information is being digitized and stored in memory, a pedestal-subtracted, gain-corrected set of channel energy measurements is sent to the AFBI. The AFBI calculates the energy sums and the first and second moments: $\Sigma E_i, \Sigma E_i x_i$, and $\Sigma E_i x_i^2$, where the sums are over calorimeter channels. These quantities are used to place cuts on the events. Neutral events must satisfy:

1. A minimum threshold (50GeV) for the energy deposited in the LAC.

2. A cut on longitudinal vertex position, derived from the energy sums and the second moment (see chapter 4.3). The calculated vertex position must be less than 55m, where the zero is defined by the position of the end of the cleaning collimator.

3. For checking purposes a fraction of events have all calculations performed with rejection inhibited.

3.7.3 The 168E On-Line Filter

Before events are written out to tape, a final reduction is achieved by the 168E system. Charged triggers which originate from three-body decays, or two-body decays outside the fiducial volume, can be rejected using wire chamber and photon counting information.

Energy clusters are used to reject $\pi^+\pi^-\pi^0$ events which have a photon more than 15cm from a charged track in the LAC. For the remaining events the longitudinal decay position is calculated, and used to calculate the opening angle between the two tracks. The vertex position and the kaon energy calculated from this opening angle are used to reject events outside a defined fiducial volume ($z > 58m$), or with energy below a defined threshold (45GeV).

In addition the 168E filter was used for 'lifetime downscaling'. A calculation was made of the number of K_S lifetimes from the target, using the momentum and vertex position of the decay. For low lifetimes a fraction of events were rejected, and a downscaling factor, representing that fraction, was applied to the events which were not rejected. This permits the accumulation of greater statistics in the more interesting region between 10 and 15 K_S lifetimes from the target, and avoids that the data acquisition is blocked by the copious number of K_S decays, whilst preserving some information on the K_S lifetime.

3.8 Data Acquisition

The data acquisition system, described in detail elsewhere [13], is FASTBUS standard, controlled by a VAX 11/750 computer. To boost the CPU capacity the VAX is connected to a Micro-VAX. During each 2.8s spill from the SPS, data from each event passing the early trigger levels is read into the 168E without intervention from the VAX. During the 11.6s between bursts, data in the buffer memory are transferred to the VAX. The data are then transferred to the Micro-VAX to be reformatted and written to tape. The data are written onto 6250 bpi tapes in the CERN standard EPIO format.

Chapter 4

Principles of the Measurement

4.1 Introduction

To measure either ϕ^{+-} or ϕ^{00}, a fit must be made of the observed time distribution of $K^0 \rightarrow \pi\pi$ decays to the formula of eqn 2.33.

$$I_{2\pi}(t) = S(p)[e^{-\Gamma_S t} + \mid \eta \mid^2 e^{-\Gamma_L t} + 2 \mid \eta \mid D(p) e^{-\frac{(\Gamma_L+\Gamma_S)t}{2}} cos(\Delta m t - \phi)] \quad (4.1)$$

Normally such a measurement relies heavily on accurate Monte Carlo simulation of the data to account for acceptance. In this experiment, however, we have two data samples from two different target stations. For each beam, the acceptance at any given momentum and vertex position should be the same, the only difference being the time of flight from the target. In this analysis we divide data from the KN station by data from the KF station, after binning in momentum and vertex position. To this ratio we fit the ratio of the two 'phase expressions' (eqn 4.1), calculated from the two targets. In this way we may measure either phase, without the use of a Monte Carlo to correct the data for acceptance. Another feature of this analysis technique is that the term S(p), a normalisation dependent on the production spectrum, is the same for the KN and KF expressions, and drops out in the division. The main disadvantage with this analysis method, in comparison with a direct fit to the time distribution from each target, using a Monte Carlo for acceptance, is that we lose statistical precision when taking a ratio.

In addition to the phase term, ϕ^{+-} or ϕ^{00}, there are other parameters in eqn 4.1 which are unknown, or have non-negligible measurement uncertainties($\Delta m, \eta, \tau_S$, D(p)). Any uncertainty in the measurement of these parameters translates, at some level, into an uncertainty in the measurement of either phase. For example, it can be shown [14] that an uncertainty of 1% in Δm corresponds to an uncertainty of 3^o in a measurement of ϕ^{+-} or ϕ^{00}. In this analysis, we present a measurement of the difference between the charged and neutral phases, $\Delta\phi = \phi^{00} - \phi^{+-}$. If the two phases (or one phase and the difference between the two), are measured in the same fit, with common values for the other parameters (either fixed or measured), then the systematic uncertainty on the phase difference should be minimised. Since ϕ^{+-} and ϕ^{00} depend in the same way, at least to first order, on the values of the other parameters, then the difference between ϕ^{+-} and ϕ^{00} should be somewhat insensitive to uncertainties in these other parameters, if the two phases are measured together. The fitting procedure will be discussed in detail in chapter 7. Here we discuss how the time of flight from the target is measured, for charged and neutral decays.

The number of K_S lifetimes between the target and the point of decay is given by

$$N = m_K \Delta z / pc\tau_S \tag{4.2}$$

where m_K is the kaon mass, Δz is the distance travelled in the laboratory frame, τ_S is the K_S lifetime, p is the kaon momentum, and c is the velocity of light. Therefore, to measure the number of lifetimes between the target and the point of decay, a necessary input for the fitting procedure, it is necessary to know the momentum and vertex position for charged and neutral decays.

4.2 Momentum and Vertex Position for Charged Decays

For charged decays, the vertex position is calculated in the normal way. Spacepoints are reconstructed in the two wire chambers, and a plane is fitted through four spacepoints (two in each chamber), to calculate the vertex position. This

is described in more detail in chapter 5.3.

The kaon momentum can, of course, be calculated from the pion energies as they are measured directly in the calorimeters. To reduce sensitivity to the hadronic energy resolution, the momentum is better calculated from kinematics, using the vertex position, and the opening angle defined by the vertex and the two tracks. It can be shown that:

$$\begin{aligned} E_{tot} &= [(m_{K^0}^2 - m_\pi^2 R)R/\theta^2]^{1/2} \\ m_{K^0} &= [m_\pi^2 R + (E_1 + E_2)^2\theta^2/R]^{1/2} \end{aligned} \tag{4.3}$$

where $R = 2 + E_1/E_2 + E_2/E_1$, θ is the opening angle between the pion tracks, and E_1 and E_2 are the measured pion energies. Let us prove this.

Let a particle four momentum be represented by P, and the three momentum be denoted by p. For a two body decay of a particle of mass M into two particles of masses m_1 and m_2, we have:

$$\begin{aligned} M^2 &= P^2 = (P_1 + P_2)^2 \\ &= P_1^2 + P_2^2 + 2P_1P_2 \\ &= m_1^2 + m_2^2 + 2E_1E_2 - 2p_1.p_2 \end{aligned} \tag{4.4}$$

Let the opening angle between the tracks be θ. In the case where the masses m_1 and m_2 are small compared with the particle momenta, we may use a Taylor expansion to second order in these masses to obtain:

$$\begin{aligned} M^2 &= 2E_1E_2[1 - (1 - m_1^2/E_1^2)^{1/2}(1 - m_2^2/E_2^2)^{1/2}cos\theta] + m_1^2 + m_2^2 \\ &= 2E_1E_2[1 - (1 - m_1^2/2E_1^2 - m_2^2/2E_2^2)cos\theta] + m_1^2 + m_2^2 \\ &= 2E_1E_2[\theta^2/2 + 1/2(m_1^2/E_1^2 + m_2^2/E_2^2)] + m_1^2 + m_2^2 \\ &= \theta^2E_1E_2 + m_1^2(1 + E_2/E_1) + m_2^2(1 + E_2/E_1) \end{aligned} \tag{4.5}$$

where, for small $\theta, cos\theta = 1 - \theta^2/2$.

If we then define :

$$\begin{aligned} r &= E_1/E_2 \\ E &= E_1 + E_2 \end{aligned} \tag{4.6}$$

it follows that

$$\begin{aligned} E_1 &= E - E_2 = E - E_1/r \\ E_1 &= rE/(r+1) \\ E_2 &= E/(r+1) \end{aligned} \tag{4.7}$$

and we find the mass to be :

$$M = [(\theta E/(r+1))^2 r + m_1^2(r+1)/r + m_2^2(r+1)]^{1/2} \tag{4.8}$$

and the energy to be:

$$E = ((r+1)/r\theta)[M^2 r - (r+1)(m_1^2 + m_2^2 r)]^{1/2} \tag{4.9}$$

These are equivalent to the equations 4.3.

Because of the two energy ratios in the term R, a poor measurement of one pion energy enters in a less serious way than if the momentum were calculated directly from the sum of the pion energies.

It should be noted that the calculated kaon mass is not used for the momentum calculation, rather the kaon mass as given in the Particle Data Booklet. The calculated kaon mass is one of the quantities used to discriminate against three-body background to $\pi^+\pi^-$ events. For such events the measured opening angle and track energies are lower than for a two-body decay, and the calculated kaon mass will be correspondingly lower.

4.3 Momentum and Vertex Position for Neutral Decays

For neutral events, the energy and longitudinal decay point are calculated from the energies and positions of the photons in the LAC.

The kaon energy is simply the sum of the photon energies in the LAC :

$$E_K = \Sigma E_i \ (i = 1, .., 4) \tag{4.10}$$

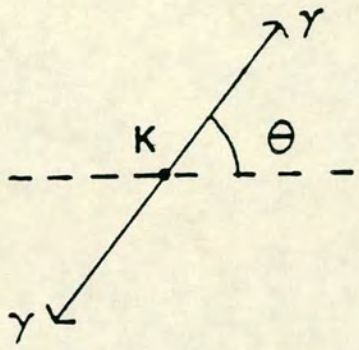

Figure 4.1: Decay into Two Photons - Centre of Mass Frame

We define the nth moments of a decay into N photons as follows :

$$\begin{aligned} X_n &= \Sigma_{i=1,N} E_i x_i^n \\ Y_n &= \Sigma_{i=1,N} E_i y_i^n \end{aligned} \tag{4.11}$$

If we assume that the decaying particle is a kaon then, using only the measured photon energies and positions, the longitudinal position of the decay is given by:

$$Z^2 = (1/m_K^2)[X_0 X_2 - X_1^2 + Y_0 Y_2 - Y_1^2] \tag{4.12}$$

where Z is the distance between the kaon vertex and the LAC.

We will prove this for the decay of a kaon into two photons; the proof for a decay into four photons being a generalisation of this. Consider the decay of fig 4.1 in the centre of mass frame:

$$\begin{aligned} p_K^2 &= (p_1 + p_2)^2 \\ &= p_1^2 + p_2^2 + 2p_1.p_2 \end{aligned} \tag{4.13}$$

Now:

$$\begin{aligned} m_K^2 &= E_K^2 - p_K^2 \\ &= 2E_1 E_2(1 - cos\theta) \end{aligned} \tag{4.14}$$

In the laboratory frame θ is small for high energy kaons, so :

$$m_K^2 = E_1 E_2 \theta^2 \tag{4.15}$$

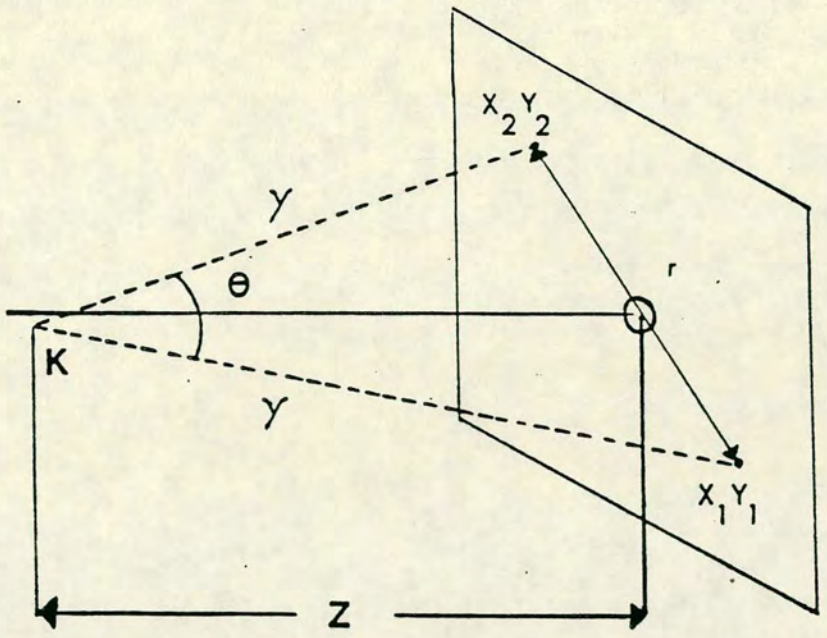

Figure 4.2: Decay into Two Photons - Laboratory Frame

In the laboratory (see fig 4.2)

$$\theta = r/z \tag{4.16}$$

where r is the distance separating the two photons at the detector. The vertex position is therefore given by:

$$Z^2 = E_1 E_2[(x_1 - x_2)^2 + (y_1 - y_2)^2]/m_K^2 \tag{4.17}$$

This can be shown, trivially, to be equivalent to eqn 4.12. For the case of a decay into four photons:

$$m_K^2 = (P_1 + P_2 + P_3 + P_4)^2 \tag{4.18}$$

leading to

$$m_K^2 = \Sigma_{i,j=1,4} E_i E_j[(x_i - x_j)^2 + (y_i - y_j)^2]/Z^2 \quad (i > j) \tag{4.19}$$

This gives, once again :

$$Z^2 = (1/m_K^2).[X_0 X_2 - X_1^2 + Y_0 Y_2 - Y_1^2] \tag{4.20}$$

We therefore have, in the general case, a reciprocal relationship between the kaon mass, m_K, and the distance between the vertex and the detector, Z. For a measured decay with four photons, it is possible to calculate two photon invariant masses for the three combinations:

$$m_{ij} = (1/Z).[E_i E_j[(x_i - x_j)^2 + (y_i - y_j)^2]]^{1/2} \tag{4.21}$$

Choosing the best mass combination, a cut is applied around the π^0 mass in the two-dimensional mass plot for the two π^0's. This will be discussed further in chapter 6.

For a $K_L \rightarrow 3\pi^0$ decay with two photons missing, the reconstructed vertex will appear closer to the calorimeter than the actual decay point. This is equivalent to saying that if we knew the vertex position, and used this to calculate the kaon mass, then the calculated mass would be below the kaon mass. We therefore expect to see a strong Z dependence of any background to the $\pi^0\pi^0$ signal due to $\pi^0\pi^0\pi^0$ decays with missing photons.

Chapter 5

Data Reduction

5.1 Introduction

The data used for this analysis represents almost the total sample collected during the 1987 run. The run started in mid June, and ended in mid September.

Data was collected from the KN and KF stations in such a way that the numbers of K_L decays recorded in the two samples are similar. Data taking was divided into mini-periods, which, under stable running conditions, lasted approximately one day. During each mini-period 20 KN and 11 KF tapes were recorded, and one K_S tape for measurement of the energy scale of the LAC. A typical KN or KF tape contained some 70,000 triggers. In all, more than 2,000 tapes (including calibration, tests, etc) were accumulated, representing 57 mini-periods. This analysis does not use mini-periods 1 or 2, where the running conditions were not yet stable, or mini-period 26 which was delayed at the production stage.

Raw data tapes were passed through the reconstruction program KORECT for the first step of reconstruction and data reduction. The events surviving this first stage were written onto Data Summary Tapes (DST's). I was responsible for this production, which was carried out at CERN, at the Rutherford Appleton Laboratory, and at the CCPN in Lyon. The production took three months, from mid-February to mid-May of 1988.

5.2 The Reconstruction Program KORECT

The main reconstruction program used by NA31 is KORECT. The DST production uses KORECT to read raw data tapes, and writes EPIO format output tapes, also readable by KORECT. These output tapes, known for historical reasons as stream 2, contain all $\pi\pi$ candidates, all e^+e^- candidates, and some fraction of $\pi^0\pi^0\pi^0$ events.

After an event has been read, the raw data information is decoded. An event will be rejected at this stage in the very rare case of a serious error in the data format. Pedestals and sensitivities for the calorimeter strips are obtained from a data base which contains information from electronic and muon calibrations. For all non-calibration events, with a charged or a neutral trigger, we attempt a charged reconstruction. If a vertex is found, the event is regarded as a charged event. If no vertex is found then the event is regarded as a neutral decay, and an attempt is made at neutral reconstruction. After reconstruction we apply a selection procedure which decides if the event should be written to stream 2.

We shall describe the charged and neutral reconstructions, and the stream 2 selection criteria.

5.3 The Charged Reconstruction

The charged reconstruction starts with the wire chamber information. First the wire address information is used to construct spacepoints, defined by a χ^2 criterium on the triangular condition. A space point contains 3 or 4 hits in the four planes. If there are at least two spacepoints in each chamber, we loop over all possible combinations of 2 spacepoints per chamber and try to fit a plane through the 4 spacepoints, provided that the distance between spacepoints is at least 10cm (20cm) in chamber 1 (2). If the most coplanar combination has an acceptable χ^2, this combination gives a provisional vertex. If the χ^2 of another combination is also acceptable, the presence of another solution is flagged. For all acceptable solutions we do a full spacepoint reconstruction using TDC in-

formation. With the more accurate spacepoints from TDC-reconstruction, we repeat the selected best plane fits, and the fit with the best χ^2 gives the final vertex position. A vertex will be rejected if one of the spacepoints is closer than 12cm (18cm) to the beam axis in chamber 1 (2). In the case that no vertex is found, we attempt a neutral reconstruction.

From the opening angle of the decay we calculate the kaon energy, assuming a symmetric two-body decay. If this energy is less than 55GeV, we stop reconstruction at this point.

Once we have the geometrical information of an event, we extrapolate each track into the calorimeters and determine it's energy by summing the energies of a well defined set of strips around the impact point. A strip belongs to the sampling region for a track if the perpendicular distance between the impact point and the centre of the strip is less than 14, 21 or 31cm in the LAC-front, LAC-back and hadron calorimeter, respectively. For each strip we add the pedestal subtracted number of ADC counts, and apply the procedure described in 3.6.3 to calculate the track energy.

After determination of the charged track energies, we do a complete photon reconstruction. This procedure gives us a rather large number of 'photons', which are real γ's or just fluctuations in pion showers. To distinguish between the two possibilities we apply a criterium based on the distance from the nearest charged track and the 'photon' energy. The 'photon' is regarded as a real photon if it's energy is at least 15GeV and it is more than 15cm from the nearest track, or if it's energy is greater than 20GeV and it is 10-15cm from the nearest track. If there is at least one photon, it's presence is flagged, and used for rejection at a later stage.

At this point the reconstruction is finished. The remaining task is π/e discrimination. A priori we consider each charged track to be a pion. Electrons are those tracks which satisfy ALL of the following conditions:

1. The energy in the hadronic calorimeter (EHAD) is less than 5GeV.
2. ELAC/EHAD is greater than 6.
3. ELAC-front/E-total is greater than 0.46.

4. The width of the track, in the LAC, is between 1.77 and 2.4cm.

These cuts reject a few permille of $\pi^+\pi^-$ events, but approximately 95% of electrons.

5.3.1 Charged Event Selection for DST's

After the complete charged reconstruction, and the identification of tracks likely to be electrons, certain kinematical cuts are applied to the $\pi^+\pi^-$ events. Events passing these cuts are written to the DST's.

1. No extra photons are tolerated, if they satisfy the distance and energy cuts above. This is primarily a rejection of $\pi^+\pi^-\pi^0$ decays.
2. No electron tracks, as defined above, are allowed.
3. The z-position of the vertex should be between -10 and 55m.
4. The total energy, calculated from the opening angle and the ratio of track energies, should be greater than 55GeV.
5. The spacepoints should not lie on the same side of the beam hole.
6. The ratio of the track energies should lie between 0.25 and 4.0. This cut is designed to exclude the $\Lambda \rightarrow p\pi$ decay of the Λ baryon, a possible background to $K_S \rightarrow \pi^+\pi^-$ decays. The proton of a $\Lambda \rightarrow p\pi$ decays has a higher energy than the pion, and from a comparison of data with Monte Carlo [15], the above cut reduces any background from Λ decay to the level of one per mille. For a given total energy, the minimum pion energy is defined by this cut.

5.4 The Neutral Reconstruction

The neutral reconstruction uses only information from the LAC. Only events where the sum over all strips is greater than 55GeV are processed. The first step is a search for one-dimensional clusters in the LAC-halfplanes. Summing

the energies E_J of the front and back strips, we find all peaks which satisfy the following conditions:

1. $E_J > 0.5(E_{J-1} + E_{J+1}) + 0.15\text{GeV}$
2. $E_{J-1} + E_J + E_{J+1} > 0.6$ GeV
3. $E_{J-1} > 0.15E_J$ or $E_{J+1} > 0.15E_J$

Peaks on neighbouring strips are merged. For isolated peaks we determine the cluster energy by summing over fifteen strips (the central strip, and seven on each side) and the cluster position is determined by a parametrisation based on the energies of the three central strips.

The next step in the neutral reconstruction is to combine one-dimensional clusters into two-dimensional photons, by associating clusters from the two projections. Pairs are made first near the boundaries between quadrants, and then inside the quadrants. When there is an ambiguity, the clusters of most similar energy are paired. We allow a maximum of 3 photons per quadrant, or 8 photons in the whole detector. At this stage some corrections are applied to the photon energy.

1. The zero suppression (see 3.5.3) clips the wings of almost all photon showers, reducing the energy recorded in the ADC's by typically 3%. A correction is applied to account for this, the correction having been determined from $\pi^0\pi^0$ events with and without zero suppression implemented in the ADC's.
2. For photons close to the beam axis there is a leakage of energy from the calorimeter into the beam hole. For photons closer than 18cm to the beam axis a correction, determined from an electron beam scan around the hole, is applied.
3. In a K_S beam it was found that 2.4% of neutral events were 5 photon events. A distribution of the distance between showers in their X and Y projections shows a peak at zero, in one projection, for 72% of these events, and typically one of these two photons with a common coordinate has a very low energy. Spurious noise, and a few consistently active channels are identified as the source of the fifth photon.

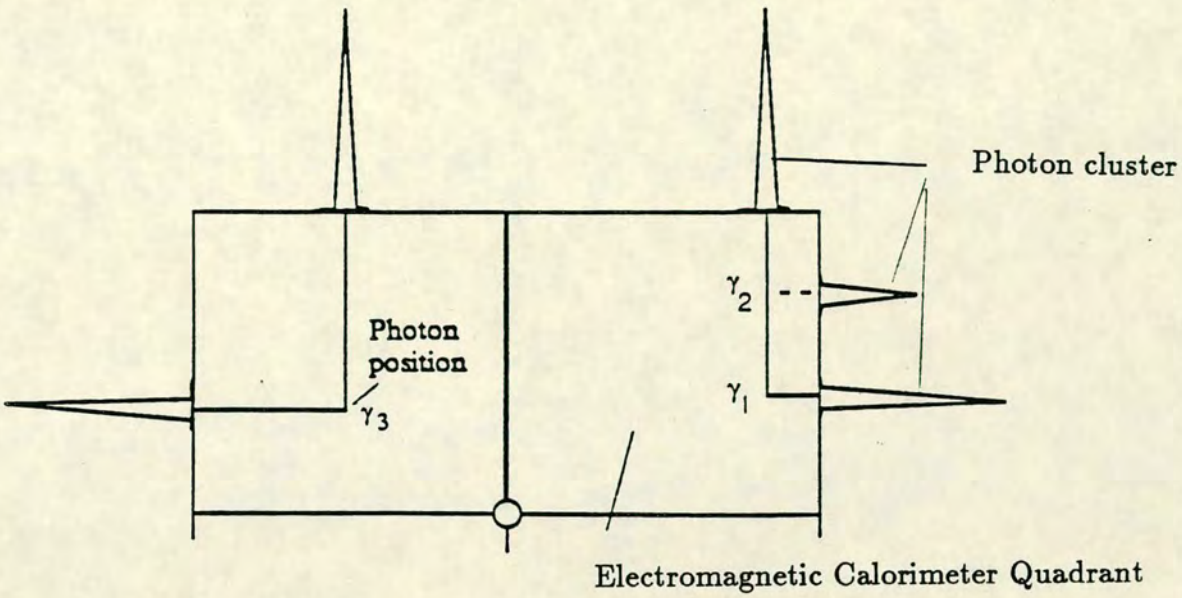

Figure 5.1: Overlap between photon and noise

The neutral reconstruction is designed to pair as many projections as possible, and mistakenly pairs this spurious activity with part of the energy of a real photon (see fig 5.1). An algorithm has been developed to correct for this problem for all events with an odd number of photons. If two photons are in the same quadrant and closer than 0.5cm in one projection and 10cm in the other, then the two photons are completely merged. If the second projection is more distant than 10cm, then only the energy of the shared projection is merged.

The last step in the neutral reconstruction looks for $K^0 \rightarrow \pi^0\pi^0$ and $K^0 \rightarrow 3\pi^0$ decays. If 4 or 6 photons have been found, the z-position of the vertex is calculated from the K^0-decay hypothesis (see 4.11), and the best pairing of two photons into π^0's is determined. Where 5 or 7 photons are found, the same algorithm is used, neglecting one of the photons below 10GeV.

5.4.1 Neutral Event Selection for DST's

To be written to DST's $\pi^0\pi^0$ events must satisfy the following conditions:

1. The total energy should be greater than 55GeV.
2. The Z-position of the vertex should lie between -10 and 55m.
3. For each photon, the invariant mass of the $\gamma\gamma$ pair should lie between 100 and 170MeV. ($m_{\pi^0} = 134.96$ MeV)

5.5 Further Data Reduction

The data reduction achieved at the level of the DST output is not sufficient to permit the fast analysis of large amounts of data. For this reason, a miniDST was produced, containing only events which are regarded as good candidates for $\pi\pi$ decays, and aiming to keep the number of words per event to a minimum. Rather than detail the cuts used to reduce the data volume at each stage, we will henceforth describe only the cuts used for the final analysis. The events on the miniDST's satisfy at least the cuts made at the stream 2 level, and, for most relevant quantities, the cut applied is between the cut at the stream 2 level, and the cut used in the final analysis. Some minor corrections are applied to the data at the miniDST level, either in the writing or reading program.

In the final stages of analysis it is convenient to run extremely fast analysis jobs, to test for stability of results against cut positions, and other systematic effects. Reading of miniDST's was too slow for this purpose, so a microDST, containing only three words per event, was produced. The microDST contains information on only the most important quantities, in many cases containing only one bit to indicate if the event would or would not satisfy a given cut.

Chapter 6

Cuts and Removal of Background

In this chapter we will discuss the cuts and background removal for charged ($\pi^+\pi^-$) and neutral ($\pi^0\pi^0$) events. The cuts applied at the level of DST and miniDST production are loose. Tighter cuts are placed at the level of miniDST reading, or microDST production. These tighter cuts, used for the final analysis, are described here.

The NA31 coordinate system is an orthogonal, right-handed coordinate system, with the Z axis along the beam axis. The zero of the Z axis is at the downstream end of the cleaning collimator (fig 3.3). The zero of both the X and Y axes is at the centre of the beam, with the positive Y direction pointing upwards.

6.1 Charged Events

6.1.1 Cuts for Charged Events

Number of Spacepoints

Only events with exactly two charged tracks are accepted. The number of spacepoints in wire chamber 1 must be exactly two. Backscattering from the calorimeters increases the number of accidental spacepoints in wire chamber 2, so there

is no cut on the number of spacepoints in this chamber.

Track Positions

The outer radius within which tracks are accepted is defined by an octagon of inscribed radius 118cm at wire chamber 2. The distance from a spacepoint to the beam axis must be at least 12cm(18cm) in chamber 1(2).

A plastic foil separates the left and right halves of the Liquid Argon Calorimeter (see fig 3.13). An electron from a $K_L \rightarrow \pi e \nu$ event hitting the foil could pass the electron rejection cuts by depositing an atypically small amount of energy in the LAC. For this reason tracks with $\mid X \mid < 0.6$ cm are rejected.

The positions of the tracks in the charged decay hodoscope are used to repeat the Q_X condition which is part of the on-line trigger. This condition demands that the tracks should be in opposite quadrants of the hodoscope.

Track Energies

The K^0 energy is determined from the opening angle and the ratio of track energies (see 4.2). In addition the sum of the energies of the two tracks must be greater than 40 GeV. This rejects mainly three body decays with small opening angles and low energy.

Centre of Gravity

The centre of gravity of a charged event is calculated from the track positions and energy :

$$\begin{aligned} X_{cog} &= (E_1.x_1 + E_2.x_2)/(E_1 + E_2) \\ Y_{cog} &= (E_1.y_1 + E_2.y_2)/(E_1 + E_2) \\ r^2_{cog} &= X^2_{cog} + Y^2_{cog} \quad . \end{aligned} \tag{6.1}$$

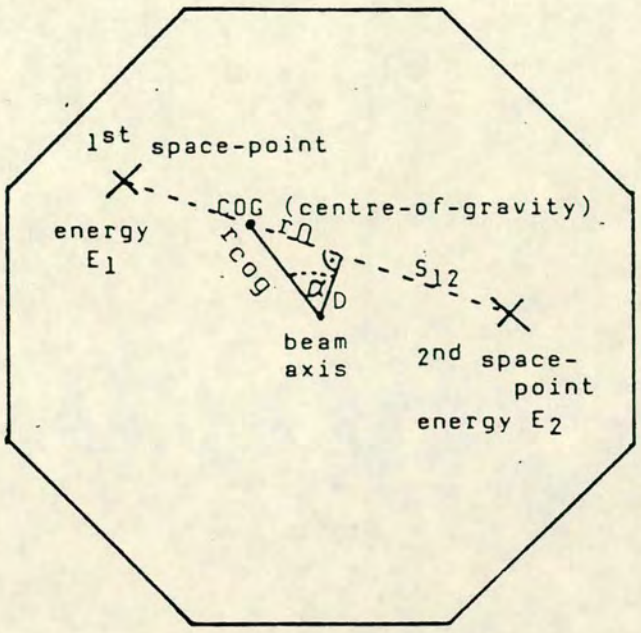

Figure 6.1: Center of Gravity for Charged events

r_{cog} may have a large measurement error due to the calorimetric measurement of the track energies. The error on r_{cog} (see fig 6.1) is given by

$$\sigma_{cog} = 0.7.sin(\alpha).S_{12}.(E_1.E_2/(E_1+E_2)^3)^{1/2} \quad . \tag{6.2}$$

σ_{cog} is typically 3cm, and events with $r_{cog} > 10cm + 2\sigma_{cog}$ are rejected. This cut mainly rejects three body decays where the third particle has a large momentum component perpendicular to the plane of the two detected tracks. Scattered kaons would also be rejected by this cut.

Closest Distance of Approach

For events with a reconstructed vertex, the closest distance of approach (CDA) of the two tracks is obtained by computing the distance in space between the two particle trajectories. Events with CDA > 2.5 cm are rejected. This cut, primarily a cut against badly reconstructed events, rejects $\approx$ 0.2% of charged events.

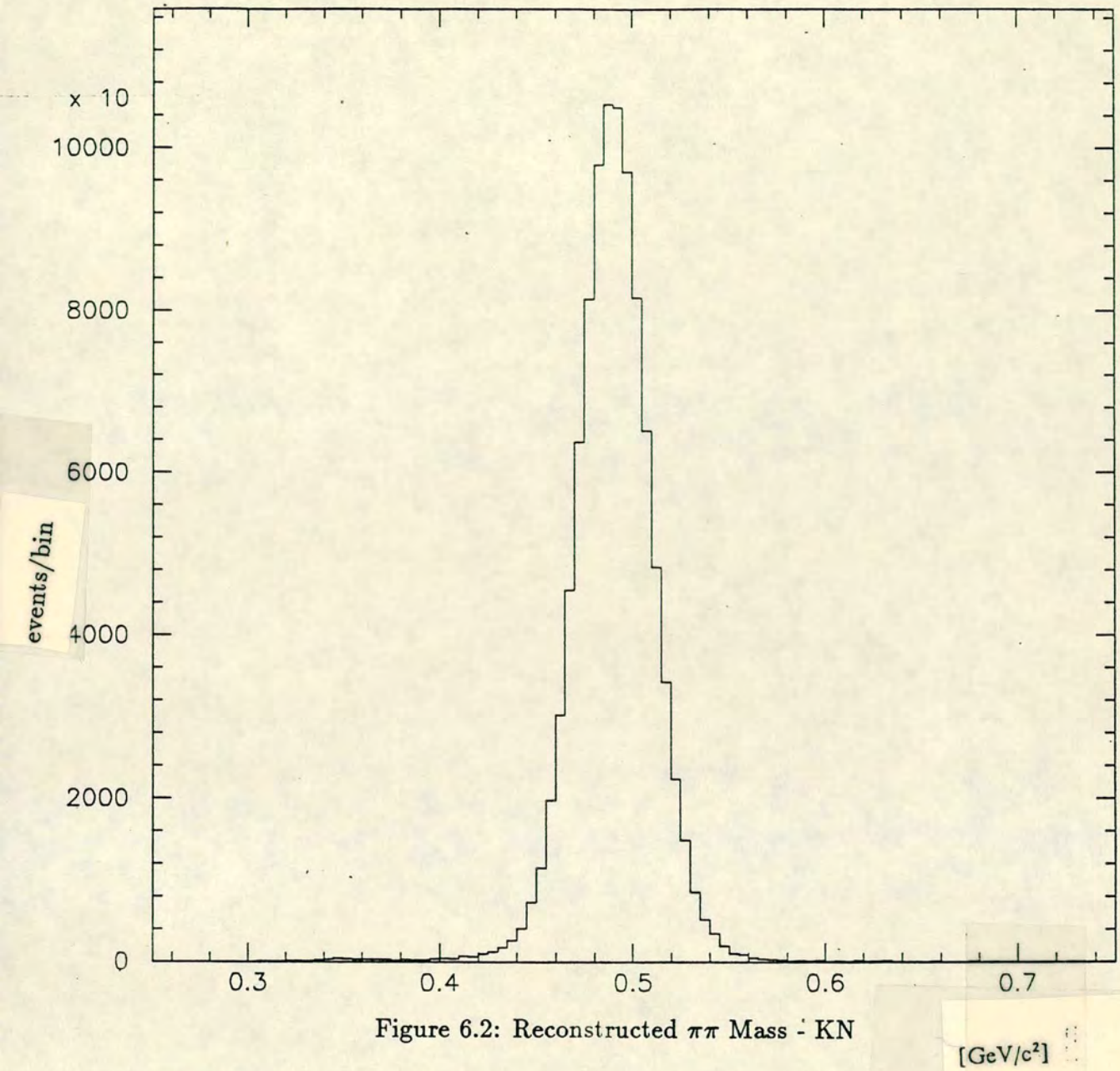

Figure 6.2: Reconstructed $\pi\pi$ Mass - KN

Mass Cut

The invariant mass of the two charged particles is shown, for the KN and KF beams, in figs 6.2 and 6.3. At lower masses one can see background from three-body decays of K_L. Due to small changes in the calibration of the hadron calorimeter, the mean value of the mass distribution varies by a few MeV from mini-period to mini-period. A resolution dependent mass cut is applied around the mean value, calculated from K_S data, on a mini-period by mini-period basis. The resolution was determined at 10 GeV intervals over the region of kaon energy between 70 and 170 GeV, and varies between 28 and 20 MeV over this region.

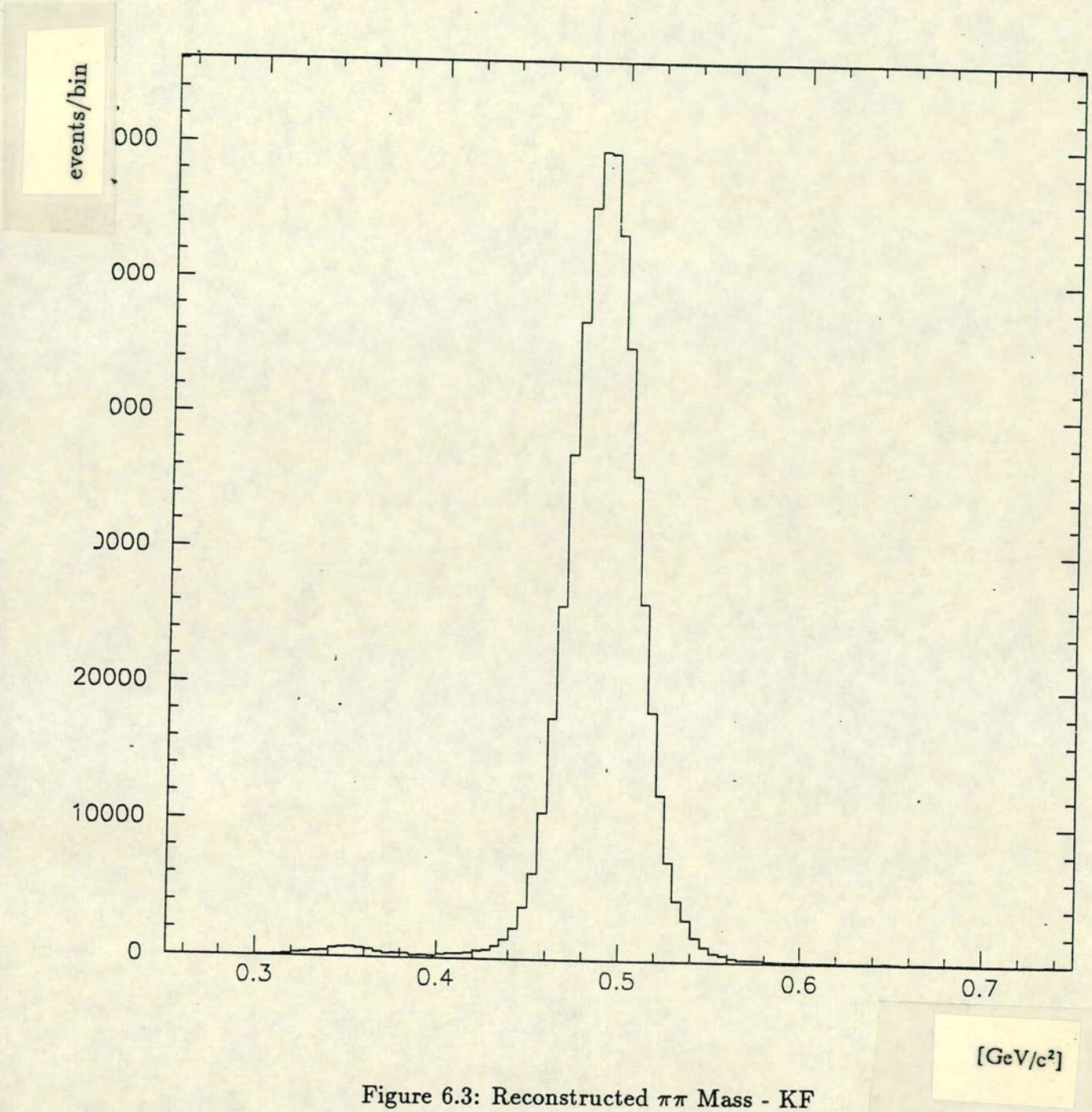

Figure 6.3: Reconstructed $\pi\pi$ Mass - KF

Events with $| m_{\pi\pi} - < m_{\pi\pi} > | > 2.1\sigma(E_K)$ are rejected.

This cut rejects roughly 4% of $\pi^+\pi^-$ events, but is a very effective cut for the removal of three body background events.

Ratio of Track Energies

Lambda hyperons (Λ) are produced at the target along with kaons. The $\Lambda \rightarrow p\pi$ decay, a potential background to the $\pi^+\pi^-$ signal, is rejected by placing a cut on the ratio of track energies (see section 5.3.1). At the DST production stage we demanded that $E_{max}/E_{min} < 4$. A tighter cut of $E_{max}/E_{min} < 2.5$, in conjuction with the tight mass cut, is used at the miniDST reading level to reject all $\Lambda \rightarrow p\pi$ decay's.

Electron Rejection

Electrons from $K^0 \rightarrow \pi e \nu$ events are recognised by the longitudinal shower developement of the electron (see section 5.3). In addition to the cuts applied at the DST production stage (5.3), we insist that the ratio of the energy in the LAC to the energy on the central strip of the shower in the HAC should be greater than 4. These cuts reject around 25% of $\pi^+\pi^-$ events, but leave a very small background from $\pi e \nu$ events.

Rejection of $\pi^+\pi^-\pi^0$ Decays

In order to reject $\pi^+\pi^-\pi^0$ events, any charged event is rejected if a photon is found. To distinguish between real photons and fluctuations in pion showers (see section 5.3), we demand that any photon candidate satisfy the following conditions on photon energy (E_γ) and distance to the nearest charged track ($D_{\gamma\pi}$).

- $E_\gamma > 2$ GeV and $D_{\gamma\pi} > 2$ cm.

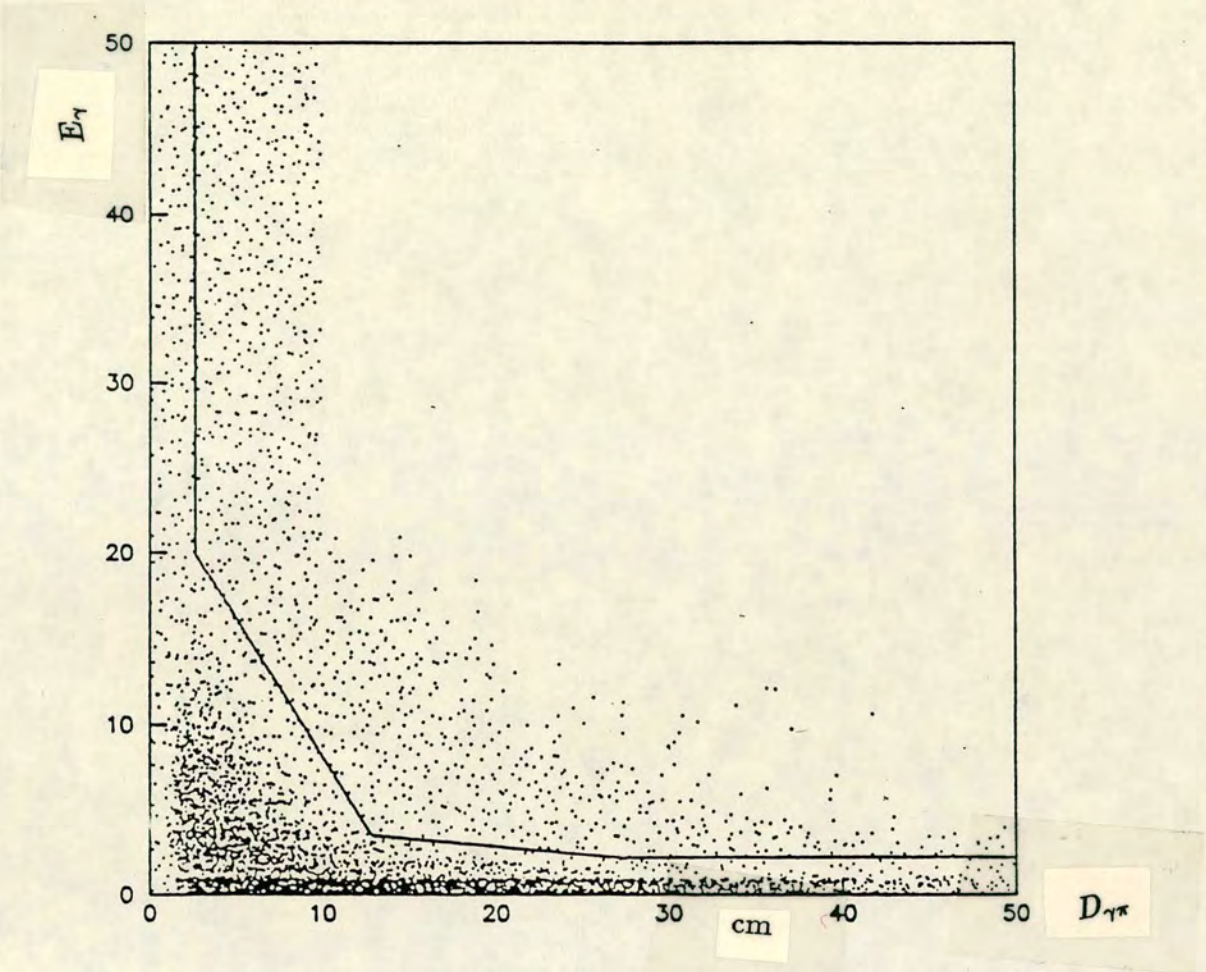

Figure 6.4: Photon energy versus distance to nearest charged track

- $E_\gamma > 15 - 0.6(D_{\gamma\pi})$
- $E_\gamma > 50 - 10(D_{\gamma\pi})$

Figure 6.4 shows E_γ versus $D_{\gamma\pi}$. On-line cuts in the 168E's, and loose cuts imposed at the DST production stage, have already removed events with a well separated energetic photon. The cut applied in the final analysis is shown by the solid line. The plot of E_γ versus $D_{\gamma\pi}$ is also used in the estimation of background from $\pi^+\pi^-\pi^0$ decays (see section 6.2.1).

Distance Between the Decay Plane and the Target

Three body decays with missing momentum carried away by an undetected neutrino are characterized by the fact that the kaon momentum vector lies in a different plane from the two charged tracks. If we assume that the kaon originates from the target, then we can determine the direction of the kaon momentum vector from the position of the vertex. The product of the normal vector to the decay plane, $\underline{n}$, and the vector from the target to the decay plane, $\underline{x}$, is a measure of the acoplanarity of the kaon momentum and the plane of the two charged tracks.

$$D_{targ} = \mid \underline{x}.\underline{n} \mid \tag{6.3}$$

The quantity D_{targ} is the distance from the target to the plane defined by the two charged tracks. D_{targ} is a quantity which has been used by the NA31 collaboration in previous analyses. To enable background subtraction to be carried out as before (see section 6.2.1), and to allow us to compare the resolution in this quantity with 1986 data, the definition of D_{targ} for the KN and KF stations is related to D_{targ} as scaled to the K_L target of 1986.

$$D_{targ} = s.D_{targ} \tag{6.4}$$

where

$$s = (Z_{WC2} - Z_{KL})/(Z_{WC2} - Z_{TARG}) \tag{6.5}$$

Z_{WC2} = 12162.4cm, Z_{KL} = −12003.0cm, and Z_{TARG} = −4800cm for KF and -3360 cm for KN.

D_{targ} distributions for KN and KF are shown in figs 6.5 and 6.6. Background from three body decays can be seen at higher values of D_{targ}. Events with $D_{targ} > 5$ cm are rejected. The quantity D_{targ} will also be used in the estimation of background due to $\pi e\nu$ and $\pi\mu\nu$ decays.

Longitudinal Vertex Position

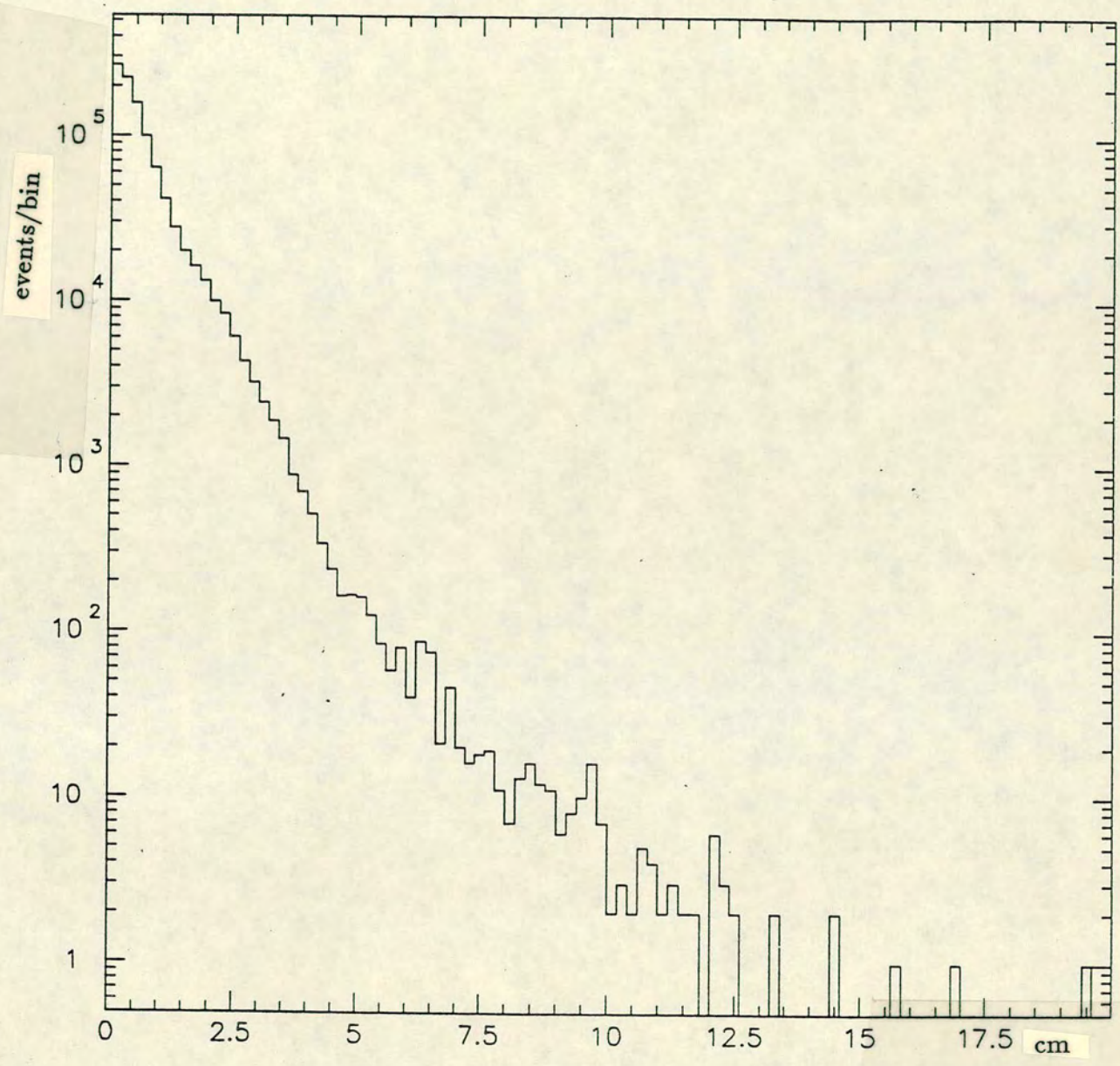

Figure 6.5: D_{targ} - KN

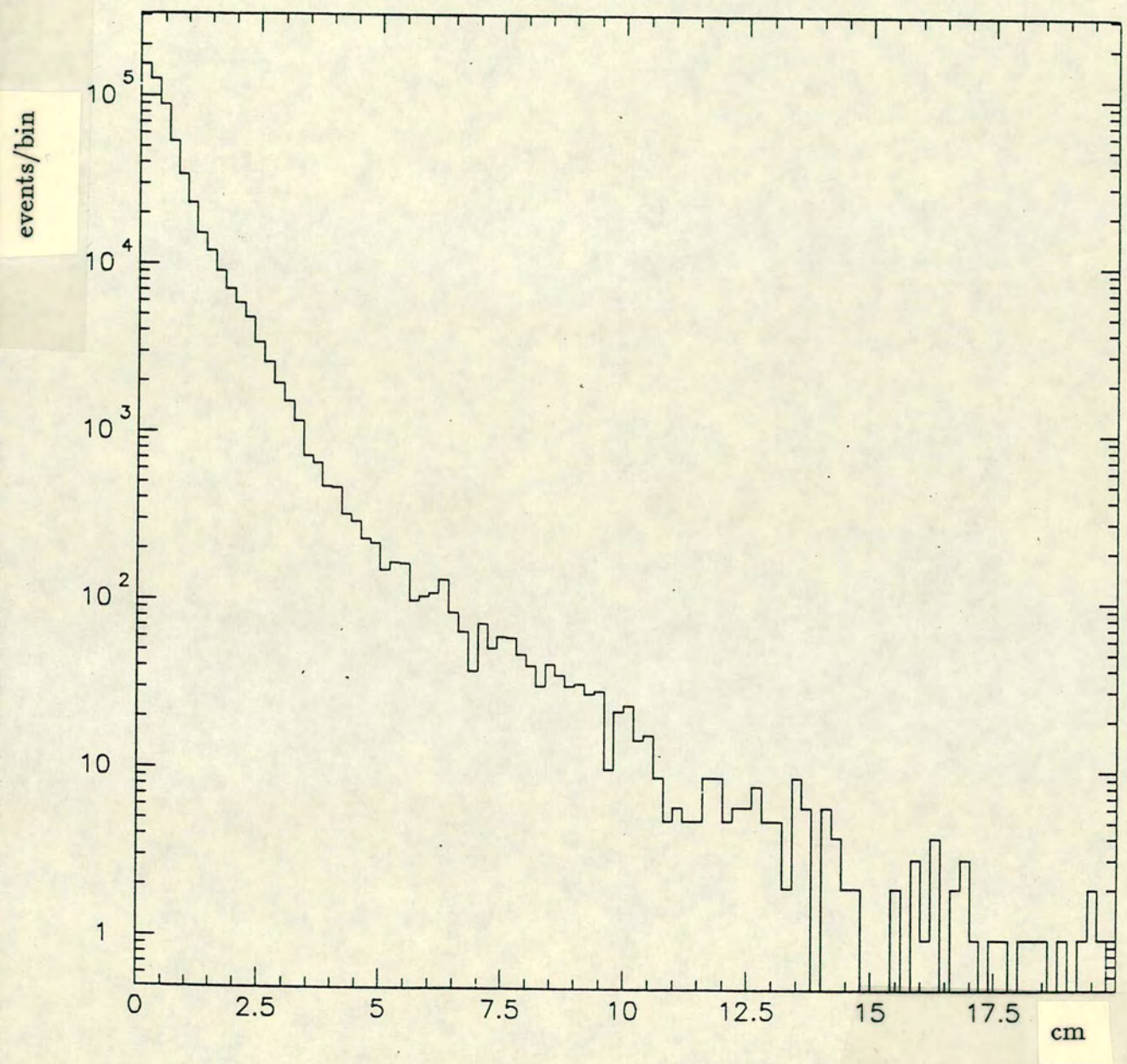

Figure 6.6: D_{targ} - KF

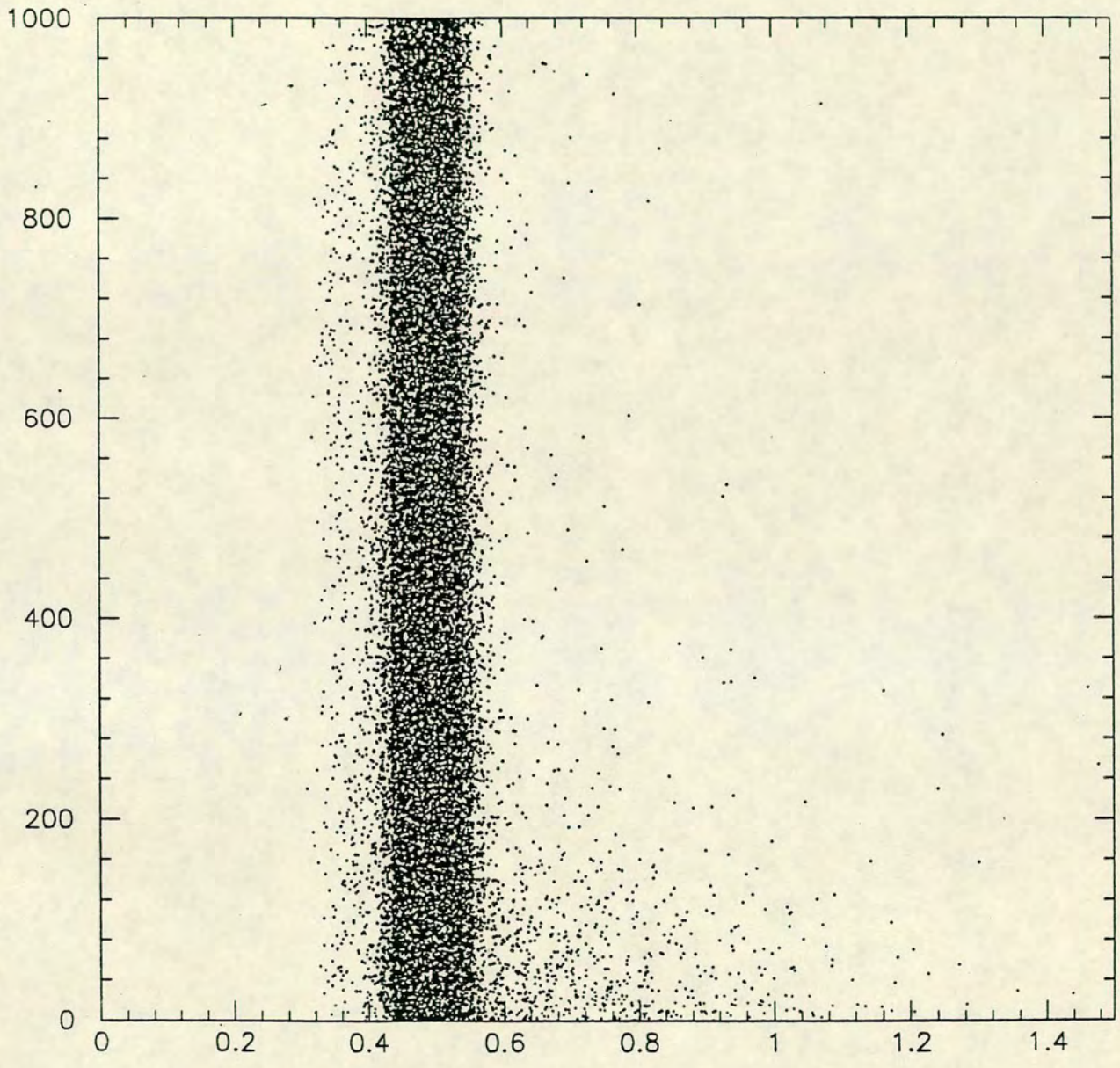

Figure 6.7: X=Reconstructed Kaon Mass, Y=Vertex Position(cm)

Figure 6.7 shows a distribution of reconstructed kaon mass versus vertex position. It can be seen that there is a tail at high kaon mass close to the collimator. This is thought to be due to neutron interactions in the cleaning collimator. Due to a lack of knowledge as to how this would extrapolate under the kaon mass peak, we cut away from the collimator. We accept only decays with $Z > 570$cm, where any background from neutron interactions is at the level of a fraction of a part per mille. The fiducial region within which decays are accepted is $570 < Z < 4890$cm.

Kaon Momentum

We accept decays where the kaon momentum is between 70 and 170 GeV. 70 GeV is thought to be a safe distance from online energy cuts (sections 3.7.2 and 3.7.3). Above 170 GeV there is very little information on the phases, since we are only a few K_S lifetimes from the KN or KF target, and we are not in the sensitive region of interference between K_L and K_S.

6.1.2 Background Subtraction for Charged Events

Background in the charged mode comes from three-body decays of K_L. Decays of K_L into $\pi^+\pi^-\pi^0$, $\pi\mu\nu$ or $\pi e\nu$ are much more numerous than decays into $\pi^+\pi^-$ (see table 3.1). In this section we shall describe the evaluation of background to the $\pi^+\pi^-$ signal from these three-body decays.

$\pi^+\pi^-\pi^0$ with a Photon close to a Pion Shower

There are two possible ways in which a $\pi^+\pi^-\pi^0$ event may become a background event to the $\pi^+\pi^-$ signal. The first is where one photon (or both) from the $\pi^+\pi^-\pi^0$ decay overlaps with a pion shower and is regarded as part of that shower. The second is where both photons pass outwith the detector and go undetected. We shall first discuss the case of overlapping photon and pion showers.

Fig 6.4 shows a distribution of photon energy against the distance of the photon from the nearest pion track, along with the cut designed to remove $\pi^+\pi^-\pi^0$ decays with an identified photon (see 6.1.1). For each photon energy, E, there is a given distance, d(E), which marks the division between what we regard as fluctuations in a pion shower, and what we regard as a genuine photon. There will, however, be $\pi^+\pi^-\pi^0$ events where the photons will lie nearer to the pion than the distance d(E). It is these events which will not be rejected, and will become background events. We need some way of estimating the number of such events.

For each energy E, we look for photons in the control region between $\sqrt{2}$d(E) and $\sqrt{3}$d(E) from the pion tracks. For every pion, and every photon energy E, we therefore have a circle of radius d(E) inside which we do not detect photons, and a ring of inner radius $\sqrt{2}$d(E) and external radius $\sqrt{3}$d(E) inside which we collect control events. These two regions have the same area. Monte Carlo studies show that photons from $\pi^+\pi^-\pi^0$ events populate the region around pion showers uniformly. Therefore by counting events with a photon in the control ring we have a measure of the number of events with a photon inside the circle of radius d(E). The background due to such decays has been measured at the level of 0.002% in KN, and 0.02% in KF. The background due to events of this configuration is so small that no background subtraction is carried out. It will be shown later that the final result is insensitive to charged background subtraction.

The second type of $\pi^+\pi^-\pi^0$ background, where neither photon enters the calorimeters, will be discussed, along with the $\pi e\nu$ and $\pi\mu\nu$ backgrounds, in the following section.

Extrapolation in the D_{targ} Distribution

The remaining backgrounds ($\pi e\nu$, $\pi\mu\nu$ and $\pi^+\pi^-\pi^0$) are subtracted together. A $\pi^+\pi^-\pi^0$ decay where the photons do not enter the calorimeters will typically fail the cut on the reconstructed kaon mass. A very small number of such events, where the photons are of low energy, will pass this cut. A $\pi\mu\nu$ event may become a background event when the muon loses it's energy by bremsstrahlung in the

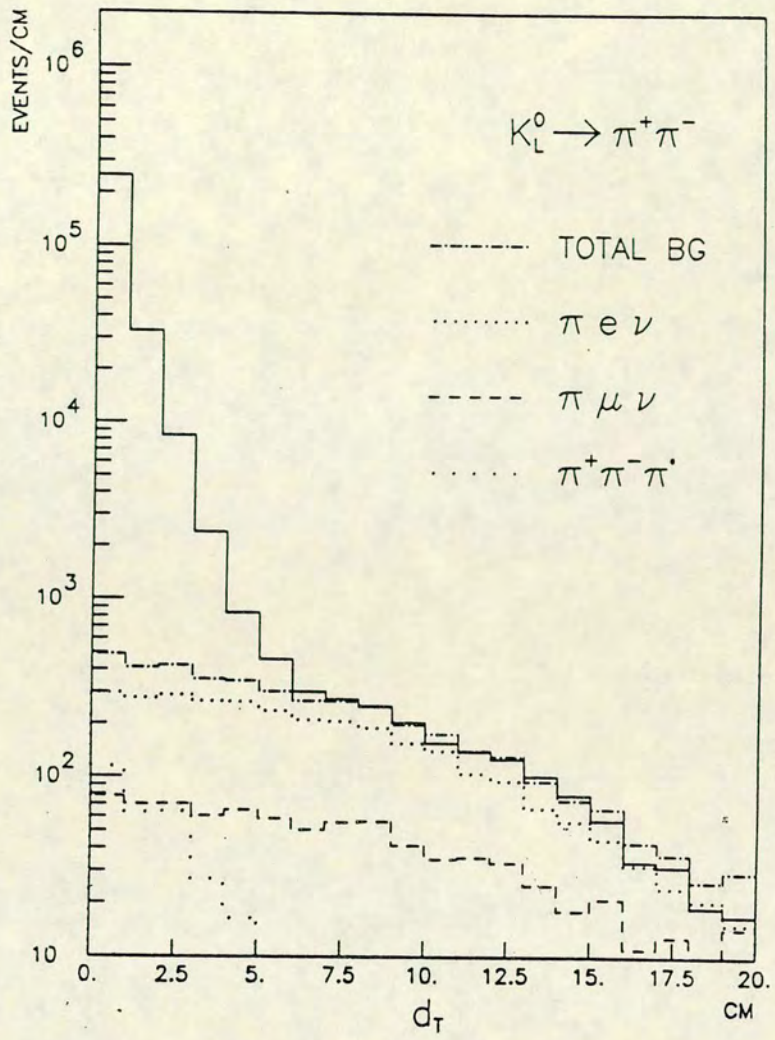

Figure 6.8: Charged Background Subtraction using the D_{targ} distribution

hadron calorimeter. A certain fraction of electrons from $\pi e\nu$ events will pass the electron rejection cuts (see 6.1.1) and the event will not be rejected.

Three body decays which provide possible background are characterised by missing momentum, carried away by a neutrino or a photon. We make use of this fact in subtracting the background due to such decays. Three-body decays have a much broader D_{targ} distribution than $\pi^+\pi^-$ decays. We reject decays with $D_{targ} > 5$cm, and use a region between 7cm and 12cm to collect background events. From an understanding of the D_{targ} distributions of the three-body decays, we may predict the number of background events under the signal region ($D_{targ} < 5$).

We make use of the knowledge which has been assimilated during previous analyses. Figure 6.8 shows the background subtraction for the K_L signal in 1986. In the background region ($7 < D_{targ} < 12$) the different types of three-body backgrounds were identified. $\pi e \nu$ events were identified by the well-defined electron shower width in the LAC. $\pi \mu \nu$ events were characterised by the shower width in the hadron calorimeter for tracks depositing less than 5GeV in the LAC, and the small number of residual events were regarded as $\pi^+\pi^-\pi^0$. Monte carlo studies, and background reference samples were used to determine the D_{targ} distribution shapes for these decay modes, and this provides enough information for background subtraction. We extrapolate from the background region under the signal region with an extrapolation factor of 1.7 . The background subtraction was carried out for each individual bin in momentum and longitudinal vertex position. The global background was $0.019 \pm 0.014\%$ in the KN beam, and $0.119 \pm 0.087\%$ in the KF beam. The background to signal ratio is a strong function of Z (because the proportion of K_L decays is a strong function of Z). This is demonstrated in figures 6.9 and 6.10.

6.2 Neutral Events

6.2.1 Cuts for Neutral Events

Number of Photons

Candidates for $K^0 \rightarrow \pi^0\pi^0$ decays are rejected unless they have exactly four photons after applying the 'merge' procedure of 5.4.

Spacepoints in Chamber 1

No space-points are tolerated in chamber 1. This leads to rejection of Dalitz decays, photon conversions, and events with accidental charged tracks.

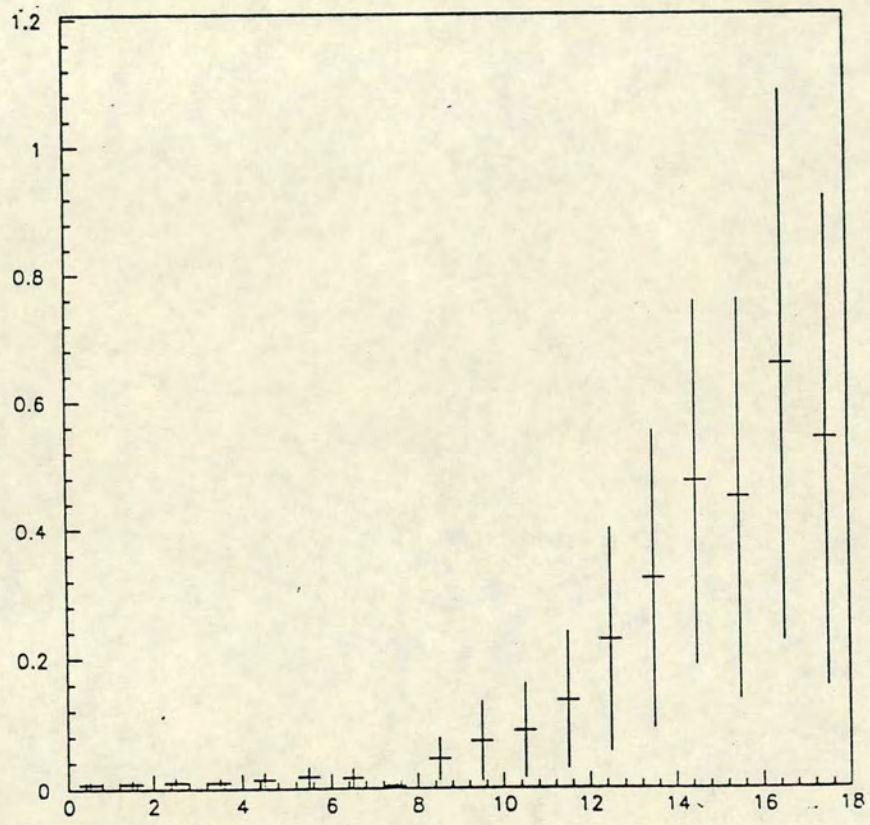

Figure 6.9: Charged Background Versus Z - KN - X=Bin Number, Y=% Background

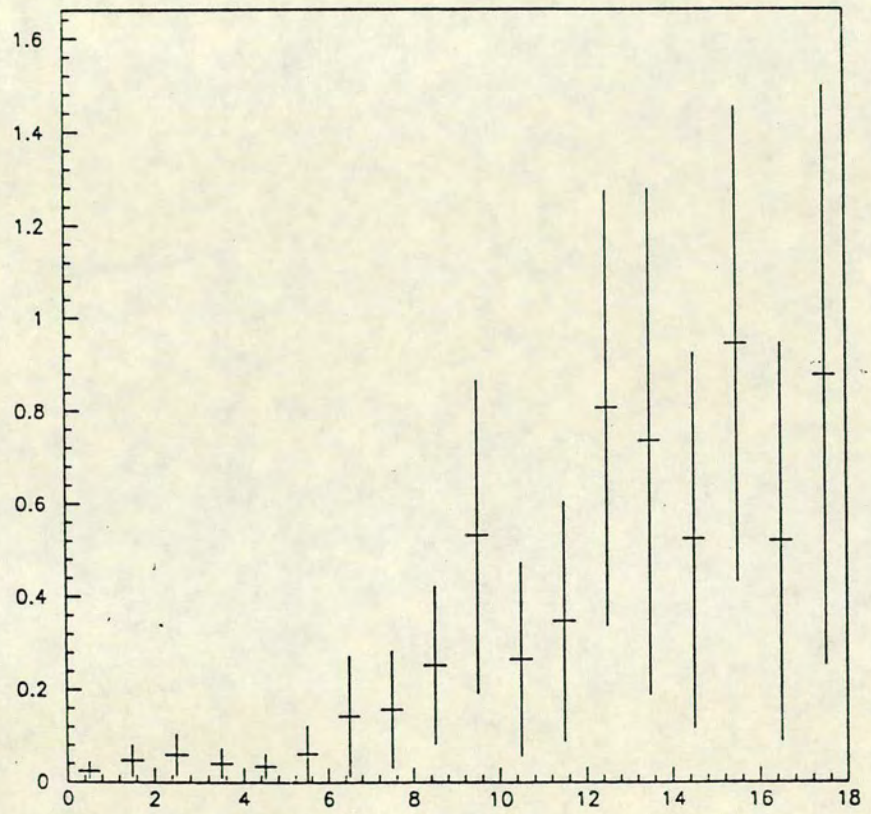

Figure 6.10: Charged Background Versus Z - KF - X=Bin Number, Y=% Background

Photon Energy

Events are accepted if all photons lie between 5 GeV and 100 GeV. Below 5 GeV detection may not be fully efficient, and the π^0 mass resolution deteriorates, since it is sensitive to the lowest energy photon. Above 100 GeV the energy on a single strip may exceed the limits of the ADC readout.

Distance Between Photons

Reconstruction problems may arise if photons are too close in space. For this reason we reject events where the minimum distance between two photons is less than 5cm.

Centre of Gravity

The distance from the beam axis to the centre of gravity of the energies (COG) must be less than 10cm. For events where all photons are recorded by the detector, the maximum COG is given by the beam divergence, and should not exceed 5cm at the LAC for either the KN or KF beam. This cut is designed to remove $3\pi^0$ events with missing photons. $2\pi^0$ decays of scattered kaons would also be rejected.

π^0 Masses

The masses of the the two reconstructed pions are correlated, due to the kaon mass constraint (see 4.3). For this reason we do not cut around the individual π^0 masses (fig 6.11), but use a cut in the two dimensional plot of the two pion masses. Figure 6.12 shows the two reconstructed pion masses. The elliptical rings shown are of equal area, and correspond to integer values of the quantity μ_{ell}, as defined below. Note the correlation between the pion masses for events inside the first ellipse. The resolution of the sum of the pion masses is 2.2 MeV,

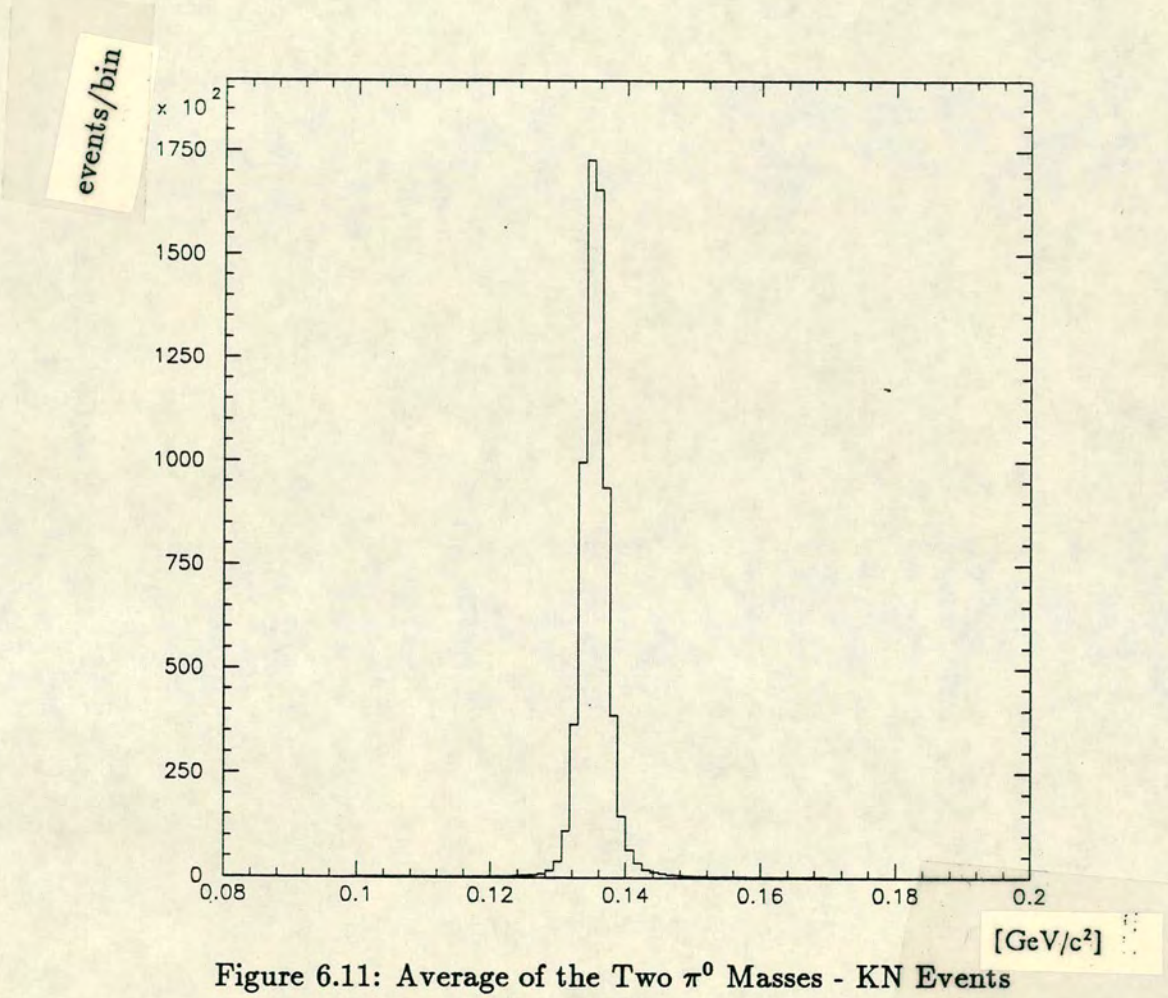

Figure 6.11: Average of the Two π^0 Masses - KN Events

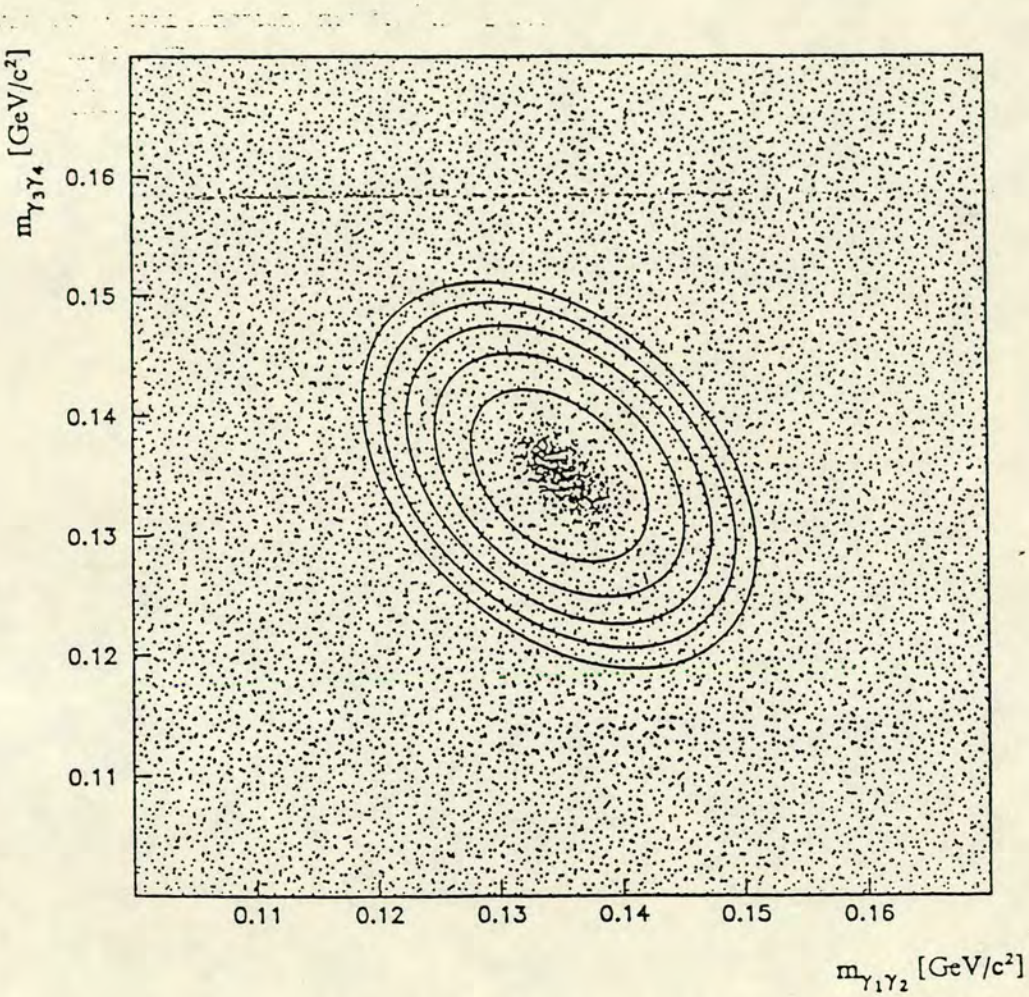

Figure 6.12: m_{π_1} versus m_{π_2}

and the difference has a resolution of 3.7 MeV.

$$\mu_{ell} = ((m_{\gamma_1\gamma_2} + m_{\gamma_3\gamma_4} - 2m_{\pi^0})/8MeV)^2 \; + \; ((m_{\gamma_1\gamma_2} - m_{\gamma_3\gamma_4})/12MeV)^2 \quad (6.6)$$

Events with $\mu_{ell} > 1$ are rejected. This is once again a cut against $3\pi^0$ events. The distribution of μ_{ell} will be used to measure the background due to $3\pi^0$ decays.

6.2.2 Background Subtraction for Neutral Events

Background to the $\pi^0\pi^0$ signal comes from $3\pi^0$ decays with missing photons. We will use the quantity μ_{ell} to determine the magnitude of this background.

Figure 6.13 shows a distribution of μ_{ell} for neutral events in the KF mode. Monte Carlo studies [16] tell us that the μ_{ell} distribution should be flat for $3\pi^0$ events with missing photons, out to high ellipse number. We know, from Monte Carlo studies, and also from K_S data in 1986, that a negligible number of $\pi^0\pi^0$ events will lie ouside the first few ellipses. We may therefore extrapolate from a background collection region, in this case $7 < \mu_{ell} < 13$, under the signal region ($\mu_{ell} < 1$), with a slope of 0. The background has been measured to be $0.253 \pm 0.029\%$ in KN, and $0.795 \pm 0.013\%$ in KF. The background to signal ratio is heavily dependent on the longitudinal decay position. This is due firstly to the short lifetime of the K_S, which has no background, and also because $3\pi^0$ events with missing photons have their reconstructed vertex shifted towards the detector relative to the real vertex position (see section 4.3). The background is subtracted on a bin by bin basis for each bin in momentum and vertex position.

Figures 6.14 and 6.15 show the background in KN and KF as a function of Z. Figures 6.16 to 6.19 show the momentum and vertex distributions, after cuts, for charged and neutral events at each target station.

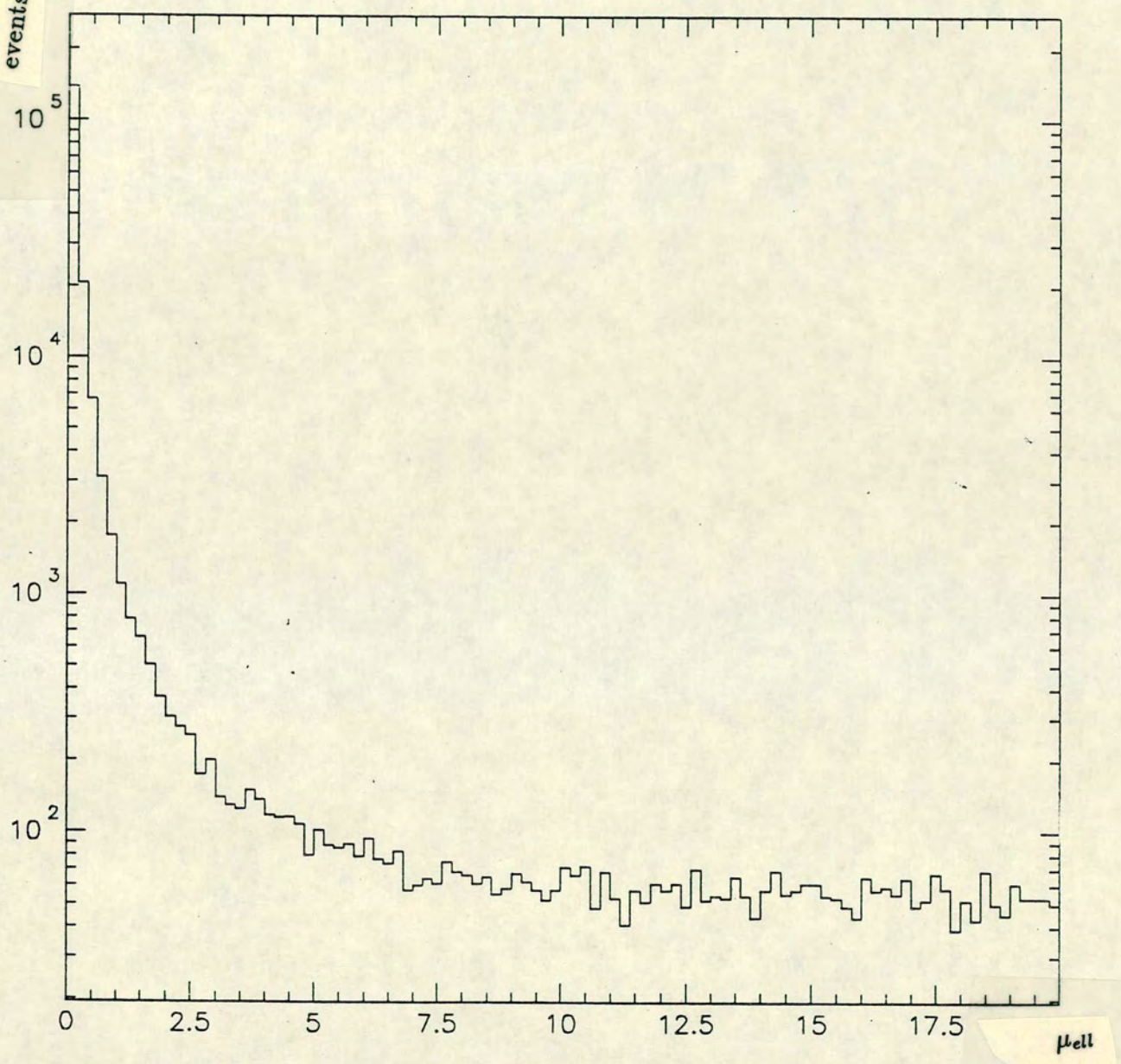

Figure 6.13: μ_{ell} Distribution - KF

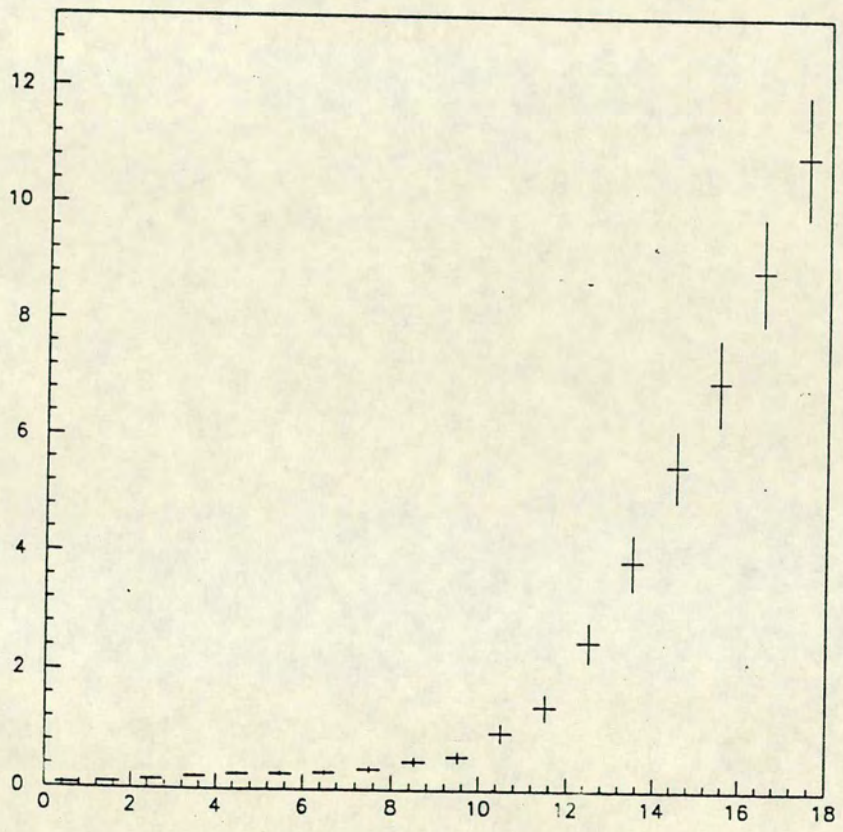

Figure 6.14: Neutral Background Versus Z - KN - X=Bin Number, Y=% Background

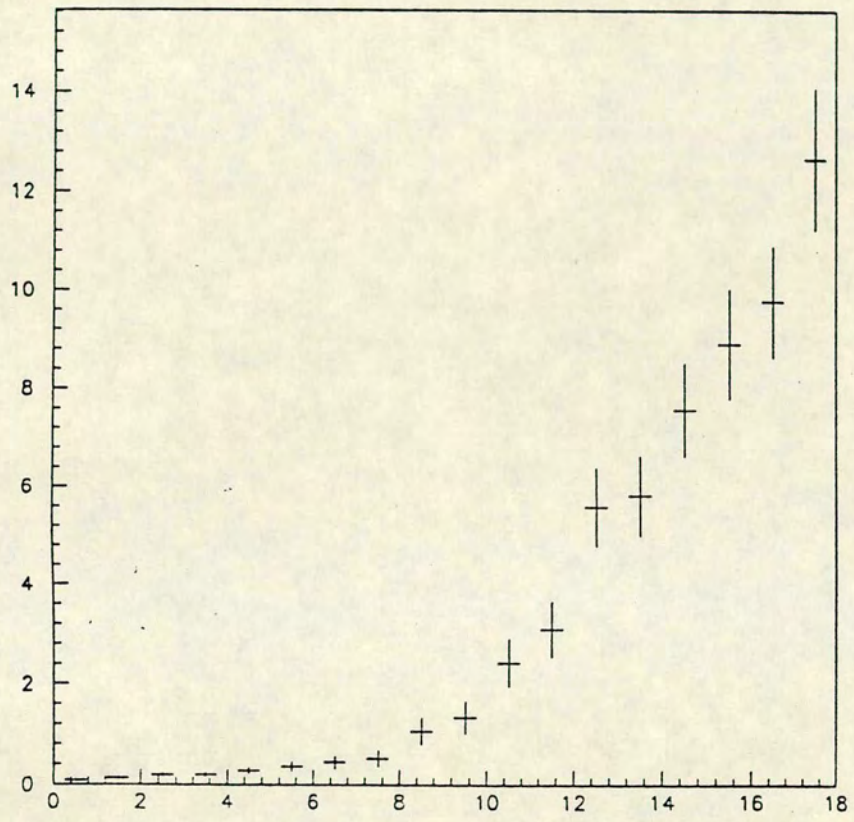

Figure 6.15: Neutral Background Versus Z - KF - X=Bin Number, Y=% Background

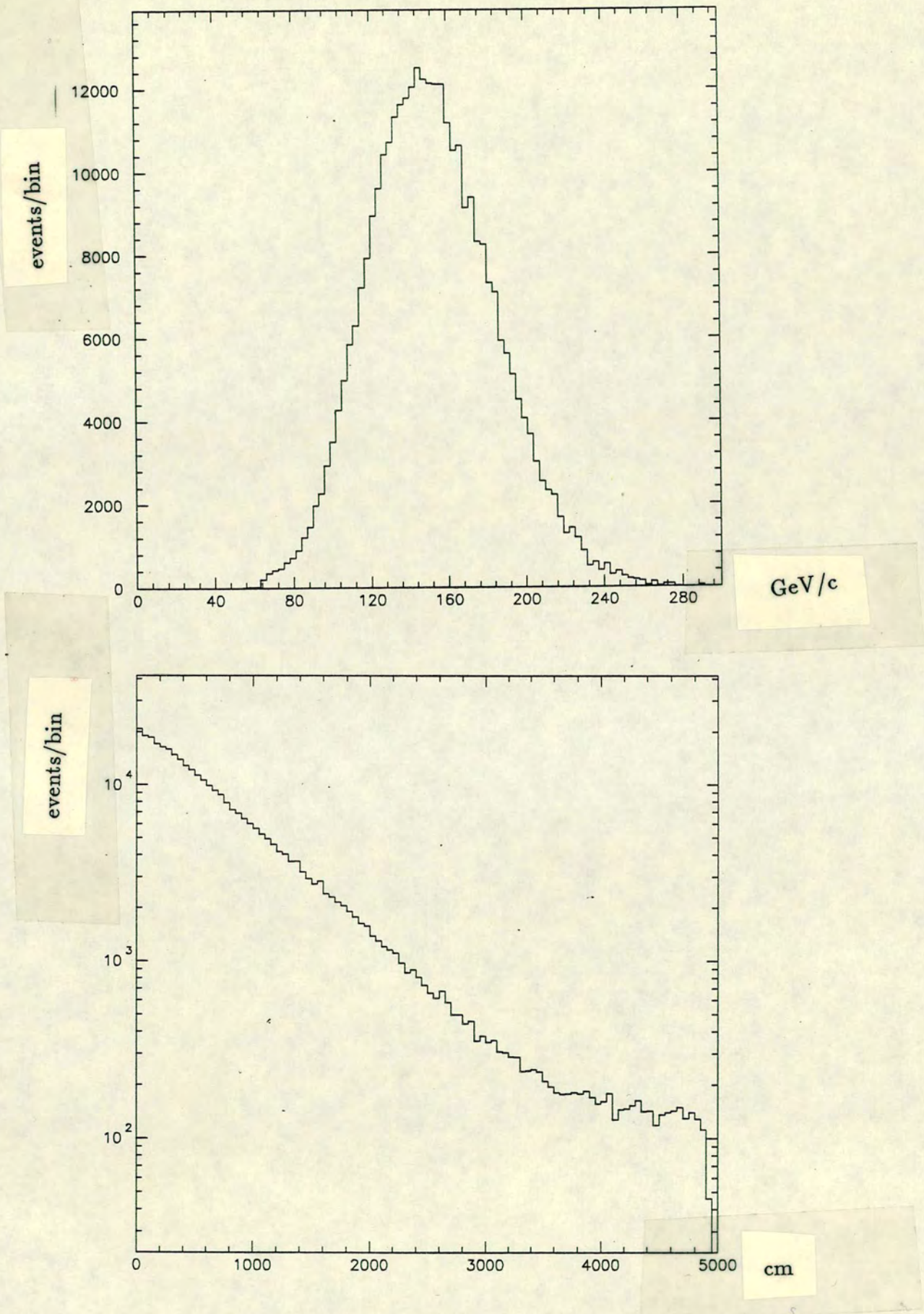

Figure 6.16: Momentum and Vertex Distributions - $\pi^0\pi^0$ - KN

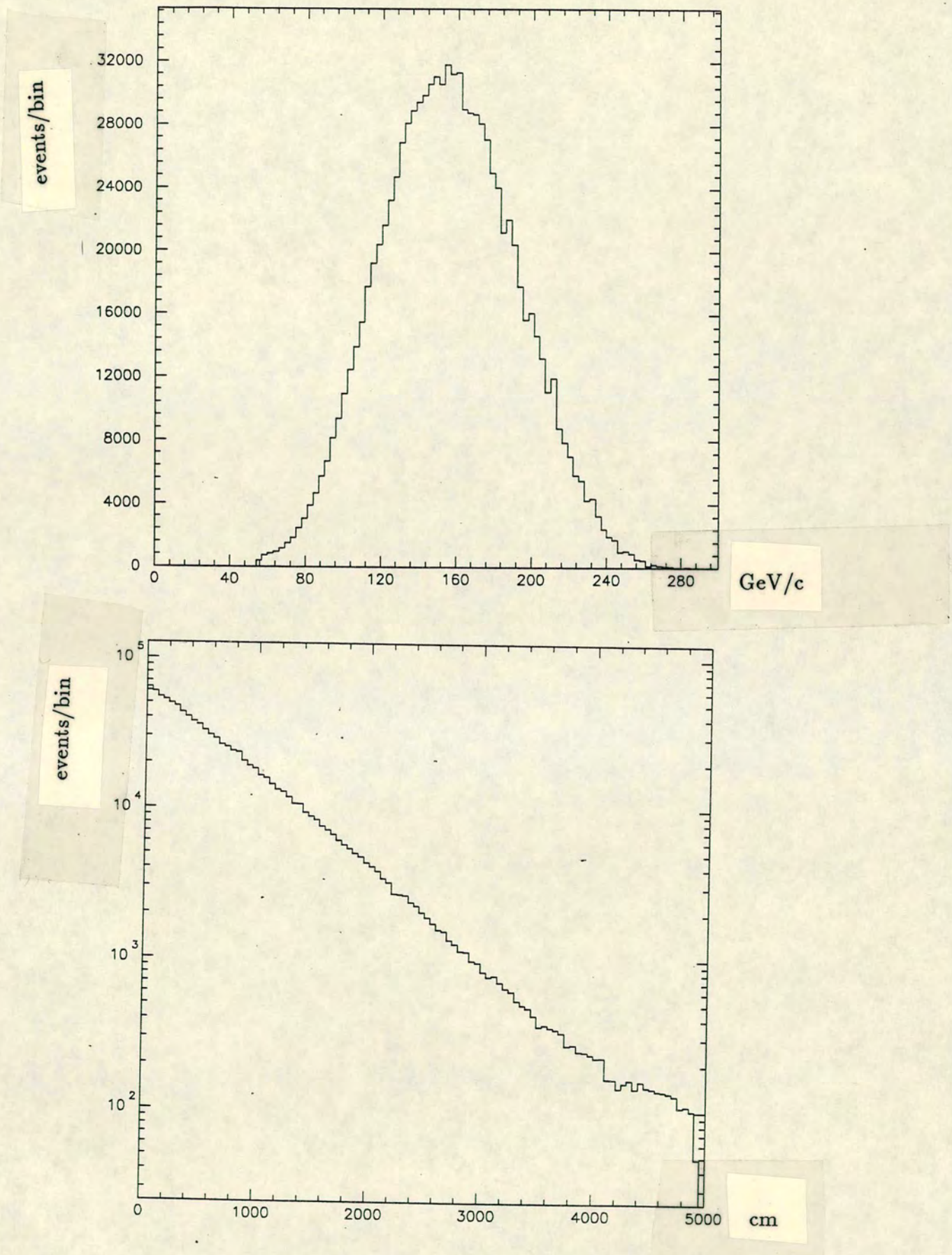

Figure 6.17: Momentum and Vertex Distributions - $\pi^+\pi^-$ - KN

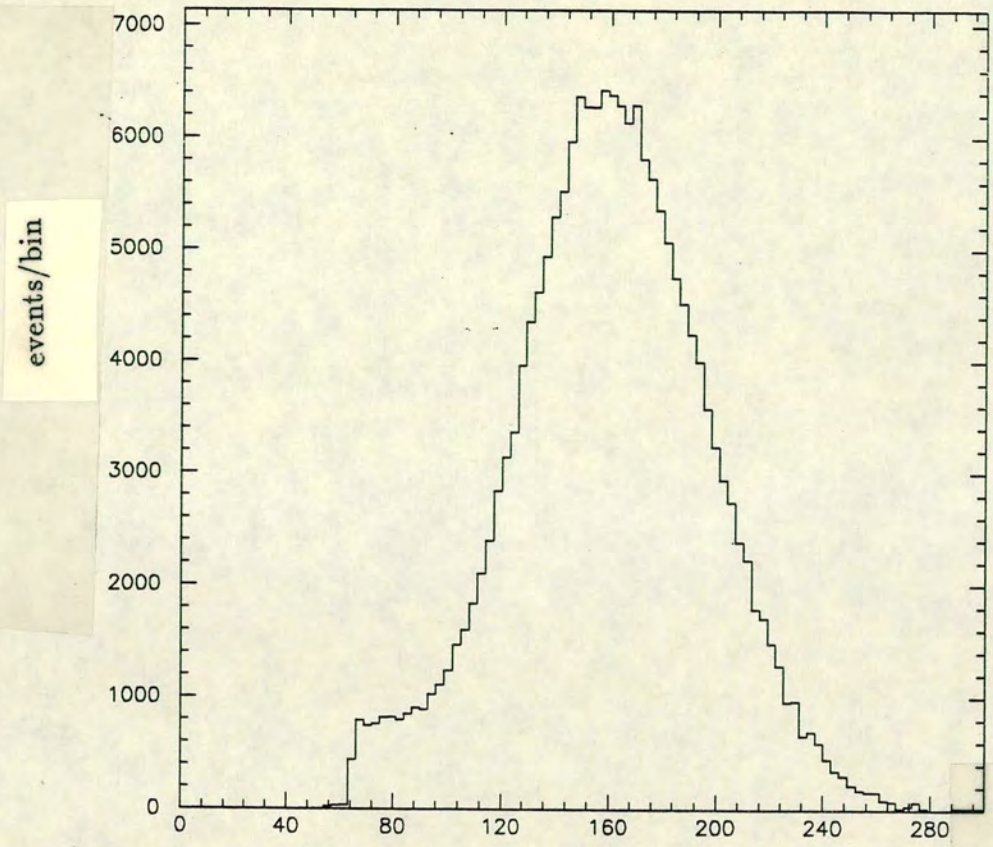

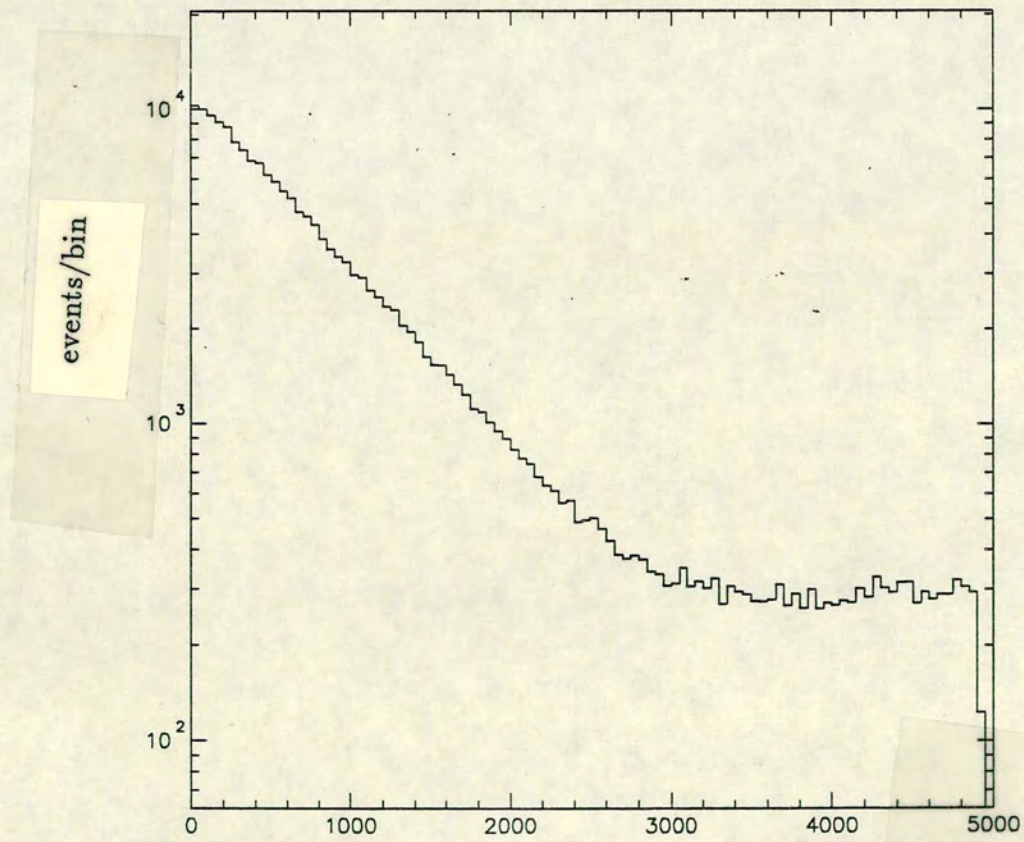

Figure 6.18: Momentum and Vertex Distributions - $\pi^0\pi^0$ - KF

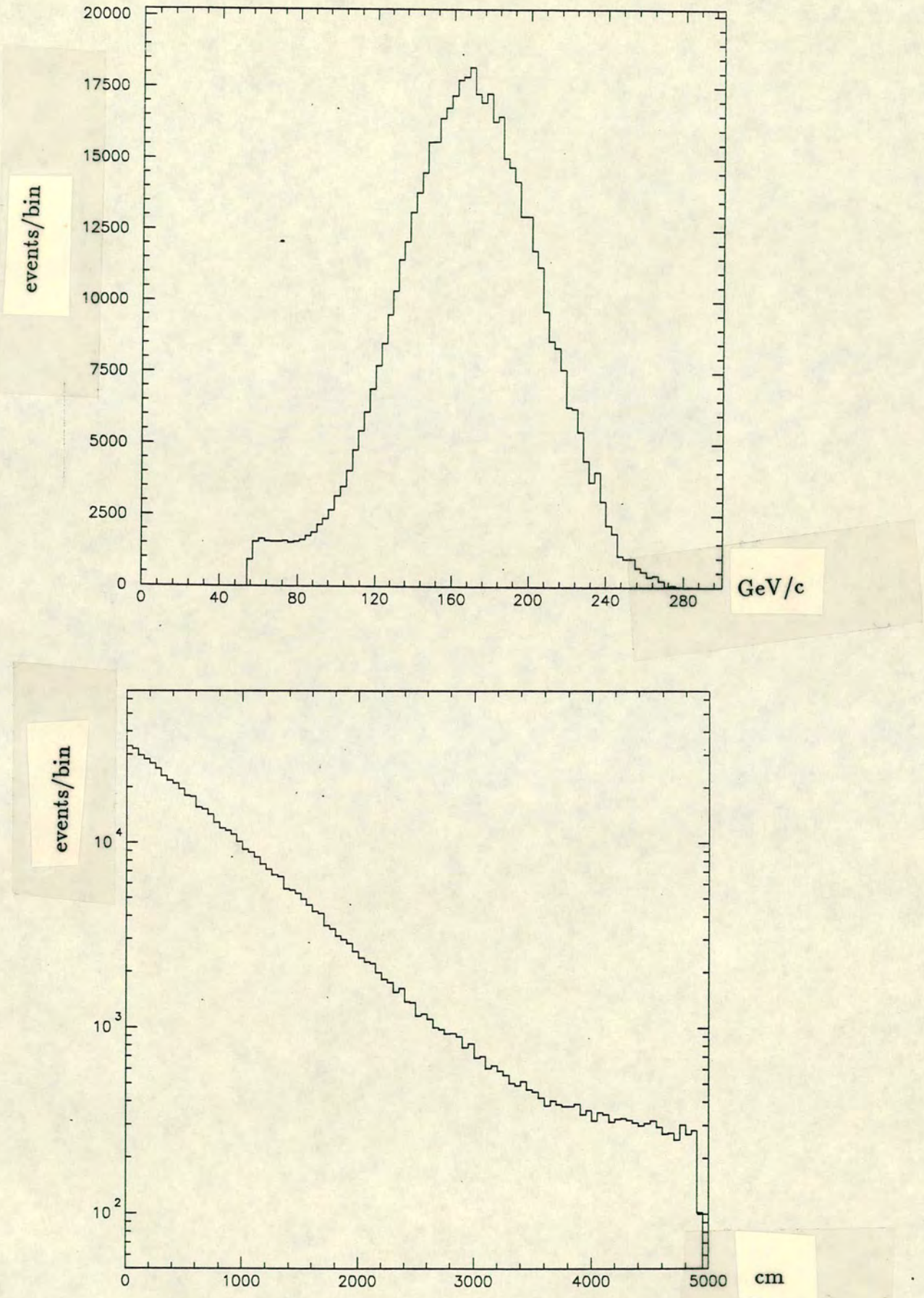

Figure 6.19: Momentum and Vertex Distributions - $\pi^+\pi^-$ - KF

Chapter 7

Results

7.1 Introduction

Having described data selection and background subtraction, we will now discuss the fitting procedure which yields results on the difference between ϕ^{+-} and ϕ^{00}.

We use bins of 5 GeV in momentum, between 70 and 170 GeV. The bins in longitudinal vertex position are 240 cm long, between 570 and 4890 cm in the NA31 coordinate system. These bin sizes were chosen to be typically a few times the resolution in both momentum and vertex. There are, therefore, 20 bins in momentum and 18 in vertex position.

As described in chapter 4, the philosophy behind the analysis is that a division of data from one target by data from the other will result in a cancellation of acceptance, and render the use of a Monte Carlo un-necessary. For all bins in momentum and vertex we count the number of events, after lifetime weighting (see section 3.7.3), in KN and KF. The numbers of events falling within these cuts (after weighting) are shown in table 7.1. The number of events in a bin for KN and KF are refered to as DATAN(I,J) and DATAF(I,J), where I and J denote the bin under consideration. The error on each of these numbers (ERRN(I,J) or ERRF(I,J)) is given by the the square root of the sum of the squares of the

KN	$\pi^+\pi^-$	3,156,997
	$\pi^0\pi^0$	1,234,691
KF	$\pi^+\pi^-$	471,966
	$\pi^0\pi^0$	182,552

Table 7.1: Final Event Statistics - After Weighting

weights for events in the bin. We define:

$$\begin{aligned} DATA(I,J) &= DATAN(I,J)/DATAF(I,J) \\ ERR(I,J) &= (ERRN(I,J)/DATAF(I,J)) \\ &+ (DATAN(I,J)ERRF(I,J)/DATAF(I,J)^2) \end{aligned} \quad (7.7)$$

We need a theoretical function in order to fit theory to data. Equation 4.1 gives the time distribution of $K^0 \rightarrow \pi\pi$ events after a target. We define :

$$\begin{aligned} F_n(I,J) &= S(p)[e^{-t_n/\tau_S} + \mid\eta\mid^2 e^{-t_n/\tau_L} + 2\mid\eta\mid D(p)e^{-\frac{(t_f/\tau_L+t_f/\tau_S)}{2}}cos(\Delta m t_n - \phi)] \\ F_f(I,J) &= S(p)[e^{-t_f/\tau_S} + \mid\eta\mid^2 e^{-t_f/\tau_L} + 2\mid\eta\mid D(p)e^{-\frac{(t_f/\tau_L+t_f/\tau_S)}{2}}cos(\Delta m t_f - \phi)] \end{aligned} \quad (7.8)$$

where t_n and t_f are calculated from the central momentum and vertex positions for the bin, and the Z position of the target. F_n and F_f describe the interference beams from the KN and KF targets respectively. Then

$$PRED(I,J) = F_n(I,J)/F_f(I,J) \ . \quad (7.9)$$

We leave certain parameters free in the expression PRED(I,J), and fit the theoretical expression to the data. This will give experimental values for the parameters left free, in particular the phases ϕ^{+-} and ϕ^{00}. The contribution to χ^2 per bin is given by

$$DCHISQ(I,J) = (DATA(I,J) - RK.PRED(I,J))^2/ERR(I,J)^2 \quad (7.10)$$

where RK is a normalisation term, the ratio of the kaon fluxes at the two targets. Figure 7.1 shows how the theoretical function PRED would look with and without interference at 100GeV. The dotted line shows the function with no interference, using typical values for all parameters, and the solid line shows the function with a phase, ϕ, of 45^0.

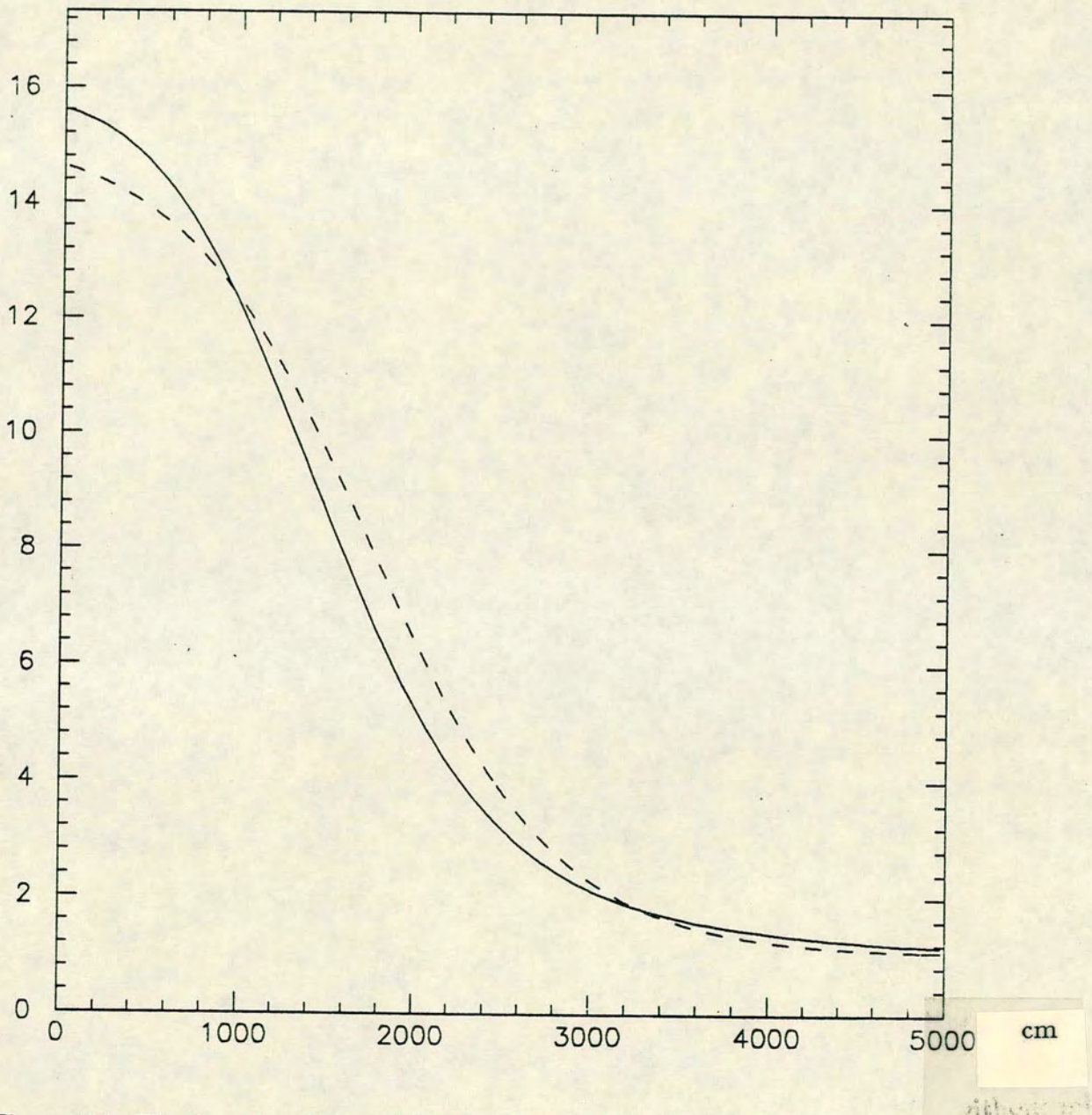

Figure 7.1: The functional form PRED at 100GeV - with and without interference

7.2 Details of the Fitting Procedure

In this section we will examine which parameters are left free in the fit, and discuss how we take care of the effects of bin-centring, and resolution in momentum and vertex position. The fit is carried out using the MINUIT [17] package available at CERN. As explained in chapter 4, we will calculate the charged and neutral phases in the same fit, thus reducing the sensitivity of the difference of these parameters to certain other parameters in the theoretical formula.

7.2.1 Free and Fixed Parameters in the Fit

Let us first consider the theoretical function PRED, and discuss which parameters must be fixed, and which fitted, during the fitting procedure. Parameters which must be left free in the fitting procedure are those which we wish to calculate, or those which are not well enough known to fix. Parameters which it is desirable to fix are those which are well measured experimentally. It may be necessary to fix some parameters which, because of the nature of the theoretical formula, are highly correlated to parameters which cannot be fixed.

To calculate the phases ϕ^{+-} and ϕ^{00} we must obviously leave them as free parameters in the fit.

The dilution factor, D(p), is as yet a poorly measured quantity, and we must leave it free in the fit. Since D(p) is momentum dependent, we will allow the value of D(p) to differ across the momentum range. We calculate a value of D(p) for each momentum bin, so the fit contains the twenty free parameters D(1)...D(20). The dilution factor is constrained to be the same in both charged and neutral modes.

The other factor which we leave free in the fit is the normalisation term RK, which is an unknown quantity. We might expect this normalisation factor to be the same for charged and neutral modes, but there are small effects which can result in the measured value being different for charged and neutral. A difference

in the rate at which accidentals kill charged and neutral events in the two beams, or a small difference between charged and neutral energy scales, for example, could result in different values for the charged and neutral normalisations. We therefore fit separate normalisation factors, RKC and RKN, for charged and neutral modes.

The K_L lifetime, τ_L, is a well-measured quantity, and may be fixed during the fitting procedure.

The mass difference Δm, the difference between the K_L and K_S masses, is not a quantity which has been precisely measured. Ideally one would like to calculate this quantity during the fit. Due to the functional form of the interference expression, this is not possible. The only place that Δm appears is inside the cosine term $cos(\Delta mt - \phi)$. The phase ϕ (ϕ^{+-} or ϕ^{00}) is a free parameter. If Δm were free then we would arrive at the situation where an increase in Δm could be compensated by an increase in ϕ without a change in the overall value of the cosine term. In fact, the two parameters are totally correlated, and since we wish to measure ϕ^{+-} and ϕ^{00}, we must fix the term Δm.

The last two parameters which we must discuss are the K_S lifetime τ_S and the CP-violation term η (η^{+-} and η^{00} are sufficiently close in value that we may neglect the difference between them without affecting the calculated values of ϕ^{+-} and ϕ^{00}). Initially these parameters were left as free parameters in the fit. The results obtained gave results for η and τ_S which did not compare favourably with the currently accepted results. Further investigation revealed that both of these parameters are highly correlated with the dilution factor D(p), which must be left free. The correlation coefficients (as defined in the MINUIT manual) between η and D(p), and between τ_S and D(p), were both greater than 0.9. This is unacceptably high. If we examine the function describing interference (equation 4.1), we see that although both η and τ_S are present in one of the first two terms, they are both present in the third term, along with D(p). Any correlation is due to the fact that both η and D(p), or τ_S and D(p), may change without altering the value of the whole interference expression. Attempts to leave either η or τ_S free, with the other fixed, still showed very high correlations between the free parameter and D(p). For this reason both η and τ_S must be

Input Parameters	τ_S	$(0.8923 \pm 0.0022)10^{-10}$s
	τ_L	$(5.183 \pm 0.040)10^{-8}$s
	η	$(2.275 \pm 0.021)10^{-3}$
	Δm	$(0.5641 \pm 0.0023)10^{-24}$J

Table 7.2: Input Parameters in the Fitting Procedure

input as fixed parameters. The values used for the fixed input parameters are taken from the Particle Data Booklet, and are shown in table 7.2, along with the measurement errors.

For parameters which are fixed during the fit, a systematic error on the phases ϕ^{+-} and ϕ^{00}, resulting from the measurement error of the fixed parameter, will be evaluated (see section 7.3).

7.2.2 Resolution and Bin-Centring Effects

In our fitting procedure we must take care of the effects of resolution in momentum and vertex position, and any effects due to the fact that the phase function changes over the finitely sized bins. The resolutions in p and z will move events from one bin to the other. If the function is not flat, then this will occur in an asymmetric way, resulting in an absolute change in the number of events in certain bins. Due to the fact that the phase function changes over the size of a bin, the values which we use to calculate the number of lifetimes from the target (namely the central values for momentum and vertex for that bin) will not represent the average value of momentum and vertex for events in the bin. This, if unaccounted for, would result in errors in the calculated values of the phases ϕ^{+-} and ϕ^{00}. The effects of resolution and bin-centring may be taken care of at the same time, and the method is described below. Let us first introduce the relevant resolutions for charged and neutral events.

The vertex resolutions for charged and neutral decays are calculated at the same time as the energy scales. This procedure involves a fit to the position of the K_S anti-counter, using K_S data, and will be described in section 7.3.2. The vertex resolution is roughly 120cm for neutral events, and 100cm for charged events.

Vertex	$\pi^+\pi^-$	$\sigma_z = 100$cm
	$\pi^0\pi^0$	$\sigma_z = 120$cm
Momentum	$\pi^+\pi^-$	$\sigma_E = 1.2\%$E
	$\pi^0\pi^0$	$\sigma_E = 8\%\sqrt{E}$

Table 7.3: Vertex and Momentum Resolutions - Charged and Neutral

The energy resolution for neutral events comes solely from the energy resolution of the liquid argon calorimeter. This has been measured, using calibration beams of known energy, to be $8\%\sqrt{E}$. The energy resolution for charged decays comes from both the calorimeter resolution and the spacepoint resolution in the wire chambers (see equation 4.3). The momentum resolution in the charged mode is typically $\sigma_E = 1.2\%$E. These resolutions will be used in the fitting procedure. They are summarised in table 7.3.

To calculate the effect on the final result due to resolution in momentum and vertex, we must calculate the numbers of events which a given bin gains and loses due to smearing in both quantities. This is achieved in the following way. For each (p,z) bin we define a region in momentum and vertex which extends beyond the bin boundaries by 5GeV in p, and by 400cm in z, in both positive and negative directions. We therefore have, for each bin, a region of 15GeV by 1040cm, the centre of which is the centre of our initial bin. This region is subdivided into 3120 regions of 0.25GeV by 20cm, some of which lie inside the original bin, and some of which lie outside. We make an initial fit of the function PRED to the data, using only our initial (5GeV,240cm) bins, to calculate the quantities ϕ^{+-}, ϕ^{00}, RKC(charged), RKN(neutral) and D(1)...D(20). There are 720 bins (360 charged, 360 neutral) and 24 free parameters (charged and neutral phases, charged and neutral normalisation terms and a dilution factor term for each of 20 momentum bins). There are, therefore, 696 free parameters. The values obtained were:

$$\begin{aligned} \phi^{+-} &= 47.1 \pm 1.5^0 \\ \phi^{00} &= 49.3 \pm 2.3^0 \\ RKC &= 1.041 \pm 0.003 \\ RKN &= 1.031 \pm 0.003 \\ \chi^2 &= 738/696 \end{aligned} \tag{7.11}$$

We use these raw results as an initial indication of the shape of the phase function PRED, for both charged and neutral modes, and re-calculate results in a way which accounts for resolution and bin-centring effects.

For each bin, and for each 0.25GeV by 20cm sub-bin, we use the above results to calculate the expressions F_n and F_f at the centre of each sub-bin. We must then calculate the contribution to the initial bin from each of the 3120 sub-bins. For this we need to know the resolution in momentum and vertex, the momentum spectrum, and the acceptance. The resolution functions in momentum and vertex are assumed to be Gaussian, and the resolution values are summarised in table 7.2. The momentum spectrum of kaons at the target is obtained from K_S data, and is parameterised as follows.

$$S(p) = p^{1.671} e^{-p/33.04} \tag{7.12}$$

The acceptance used is a parameterisation obtained from K_L data in 1986. It should be remembered that a division of data occurs, and that this will result in a cancellation of the effects of the momentum spectrum and the acceptance. These are included for completeness, but a fit neglecting these terms yielded the same results. The contribution to each bin from each of the sub-bins was determined as follows:

$$SM = F_i.A.S(p).e^{-(z-z_0)^2/2\sigma_z^2}.e^{-(p-p_0)^2/2\sigma_p^2}. \tag{7.13}$$

where F_i is either F_n or F_f calculated at the centre of the sub-bin, A is the acceptance in the sub-bin, S(p) is the momentum spectrum, z and p represent the centre of the sub-bin, and z_0 and p_0 represent the centre of the initial 5GeV by 240cm bin. The functions F_n(I,J) and F_f(I,J) are simply the sum of the contributions to these functions from each of the sub-bins.

Using this technique, the results obtained were as follows:

$$\begin{aligned} \phi^{+-} &= 46.8 \pm 1.5^0 \\ \phi^{00} &= 48.9 \pm 2.3^0 \\ RKC &= 1.039 \pm 0.003 \\ RKN &= 1.031 \pm 0.003 \\ \chi^2 &= 739/696 \end{aligned} \tag{7.14}$$

The values for the dilution factor are shown in figure 7.2. A second iteration, using these results as input parameters, gave the same results. Because we are now dealing with very small sub-bins in momentum and longitudinal vertex position, the functions F_n and F_f will not change much over a sub-bin. Therefore the values used to calculate the number of lifetimes from each target will be very close to the average value of momentum and vertex in the sub-bin, and we will have very small errors due to bin-centring effects. The errors quoted above are purely statistical. We will now consider systematic errors. It should be noted that if we fit for one of the phases and the difference between the two, then the difference between the two phases is the same as above, and the statistical error is the error obtained if the errors on each phase are added in quadrature.

Figures 7.3 to 7.8 show typical plots of the fit result for charged and neutral data. The data points represent DATA(I,J) points for KN/KF over the longitudinal decay region, and the solid line is the function PRED using the output values of the fitting procedure.

7.3 Systematic Errors and Corrections

In this section we will discuss systematic errors to the result. There is one correction to be made to the above results, and we will consider this first.

7.3.1 Correction due to Acceptance Non-Cancelletion

Central to the analysis is the assumption that, for any given bin in momentum and vertex position, the acceptance is the same for KN and KF beams. When making this assumption we must consider any differences between the two beams which might invalidate the assumption, and how they might effect the calculated results. The only major difference between the two beams is the fact that they originate from different target stations. This, when coupled with the collimator geometries, means that the two beams have different divergences, and a different

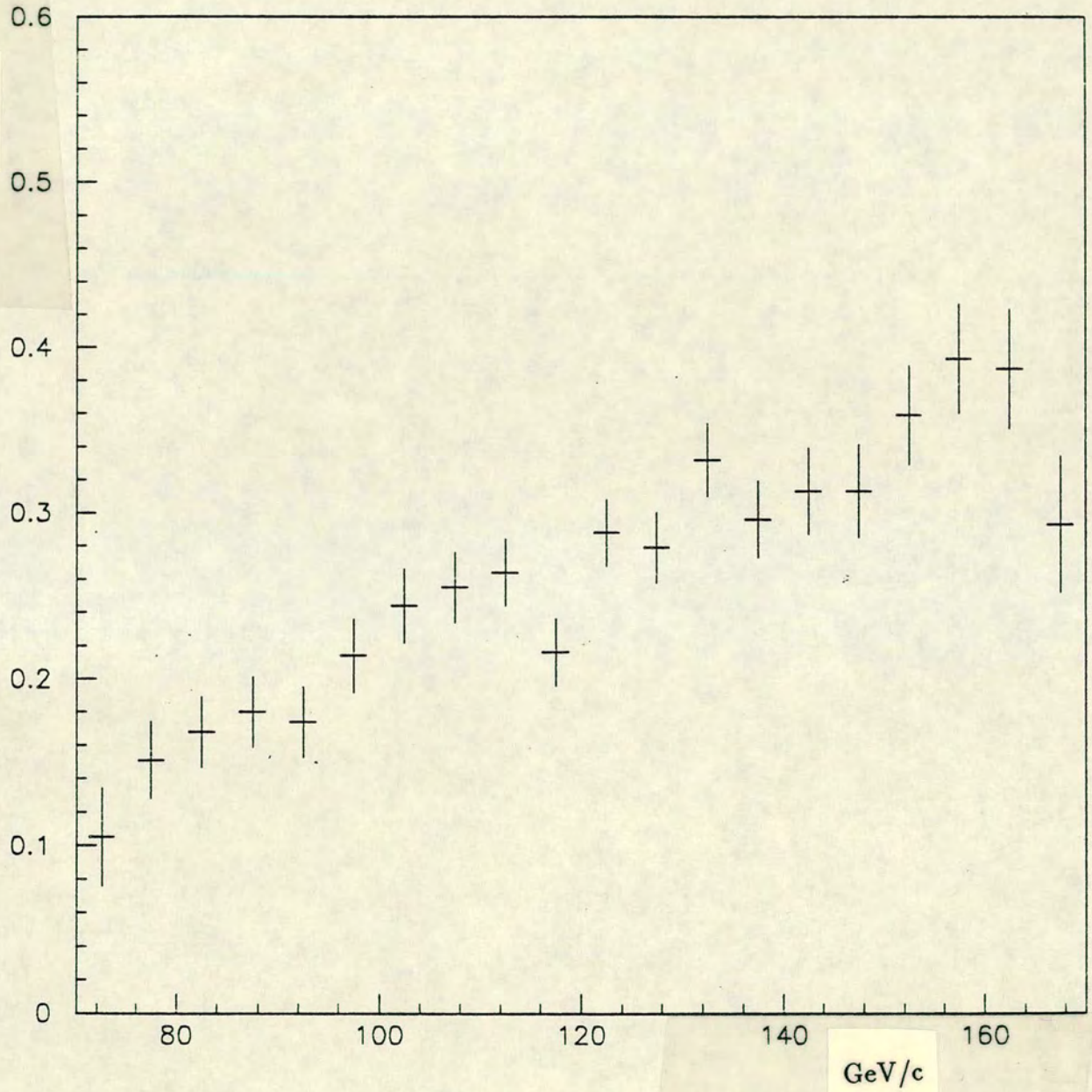

Figure 7.2: The Dilution Factor

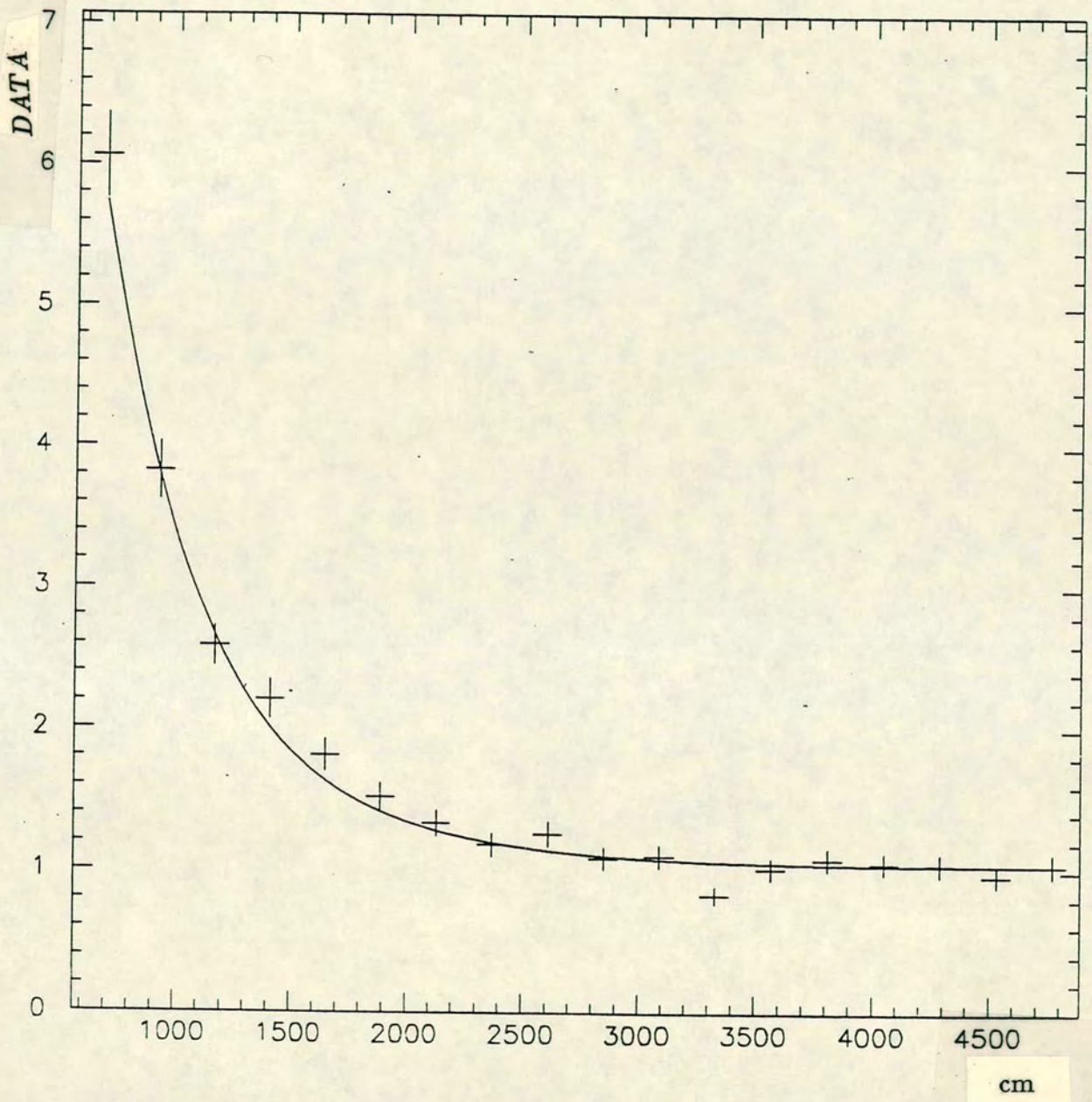

Figure 7.3: Fit Result - Charged Data - 70 to 75 GeV

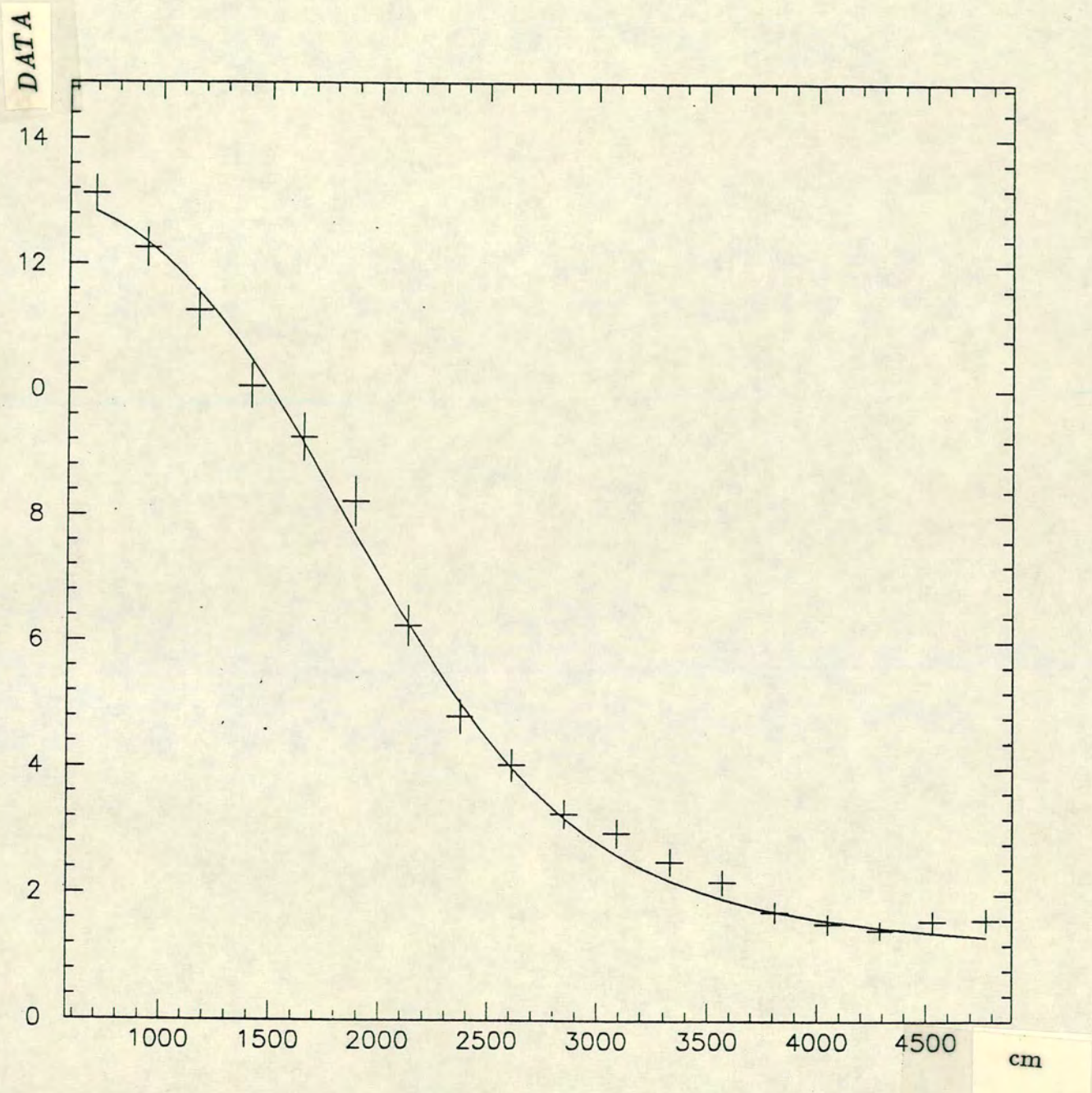

Figure 7.4: Fit Result - Charged Data - 105 to 110 GeV

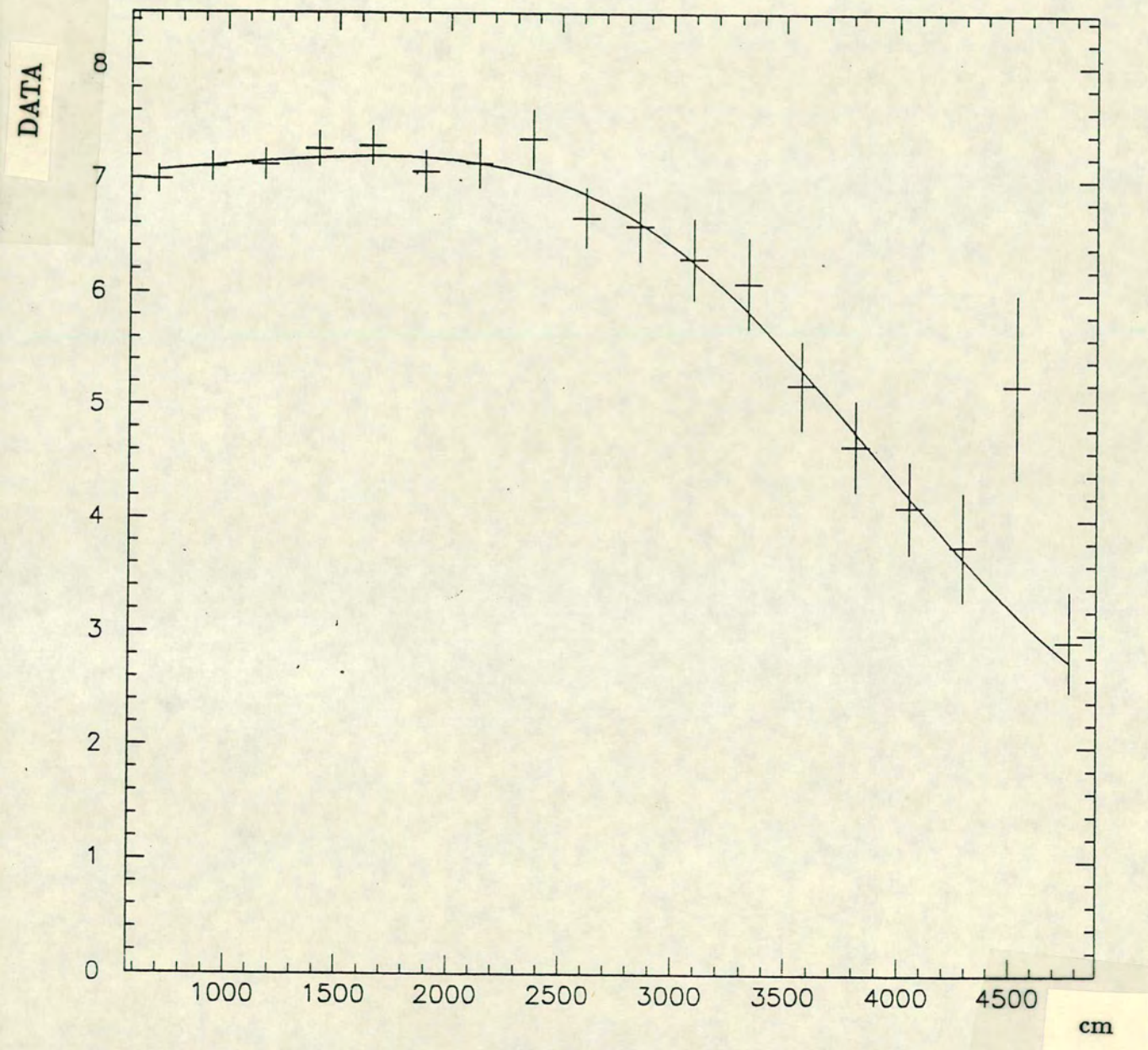

Figure 7.5: Fit Result - Charged Data - 140 to 145 GeV

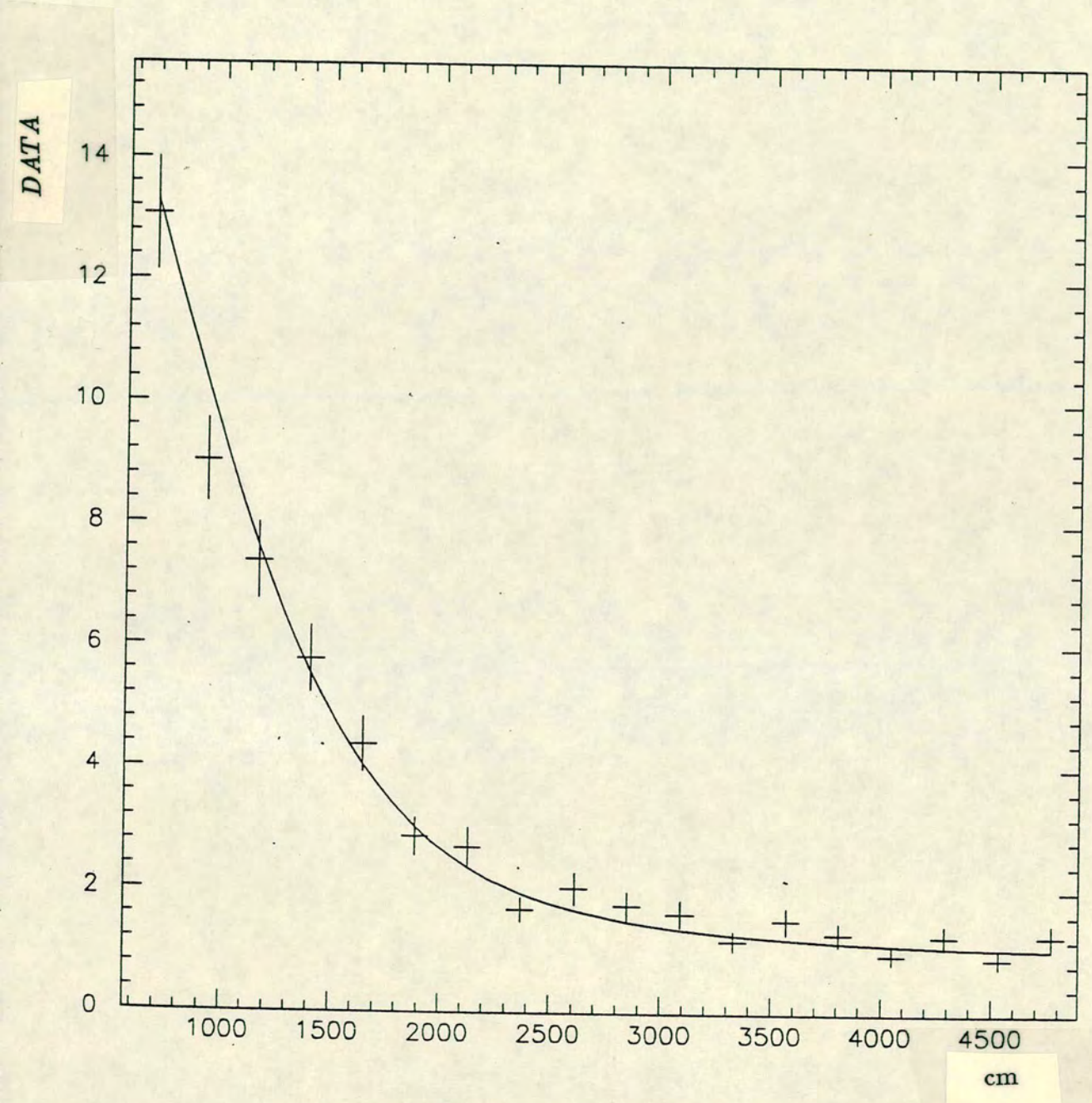

Figure 7.6: Fit Result - Neutral Data - 85 to 90 GeV

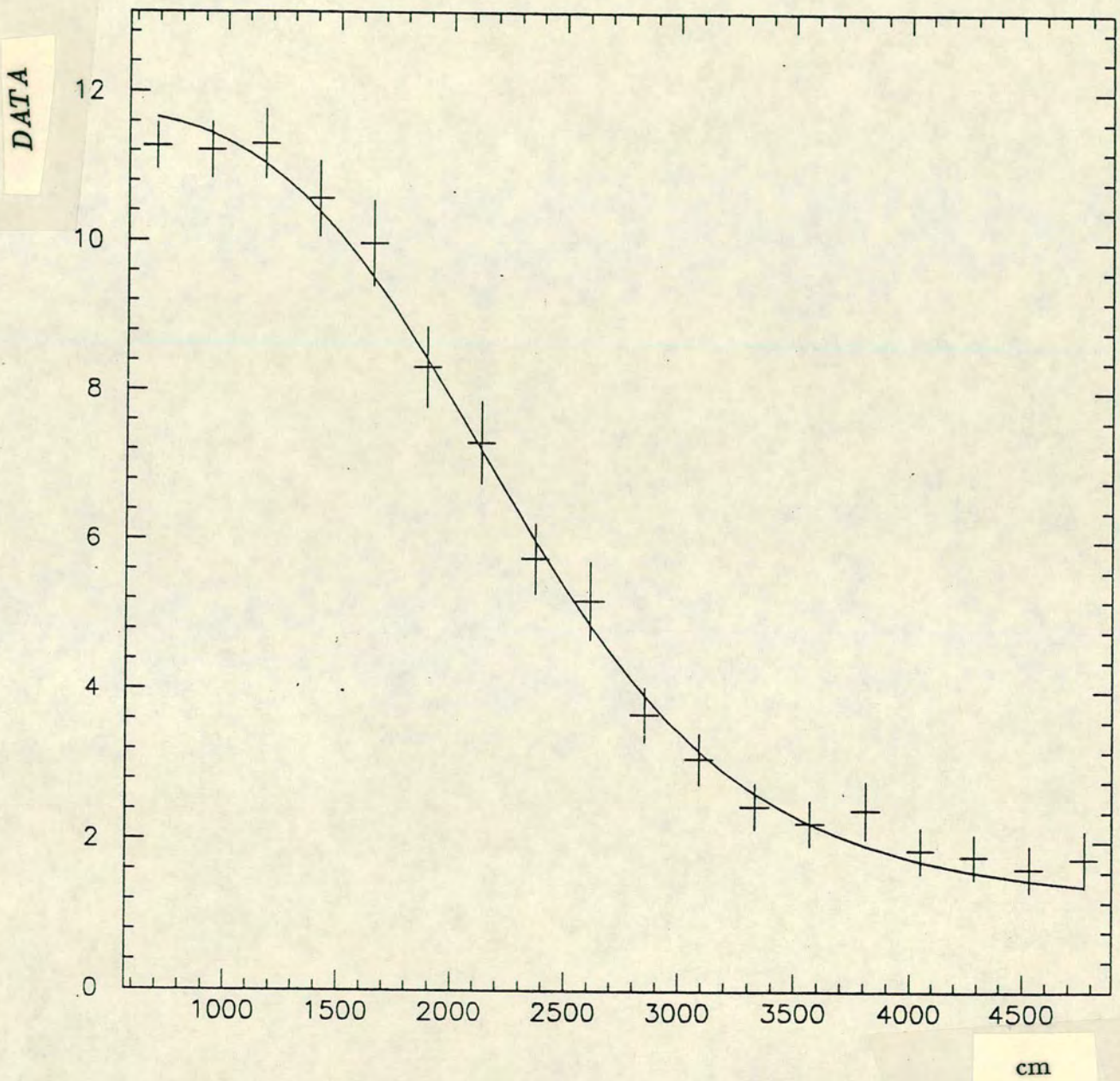

Figure 7.7: Fit Result - Neutral Data - 110 to 115 GeV

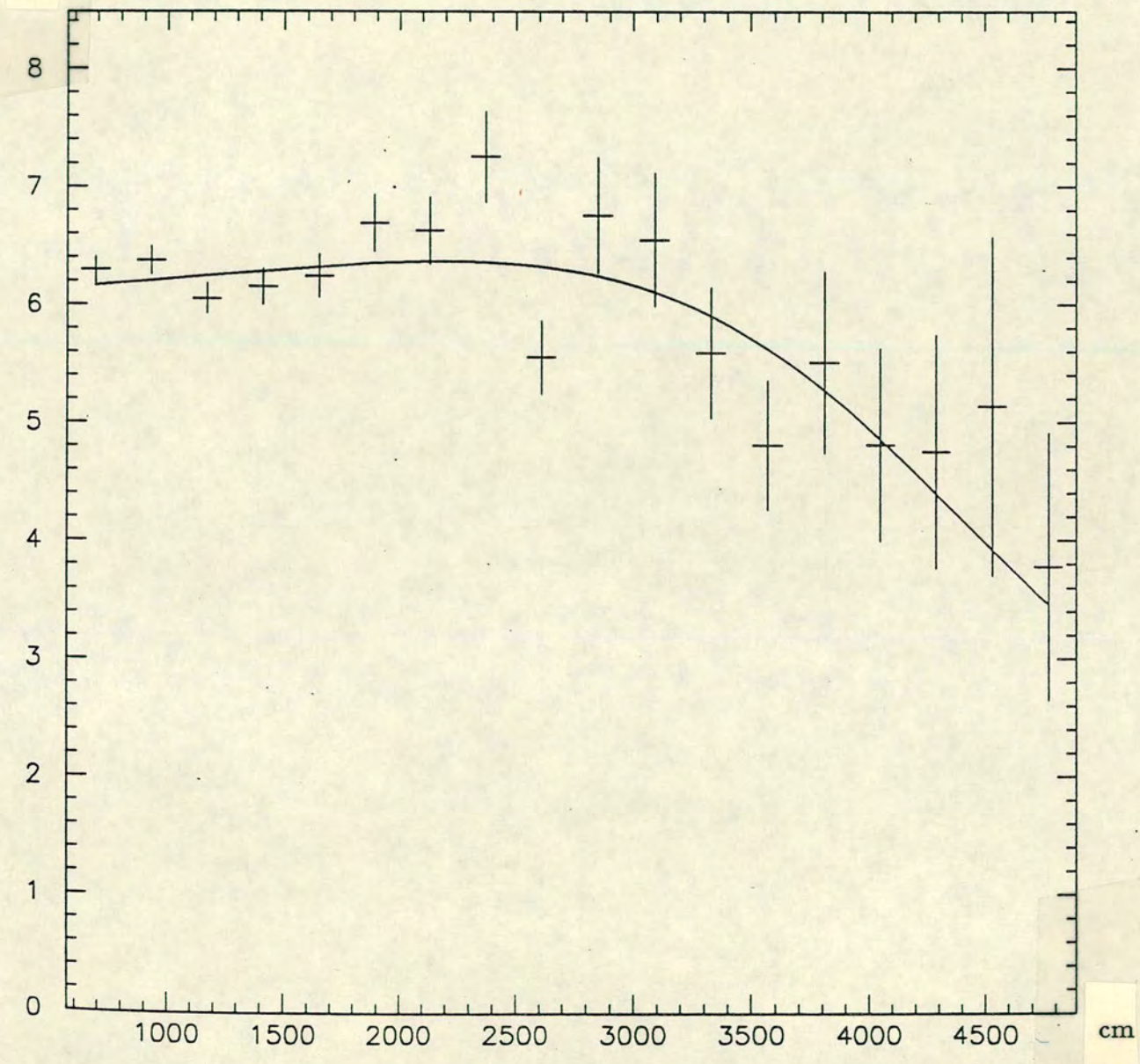

Figure 7.8: Fit Result - Neutral Data - 150 to 155 GeV

width, at any Z position within the decay volume. This could, in principal, result in different acceptances for the two beams, and must be examined further.

The KN beam, produced nearer to the detector than the KF beam, is narrower at any given Z. To examine any possible effects due to the different beam widths, we expand the KN beam to have the same width as the KF beam, and then re-calculate the results in the standard way.

For charged events we calculate the X,Y and Z co-ordinates of the vertex. For KN events we increase the radial position of the vertex relative to the beam axis, by a factor designed to expand the KN beam cone to the same size as the KF beam cone. This factor is simply the ratio of the two beam radii under normal conditions. We then alter the wire chamber hits so that the decay has the same orientation relative to the vector between target and vertex. Having done this, we impose the usual cuts, perform the standard background subtraction, and bin the data in the normal way.

For neutral events we calculate no radial vertex position. We therefore move the centre of gravity of the photons at the LAC in such a way as to expand the KN beam cone to the size of the KF beam. We then move photon positions relative to the new COG, impose standard cuts and background subtraction, and bin the data in the standard way.

When the results were calculated after these modifications , we found that the value for ϕ^{+-} was the same as previously calculated, but that ϕ^{00} had increased by 0.3^0 relative to the standard result. It can be argued that the acceptance cancellation is better when the beam cones are the same, so a correction should be applied to the previous result. The value quoted for ϕ^{00} is therefore 49.2^0 as opposed to 48.9^0.

7.3.2 Systematic Errors

Accuracy of Momentum and Vertex Calculations

When calculating the number of K_S lifetimes a kaon has travelled between the target and it's decay point (eqn 4.2), we require accurate knowledge of the momentum and vertex position. For both charged and neutral events, the longitudinal length scale is coupled with the energy scale. In neutrals this is due to the kaon mass constraint which gives a direct relationship between energy and vertex position (eqn 4.16). In the charged case the energy is calculated from the opening angle between the tracks, and the opening angle is dependent on the vertex position (eqn 4.3). In each case, a decrease in energy equates with an increase in the distance between target and vertex, and both of these effects increase the calculated number of K_S lifetimes (eqn 4.2). It can be shown that an uncertainty in length scale which is the same for charged and neutral events will result in systematic errors of the same magnitude for ϕ^{+-} and ϕ^{00}.

The length scales are measured as follows. The K_S anti-counter (section 3.3.1) is used as a fixed position in Z. Using K_S data, it's position is precisely measured from the rising edge of the $2\pi^0$ vertex distribution. The distance from the anti-counter to the LAC is 120m. In order to fix the energy scale to 0.1%, the position of the anti-counter must be measured to a precision of 10cm, which is approximately 10% of the resolution. The energy scale was determined for each mini-period, and any small corrections necessary to reproduce the position of the anti-counter were applied at the level of the photon energies. For charged events, the position of the anti-counter was measured in the same way.

The uncertainty in the length scale was 0.2% for neutral events, and 0.1% for charged. The systematic uncertainty on the agreement of charged and neutral length scales is estimated to be two per mille.

The systematic error on the phases due to systematic uncertainties in momentum and vertex position was calculated as follows. Using the standard neutral events in KN and KF, all photon energies were increased by two per mille. After the standard procedure the calculated value of ϕ^{00} differed from the result calculated

under normal conditions by 2.4^0. Since the neutral energy scale is known to two per mille, this translates to a systematic error of 2.4^0 on ϕ^{00} due to uncertainty in the energy and length scales for neutral events. The corresponding systematic errors for the charged phase and the phase difference are therefore 1.2^0 and 2.4^0, since the energy scale for charged events enters in the same way as for neutrals.

7.3.3 Background Subtraction

Charged and neutral background subtractions are described in sections 6.1.2 and 6.2.2. For charged background, which is at a very low level, if we subtract only half of the background, or subtract the background multiplied by a factor of 1.5, then the value of the charged phase does not change from the previously calculated value. We understand the background to a precision much better than $\pm 50\%$, so there is no systematic error on ϕ^{+-} due to background subtraction. For neutral decays we understand the slope of the ellipse distribution (see fig 6.12) to better than 20%. If we add or subtract 20% to the background which we subtract, then the calculated value for ϕ^{00} changes by 0.2^0. We quote a systematic error of 0.2^0 on the neutral phase due to background subtraction.

7.3.4 Fit Parameters

During the fit procedure certain parameters have to be input as fixed values, and not calculated in the fit. These values were taken from the Particle Data Booklet, and have associated measurement errors. To calculate systematic errors on ϕ^{+-} and ϕ^{00} due to the errors on the input parameters, these parameters were individually increased or decreased by one sigma, and the phase values re-calculated in a new fit. The systematic errors, due to the measurement errors of fixed parameters, are shown in table 7.4. It should be noted that the systematic errors on $\Delta\phi$ are much lower than for ϕ^{+-} or ϕ^{00}, since a change in any of the fixed parameters tends to have the same effect on the calculated values of ϕ^{+-} and ϕ^{00}.

	ϕ^{+-}	ϕ^{00}	$\Delta\phi$
Δm	1.3^0	1.3^0	-
τ_S	0.5^0	0.4^0	0.2^0
τ_L	-	-	-
η	0.2^0	0.3^0	0.1^0

Table 7.4: Systematic Errors due to Fit Parameters

7.3.5 Target Position

Due to slight uncertainty as to the beam steering, we allow an error of $\pm$10cm for the Z position of either target. We know the exact geometrical position of both targets; this error represents the level of uncertainty as to the average position of kaon production in the targets which are 40cm long. This error translates to a systematic error of 0.5^0 on either phase, but there is no systematic error on the phase difference, since a change of target position effects both phases in the same way.

7.3.6 Magnetic Field

It was discovered, during analysis of the 1986 data, that there is a small magnetic field present in the vacuum tank from which decays are collected. Further investigation showed that this came from two sources. The first source was the rail along which the K_S train runs, giving a horizontal field of roughly 1.6 Gauss throughout the decay region. The second field is a remnant field from the neighbouring experiment, NA36. Once again the field is horizontal, and the net effect over the decay region is roughly 70 Gauss-metres. The magnetic field will alter the trajectories of charged particles, and so alter the calculated vertex and energy (from the opening angle) of charged events. A careful analysis [18] shows that a typical decay will have it's vertex position shifted by $\pm$120cm, and it's energy shifted by $\pm$1%. If the distance from target to vertex is increased, then the energy is decreased, and vice versa. If all charged events are altered so that alternate events are shifted forward or backward in Z, and downwards or upwards in E, by typical values, then the value of ϕ^{+-} changes by 0.4^0. We

	ϕ^{+-}	ϕ^{00}	$\Delta\phi$
Energy scale	1.2^0	2.4^0	2.4^0
Bgd Subtraction	-	0.2^0	0.2^0
Δm	1.3^0	1.3^0	-
τ_S	0.5^0	0.4^0	0.2^0
τ_L	-	-	-
η	0.2^0	0.3^0	0.1^0
Target position	0.5^0	0.5^0	-
Magnetic field	0.4^0	-	0.4^0

Table 7.5: Systematic Errors due to Fit Parameters

quote this as a systematic error due to the presence of the magnetic field.

7.4 Summary

Table 7.5 gives a summary of all systematic errors. These errors are regarded as independent, and are added to the statistical errors in quadrature. The results for ϕ^{+-}, ϕ^{00}, and $\Delta\phi$, with the correction to ϕ^{00} and the respective errors are, therefore:

$$\begin{aligned} \phi^{+-} &= 46.8 \pm 1.5 \pm 1.9^0 \\ \phi^{00} &= 49.2 \pm 2.3 \pm 2.8^0 \\ \Delta\phi &= 2.4 \pm 2.7 \pm 2.4^0 \end{aligned} \tag{7.15}$$

where the first error is statistical, and the second is the systematic error.

The final results are :

$$\begin{aligned} \phi^{+-} &= 46.8 \pm 2.5^0 \\ \phi^{00} &= 49.2 \pm 3.6^0 \\ \Delta\phi &= 2.4 \pm 3.6^0 \end{aligned} \tag{7.16}$$

7.5 Stability of the Result

To test the stability of the result versus momentum and time, we restricted our data sample to smaller momentum regions, or divided our data into smaller samples according to time, before fitting. The results are shown in figures 7.9 to 7.14. Figure 7.15 shows the charged phase calculated as a function of azimuthal angle. The first point plotted is ϕ^{+-} calculated over 360^0 of azimuth, and the following three points are ϕ^{+-} in three separate bins of azimuthal angle. This excercise was carried out to see if there was any effect due to the magnetic field. We would expect to see any effect in the final bin, where the magnetic field is at a maximum.

We conclude that there is no trend to suggest that either phase, or the difference between the two, depends on momentum, time, or azimuthal angle.

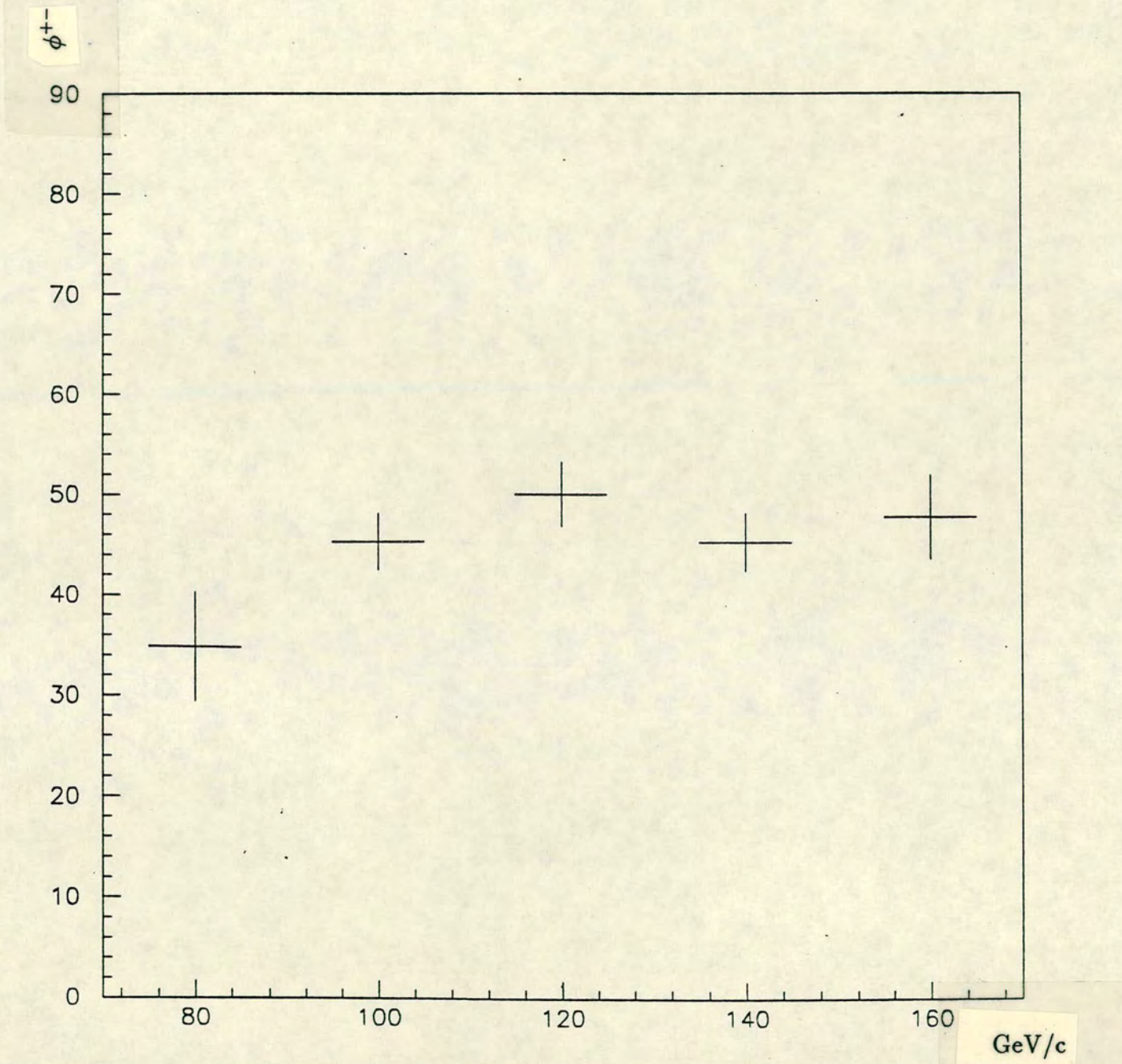

Figure 7.9: Momentum Dependence of ϕ^{+-}

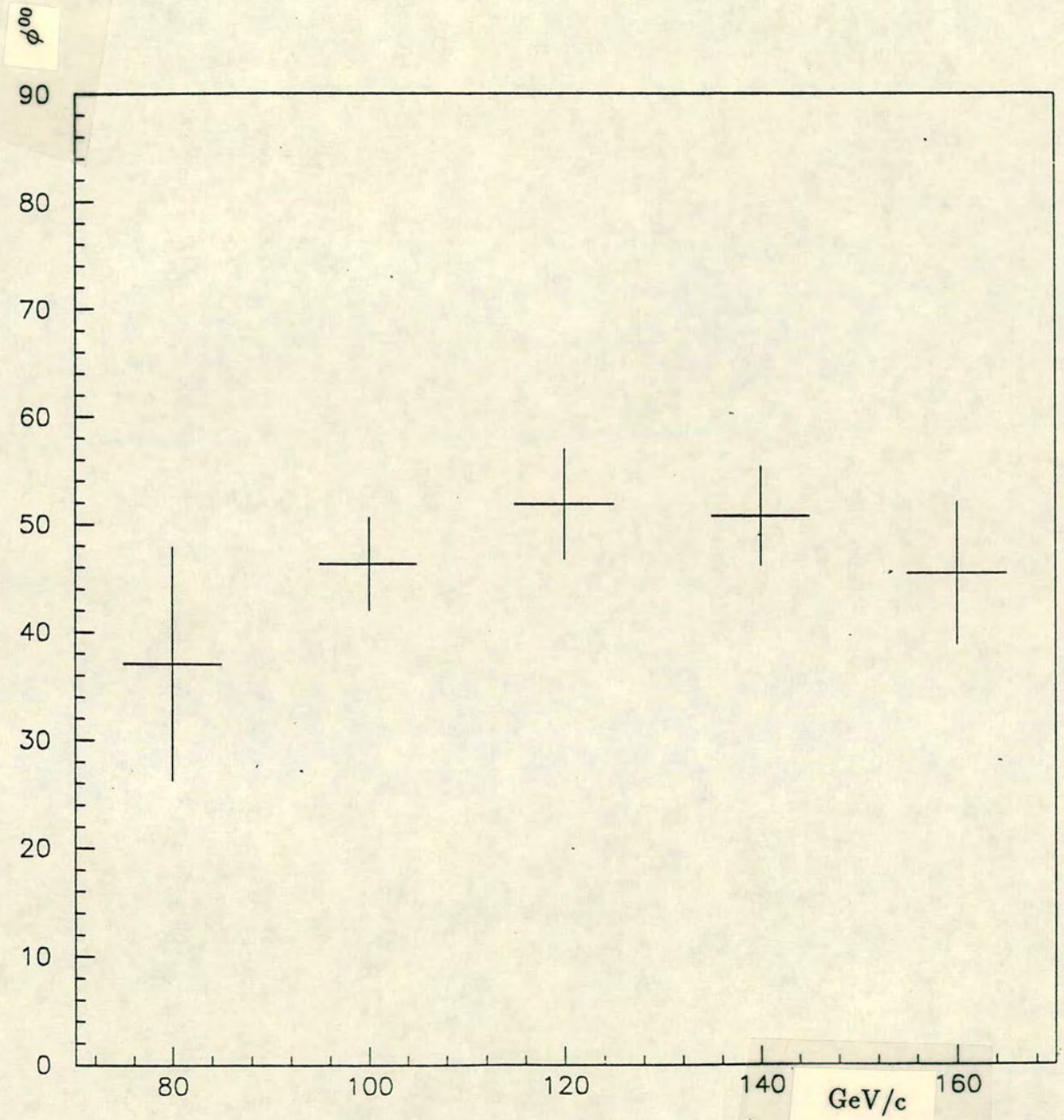

Figure 7.10: Momentum Dependence of ϕ^{00}

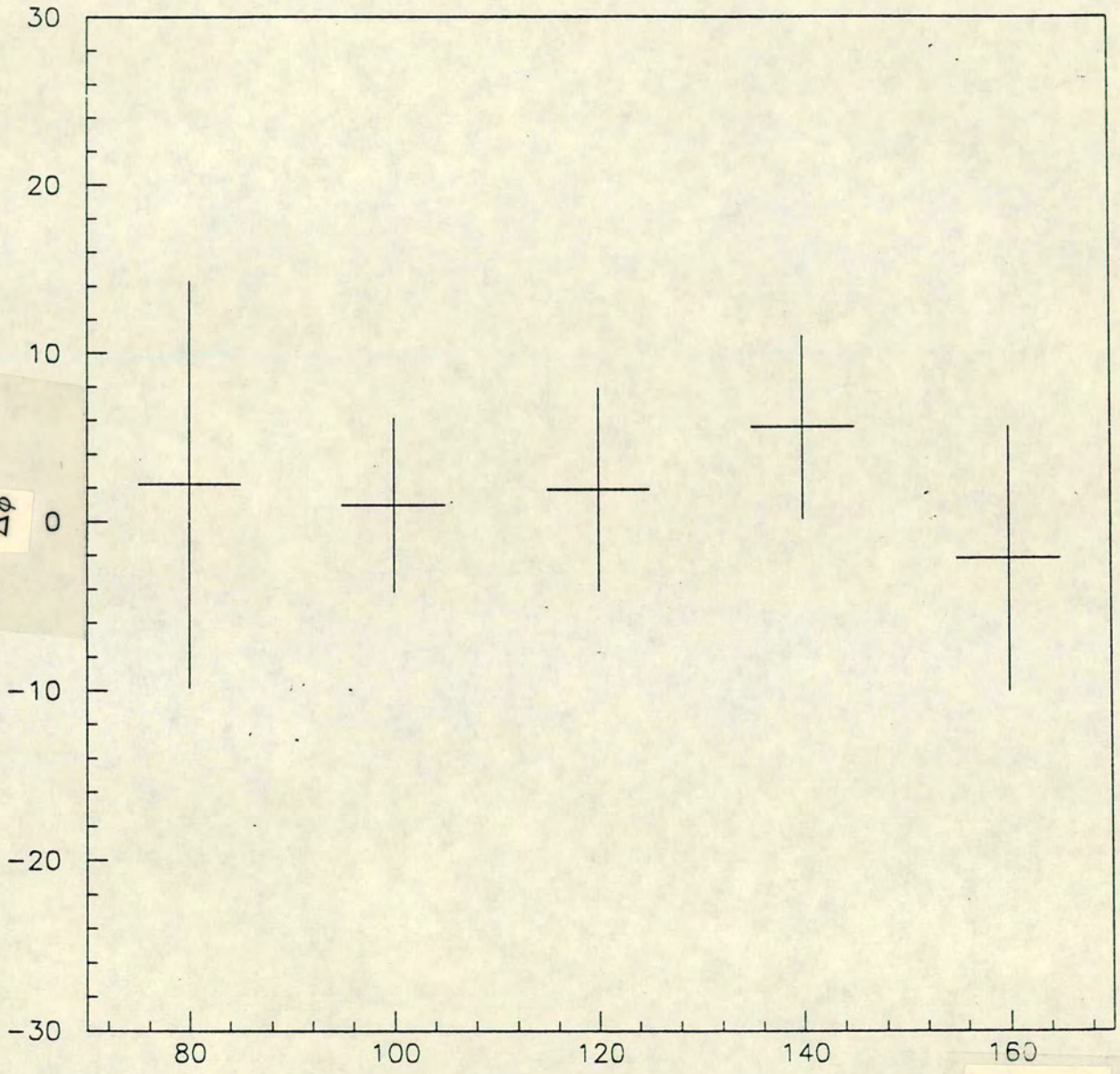

Figure 7.11: Momentum Dependence of $\Delta\phi$

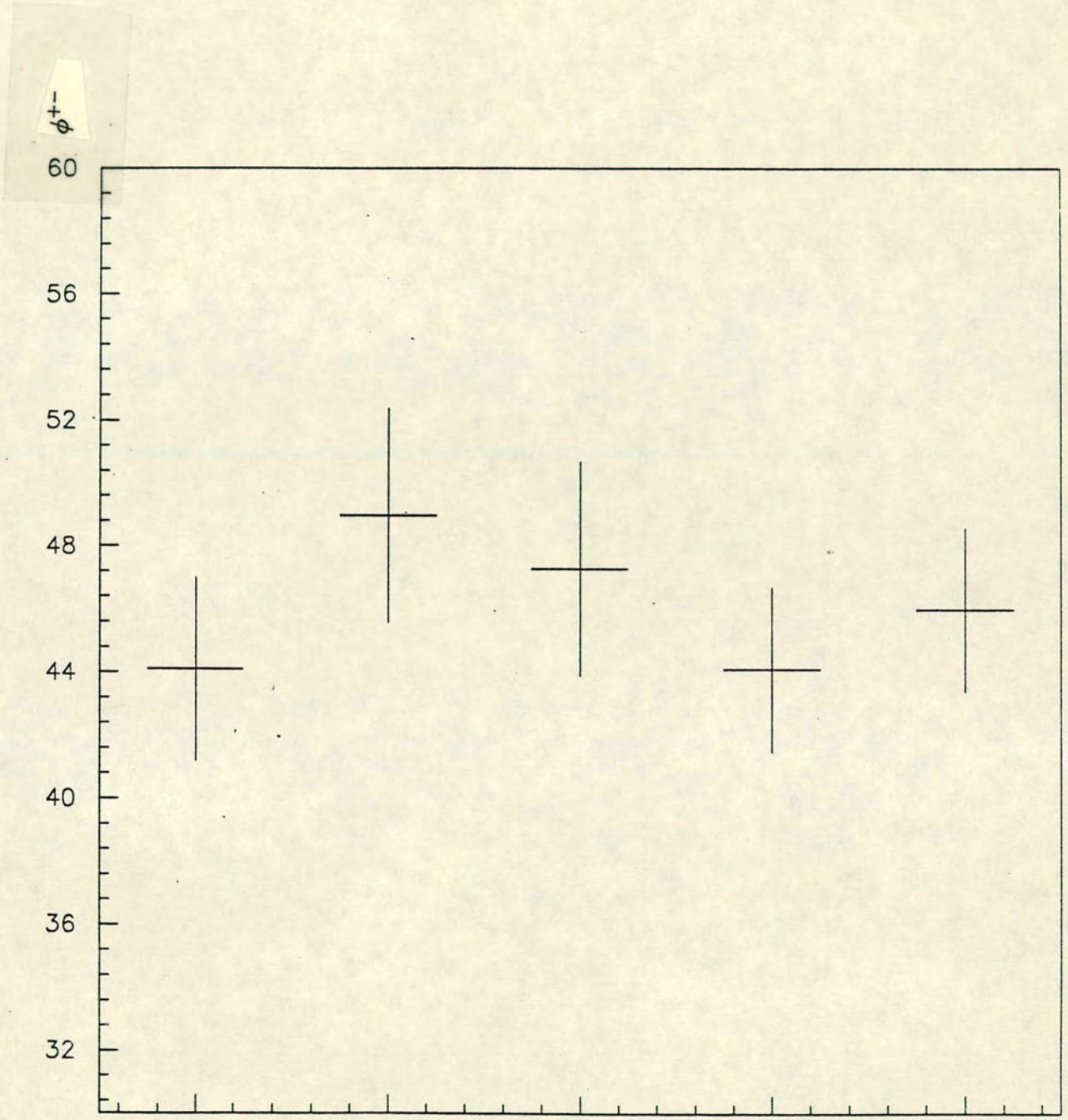

Figure 7.12: Time Dependence of ϕ^{+-}

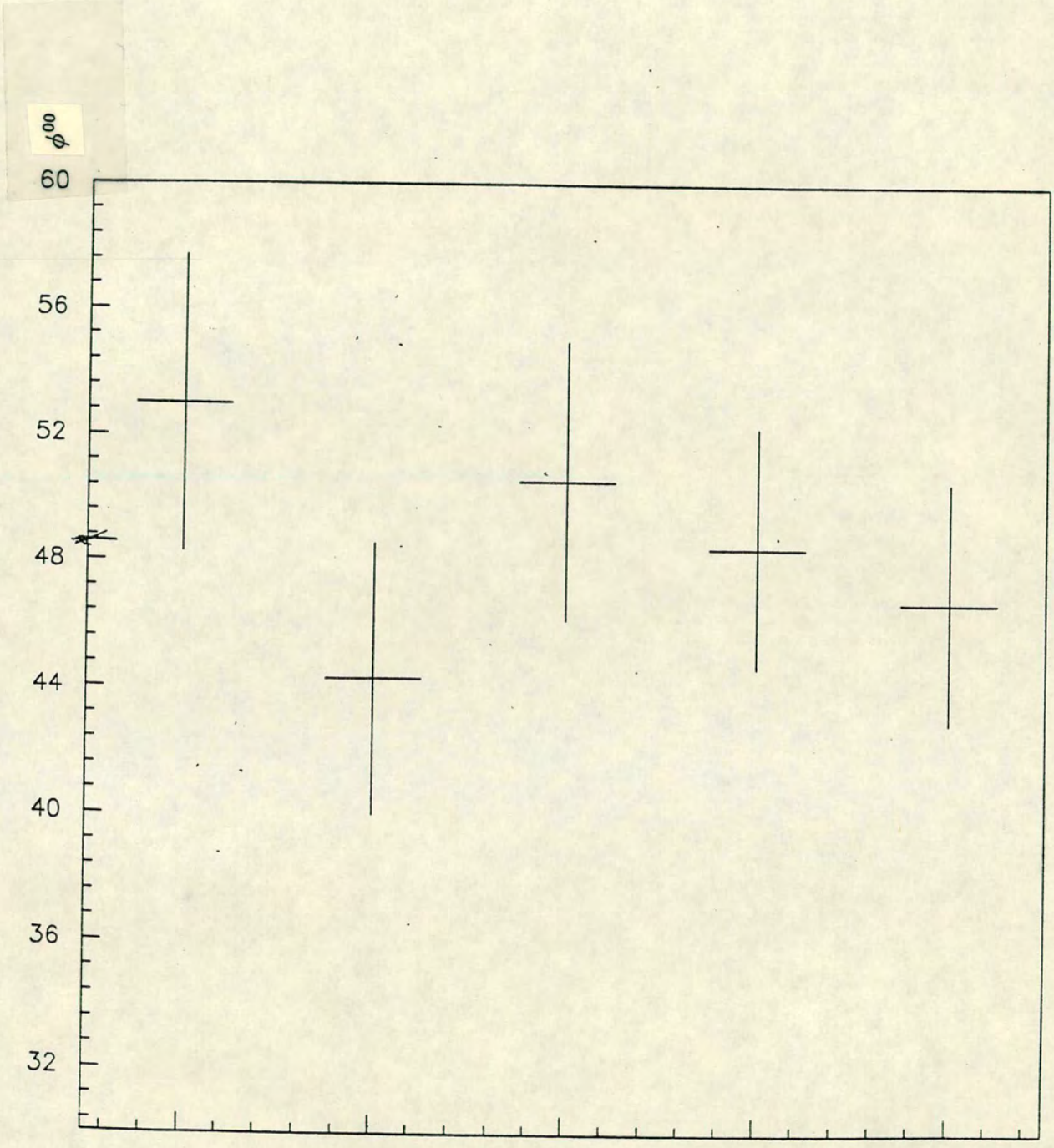

Figure 7.13: Time Dependence of ϕ^{00}

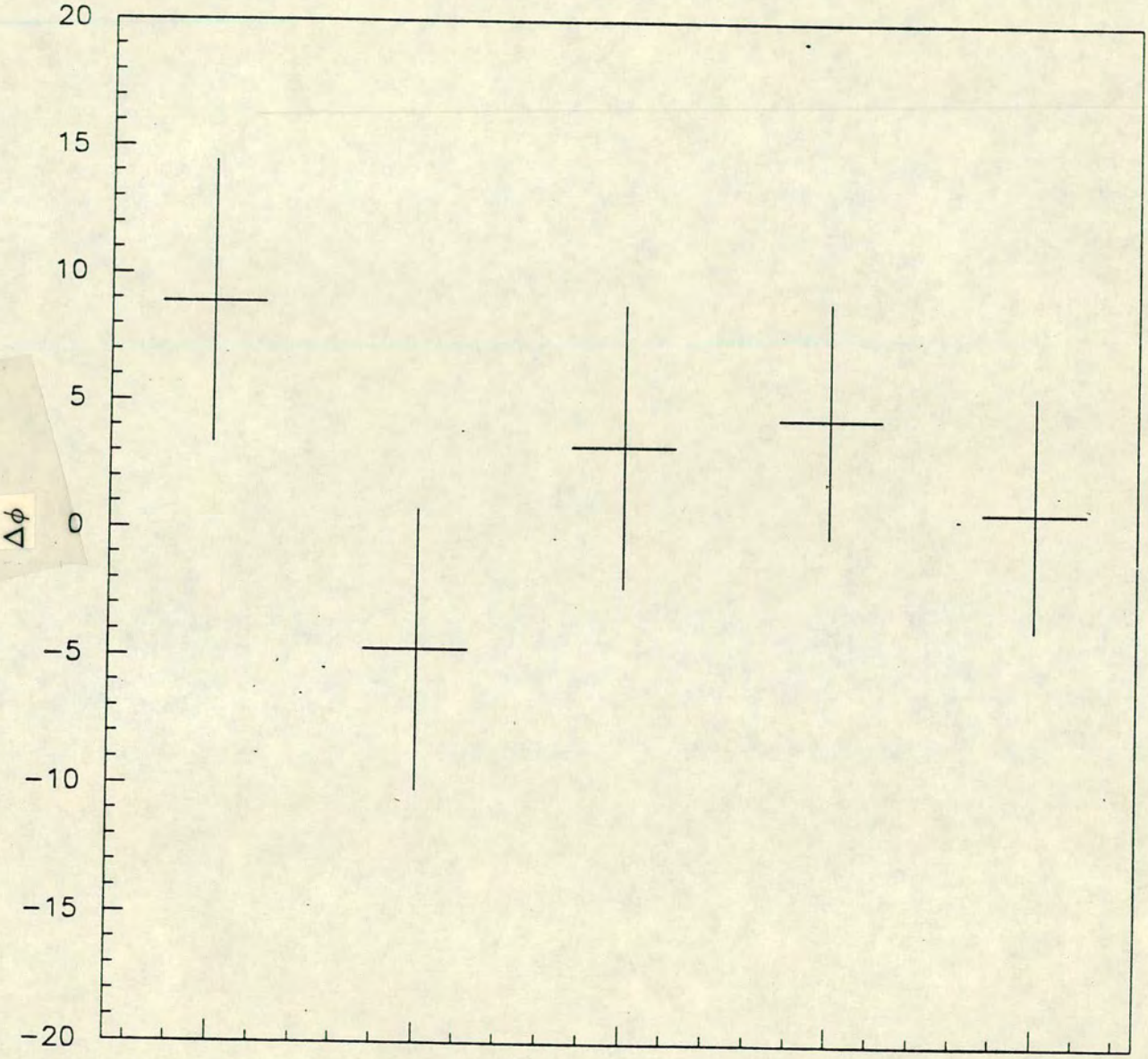

Figure 7.14: Time Dependence of $\Delta\phi$

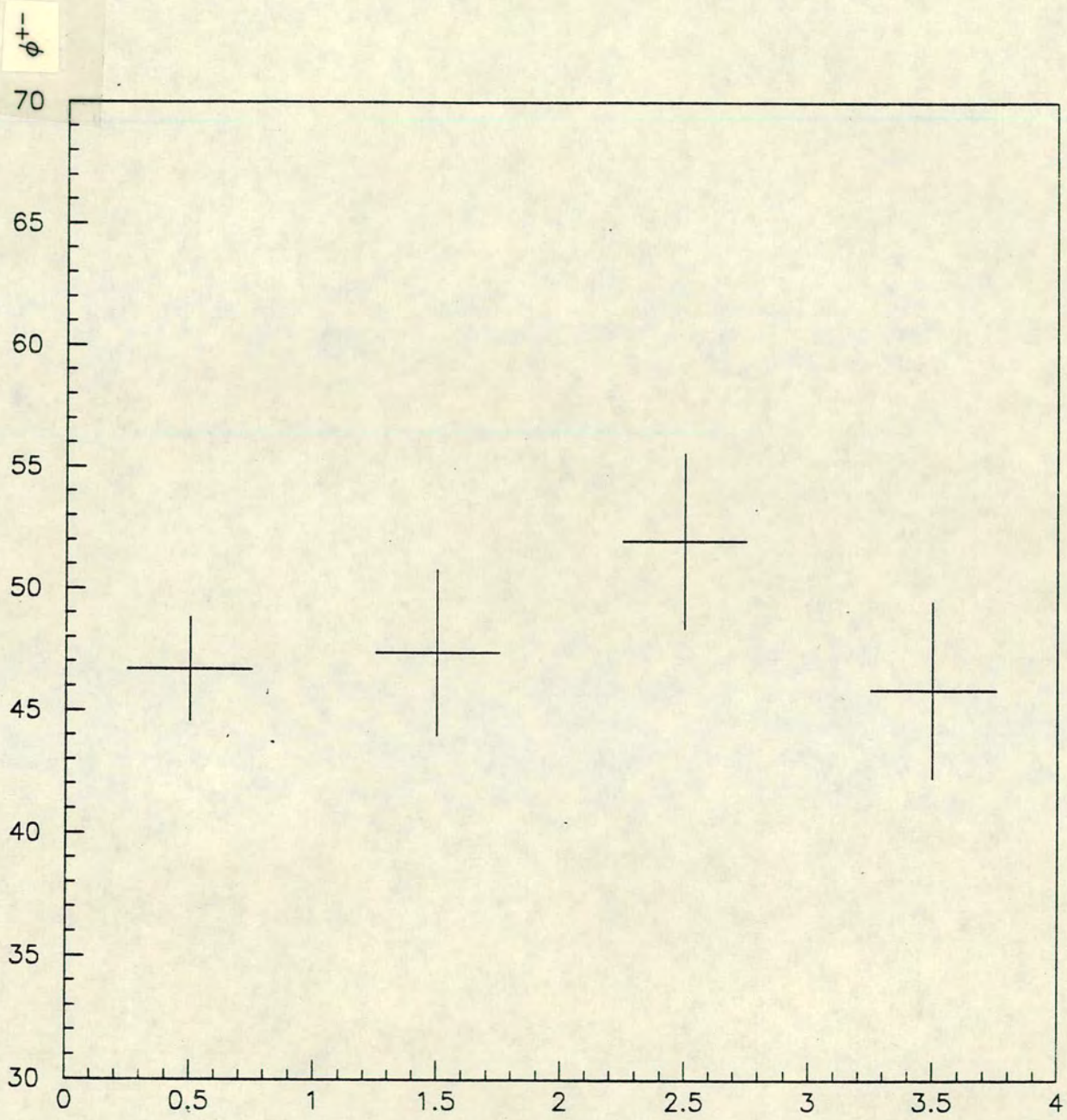

Figure 7.15: Charged Phase as a Function of Azimuthal Angle

Chapter 8

Discussion of Result

8.1 The Dilution Factor

The dilution factor, D(p), has been measured, and the results are shown in figure 7.2. This is the first measurement of the dilution factor at this energy range, and there is nothing to which we may directly compare our measurement. The only other relevant information comes from data concerning K^+ and K^- production [19]. A simple model, concerning only the relative abundance of u, d and s quarks in the incident proton and the quark sea, predicts

$$(K^0 - \bar{K^0})/(K^0 + \bar{K^0}) = (K^+ - K^-)/(K^+ + 3K^-) \qquad (8.17)$$

Our measured value for the dilution factor agrees broadly with this prediction, and the energy dependence of D(p) is adequately described.

8.2 The Phase Difference

The charged and neutral phases, ϕ^{+-} and ϕ^{00}, are measured to be 46.8 ± 2.5^0 and 49.2 ± 3.6^0 respectively. These phases are expected to agree with the 'superweak' phase, the phase ϕ_ϵ of the parameter ϵ. ϕ_ϵ is 43.72 ± 0.14^0 (see section 2.4), so ϕ^{+-} and ϕ^{00} agree with this to within 1.5σ.

	NA31	PBM	PWA
ϕ^{+-}	46.8 ± 2.5	46.5 ± 1.6	44.6 ± 1.2
ϕ^{00}	49.2 ± 3.6	55.7 ± 5.8	54.5 ± 5.3
$\Delta\phi$	2.4 ± 3.6	12.6 ± 6.2	9.8 ± 5.4

Table 8.1: Comparison with previous best measurment, and previous world average

The difference, $\Delta\phi$, between charged and neutral phases, has been measured to be 2.4 ± 3.6^0. Table 8.1 compares our measurement for these parameters with the previous best measurement, and with the previous world average. There have been few previous measurements of either the neutral phase or the phase difference, but several measurements of ϕ^{+-} have been made. Figure 8.1 compares our measurement of $\phi^{+-}$with all previous measurements having an error of less than 10^0.

If we return to section 2.4 and re-calculate the parameter $\epsilon'_\perp$, using our measured value of $\Delta\phi$ as input, then we find

$$\epsilon'_\perp = (3.2 \pm 4.8)10^{-5} \tag{8.18}$$

The parameter $\epsilon'_{||}$ is unchanged at $(6.8 \pm 2.3)10^{-6}$, so we now have no evidence that $\epsilon'_\perp$ is greater than $\epsilon'_{||}$. This is in full agreement with the requirements of the CPT-theorem. To measure $\epsilon'_\perp$ to the precision of $\epsilon'_{||}$, it is necessary to measure $\Delta\phi$ to a precision of 0.4^0. This would seem to be well beyond the limits of the current generation of experiments.

Section 2.5 concluded that the agreement between theory and data, for the parameters argϵ and Δ, was not good, and that this was due to the 2σ disagreement in the measured values of ϕ^{+-} and ϕ^{00}. Our more accurate result for $\Delta\phi$ would remove the disagreement between theory and data, and is once again in full agreement with the reqiurements of CPT.

The results presented here are from a preliminary analysis of the 1987 NA31 data. A full analysis, using Monte Carlo simulation for acceptance calculations, is currently in progress at CERN. It is expected that the error on $\Delta\phi$ will be in the region of 2^0, and the results should be published early in 1989.

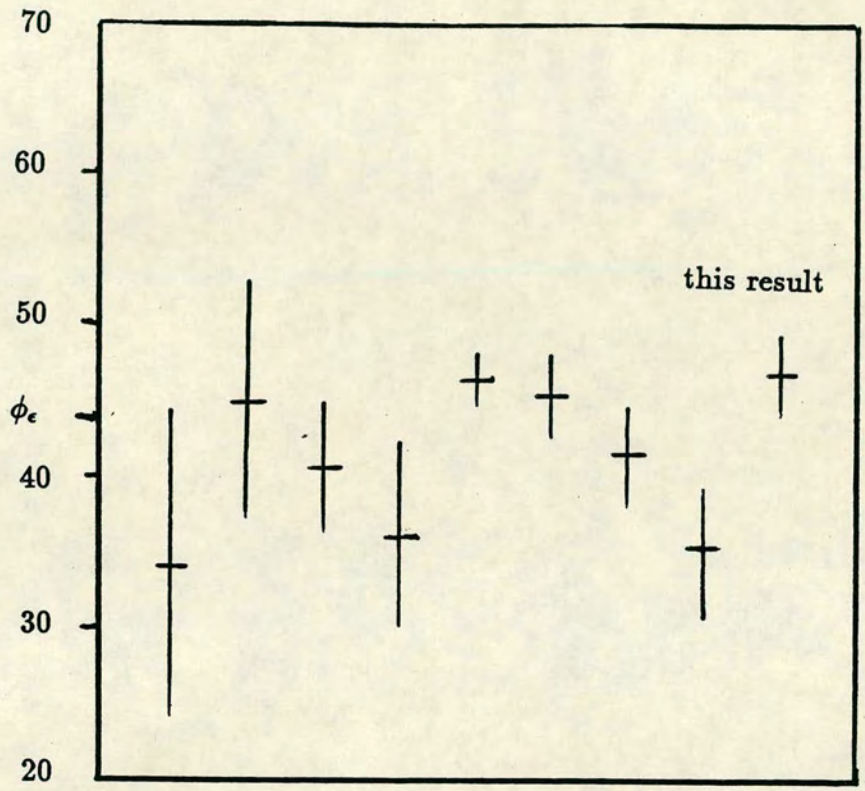

Figure 8.1: Comparison with previous results for ϕ^{+-}

References

[1] G.Luders, Ann.Phys.2(1957),1.

[2] C.S.Wu et al, Phys.Rev.105(1957),1413

[3] R.L.Garwin et al, Phys.Rev.105(1957),1681.

[4] J.H.Christenson et al, Phys.Rev.Lett.13(1964),138.

[5] Phys.Lett.170B(1986)67

[6] Phys.Lett.170B(1986)139

[7] J.H.Christenson et al, Phys.Rev.Lett.43(1979)1209

[8] T.T.Wu and C.N.Yang, Phys.Rev.Lett.13(1964)360

[9] L.Wolfenstein, Phys.Rev.Lett.13(1964)569

[10] M.Kobayashi and K.Maskawa, Prog.Theor.Phys.49(1973)652

[11] H.Burkhardt et al.; Phys.Lett.206B(1988)169

[12] V.V.Barmin et al., Nucl.Phys.B247(1984)293

[13] H.Burkhardt et al., Nucl.Inst.Meth.A268(1988)403

[14] L.Wolfenstein, Ann.Rev.Nuc.Part.Sci.36.137.70

[15] S.Roehn, Diploma Thesis, Mainz(1988) (unpublished)

[16] H.Burkhardt et al., Phys.Lett.B,199(1987)

[17] F.James and M.Roos, Computer Physics Communications 10(1975)343

[18] G.Barr, NA31 Note 43(1988)

[19] H.W.Atherton et al, CERN Yellow Report 80-07

[20] F.Gilman and M.Wise, Phys.Rev.D20(1979)2392;Phys.Lett.83B(1979)83